The Use of Multi-Sensor Quantitative Precipitation Estimates for Deriving Extreme Precipitation Frequencies with Application in Louisiana

A Thesis

Presented to the

Graduate Faculty of the

University of Louisiana at Lafayette

In Partial Fulfillment of the

Requirements for the Degree of

Master of Science

Hisham Abd El-Kareem El-Dardiry

Fall 2014

UMI Number: 1585854

All rights reserved

INFORMATION TO ALL USERS
The quality of this reproduction is dependent upon the quality of the copy submitted.

In the unlikely event that the author did not send a complete manuscript
and there are missing pages, these will be noted. Also, if material had to be removed,
a note will indicate the deletion.

UMI 1585854

Published by ProQuest LLC (2015). Copyright in the Dissertation held by the Author.

Microform Edition © ProQuest LLC.
All rights reserved. This work is protected against
unauthorized copying under Title 17, United States Code

ProQuest LLC.
789 East Eisenhower Parkway
P.O. Box 1346
Ann Arbor, MI 48106 - 1346

© Hisham Abd El-Kareem El-Dardiry

2014

All Rights Reserved

The Use of Multi-Sensor Quantitative Precipitation Estimates for Deriving Extreme Precipitation Frequencies with Application in Louisiana

Hisham Abd El-Kareem El-Dardiry

APPROVED:

_____	_____
Emad Habib, Chair Professor of Civil Engineering	Kenneth McManis Professor and Head of Civil Engineering
_____	_____
Daniel Gang Professor of Civil Engineering	Luis G. León Novelo Assistant Professor of Statistics

_____

Mary Farmer-Kaiser
Interim Dean of Graduate School

Dedication

I would like to dedicate this thesis to my parents.

Acknowledgments

I would like to express my gratefulness to Allah, the most graceful, the most merciful. I would like to thank Allah for giving me the strength and patience to accomplish this achievement.

I would like to express my sincere gratitude to Dr. Emad Habib for his support, assistance, encouragement, and his aspiring guidance throughout the period of my study. It was a great privilege to work under his supervision.

I appreciate Dr. Kenneth McManis and Dr. Daniel Gang for serving on my thesis committee. I also appreciate the contribution of Dr. Luis Novelo in the statistical analysis of my study and his serving on my thesis committee as well.

I would like to thank Dr. Yu Zhang, from the National Weather Service (NWS), and Jeffrey Graschel, from the Lower Mississippi River Forecast Center (LMRFC), for providing me with valuable comments and suggestions that were key for the execution of this research work.

Finally, I would also like to thank my parents, elder brother, and elder sister for all their prayers. They were always supporting and encouraging me with their best wishes to keep me concentrated and motivated on my research work.

Table of Contents

List of Tables

List of Figures

List of Abbreviations

ARF	Areal Reduction Factor
AES	Annual Exceedance Series
AMS	Annual Maximum Series
CONUS	Continental United States
DDF	Depth-Duration-Frequency
DSD	Drop Size Distribution
DPA	Digital Precipitation Array
GEV	Generalized Extreme Value
GB	Grubbs-Beck
HDSC	Hydrometeorological Design Studies Center
HRAP	Hydrologic Rainfall Analysis Project
IDF	Intensity-Duration-Frequency
LMOM	Linear Moments
LMRFC	Lower Mississippi River Forecast Center
MAM	Mean Annual Maxima
MAP	Mean Annual Precipitation
ML	Maximum Likelihood
MPA	Multi-Satellite Precipitation Analysis
MPE	Multi-sensor Precipitation Estimate
MQPE	Multi-sensor Quantitative Precipitation Estimate
NCEP	National Centers for Environmental Prediction
NEXRAD	Next Generation Radar

NOAA	National Oceanic and Atmospheric Administration
NWS	National Weather Service
PFE	Precipitation Frequency Estimate
PDS	Partial Duration Series
PPS	Precipitation Processing System
POT	Peaks-Over Threshold
QC	Quality Control
QPE	Quantitative Precipitation Estimate
RFC	River Forecast Center
ROC	Radar Operational Center
TRMM	Tropical Rainfall Measuring Mission
VCP	Volume Coverage Pattern
VPR	Vertical Profile of Reflectivity
WSR-88D	Weather Surveillance Radar 1988-Doppler

Chapter 1 Introduction

1.1 Background

Rainfall plays a critical role in terrestrial and atmospheric mass and energy balances over a wide range of spatiotemporal scales. Therefore, accurate quantitative estimation of rainfall is extremely important to numerous applications in Earth, environmental, agricultural and other science and engineering disciplines (*Seo, et al.,* 2010). Rainfall is also a critical input for engineering design applications where Precipitation Frequency Estimates (PFE) are highly sought. The purpose of a precipitation frequency analysis is to determine the frequency at which certain rates or depths of precipitation are expected to occur. The PFE information can also be used to define the rainfall depth that corresponds to a certain probability of occurrence. For example, the daily rainfall depth that has a 1% probability of occurrence is referred to as the 24-hour, 100-year rainfall depth. An example of a spatial map for the 24-hour, 100-year rainfall depth for the United States is presented in Figure 1. Probabilistic modeling and statistical analysis techniques for extreme rainfall are used to provide PFE information and characterize the relationships between three important variables of rainfall: depth, duration, and frequency (*Pecho, et al.,* 2009). These relationships are usually referred to as Intensity-Duration-Frequency (IDF) curves, or Depth-Duration-Frequency (DDF) curves (see Figure 2 and Figure 3 for typical examples of IDF and DDF curves).

Statistics derived from IDF or DDF curves are typically used to develop “design storms”, which are then used as an input for a variety of engineering designs such as: dam design and operation, levee design, design of urban sewer systems, determination of required discharge capacity of channels, and pump sizing. The selection of a specific return period or a

frequency of occurrence (e.g., 100-year or 1%) depends on the design criterion and the importance of the structure under development.

Figure 4 shows ranges for hydrologic design scales of different types of structures depending on their economic and societal importance. For major structures, it is practical to use an Estimated Limiting Value (ELV) to define the largest possible magnitude of a hydrologic event based on available information (for more details on hydrologic design criteria, see *Chow, et al.,* (1988)). A proper design of these water resources systems will prevent flooding, reduce loss of life and property, and reduce pollution of surface waters (*Overeem, et al.,* 2008).

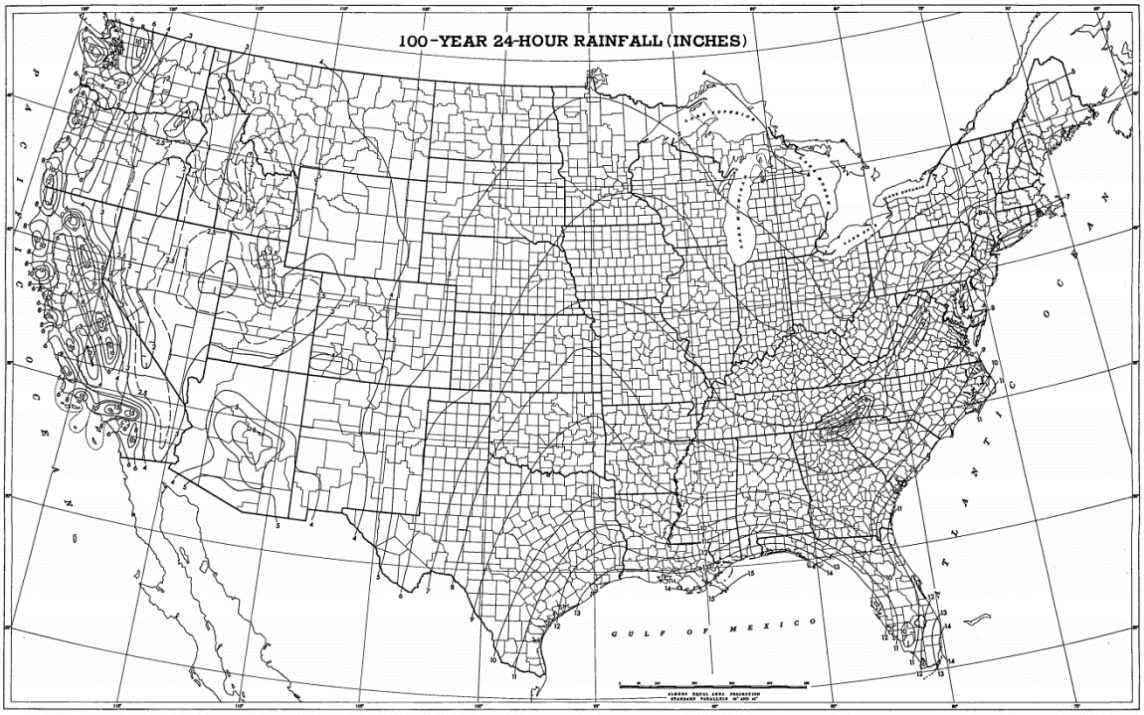

Figure 1 The 100-year 24-hour rainfall depth in the United States (Source: *Hershfield,* (1961)).

The PFE estimates are typically obtained from analysis of long records of rain gauges. However, due to the sparsity of rain gauges in many regions in the US and other world

countries, an interpolation technique is typically applied to produce a spatial map for the estimated frequencies (see Figure 1). However, the low spatial density of rain gauges significantly affects the reliability of the PFE estimates. Furthermore, the PFEs and the DDF/IDF curves derived from rain gauge observations are typically considered as point estimates, and as such, only applicable for relatively small areas (<4km2) (*Srikanthan,* 1995). These point estimates become inadequate for design applications that involve large areas such as river catchments or drainage basins.

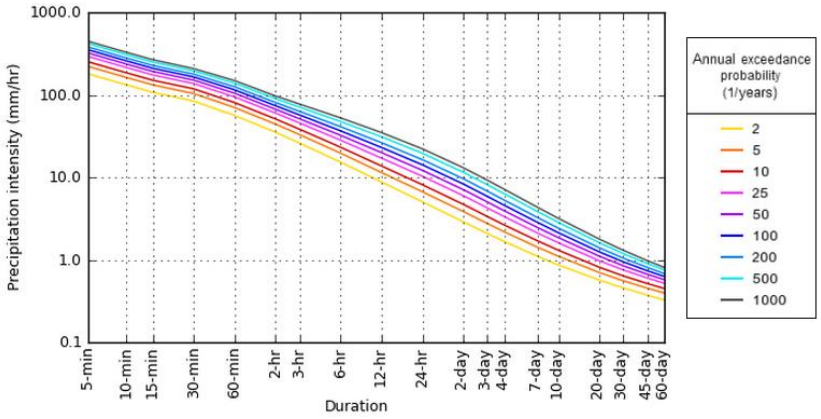

Figure 2 Intensity-Duration-Frequecny (IDF) curves for a station in Lafayette, Louisiana (Latitude:30.2050,Longitude:-91.9875) (Source: *NOAA ATLAS 14, Precipitation Frequency Data Server*).

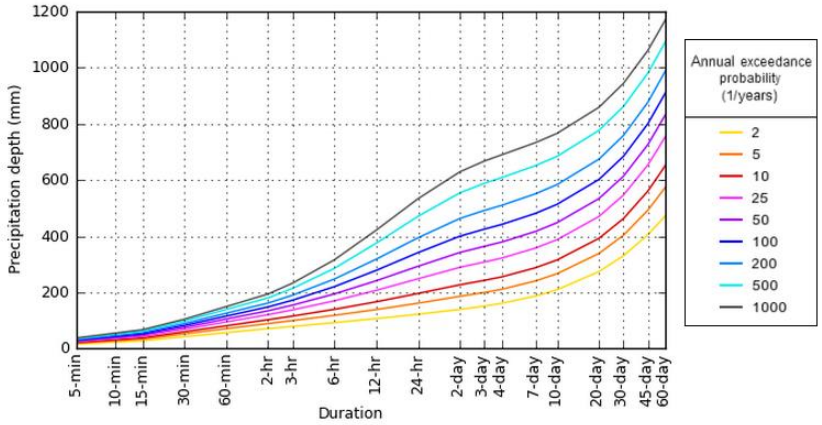

Figure 3 Depth-Duration-Frequecny (IDF) curves for a rain gauge in Lafayette, Louisiana (Latitude:30.2050,Longitude:-91.9875) (Source: *NOAA ATLAS 14, Precipitation Frequency Data Server*).

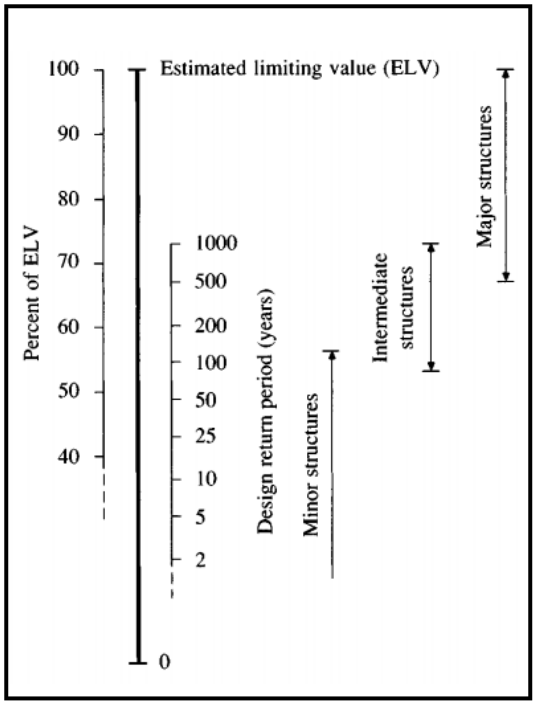

Type of structure	Return period (years)	ELV
Highway culverts		
Low traffic	5–10	—
Intermediate traffic	10–25	—
High traffic	50–100	—
Highway bridges		
Secondary system	10–50	—
Primary system	50–100	—
Farm drainage		
Culverts	5–50	—
Ditches	5–50	—
Urban drainage		
Storm sewers in small cities	2–25	—
Storm sewers in large cities	25–50	—
Airfields		
Low traffic	5–10	—
Intermediate traffic	10–25	—
High traffic	50–100	—
Levees		
On farms	2–50	—
Around cities	50–200	—
Dams with no likelihood of loss of life (low hazard)		
Small dams	50–100	—
Intermediate dams	100 +	—
Large dams	—	50–100%
Dams with probable loss of life (significant hazard)		
Small dams	100 +	50%
Intermediate dams	—	50–100%
Large dams	—	100%
Dams with high likelihood of considerable loss of life (high hazard)		
Small dams	—	50–100%
Intermediate dams	—	100%
Large dams	—	100%

Figure 4 (Left) Approximate ranges of the design level for different types of structures, (Right) Generalized design criteria for water-control structures. (Source: *Chow, et al.,* (1988)).

Weather radar technologies provide a viable resource for improving the current knowledge and estimation practices on precipitation frequency analysis. In the late 1980's, the US National Weather Service (NWS) installed the Next-Generation Weather Radar (NEXRAD) system at weather forecast offices across the country. The NEXRAD system consists of a network of Weather Surveillance Radar-1988 Doppler (WSR-88D) radars. The deployment of these radars in the United States has made spatially and temporally distributed rainfall data available in an operational environment. Reflectivity observations from each WSR-88D are used to generate radar-based Quantitative Precipitation Estimates (QPE) that can be used in a wide array of hydrologic and engineering applications (*Young, et al.,* 2000).

Unlike rain gauges, radar-based Quantitative Precipitation Estimates (QPE) have an important advantage over sparse rain gauges since they provide high temporal and spatial resolutions with large spatial coverage. A single weather radar station typically samples an area with a radius in the order 100-200 km, with a spatial resolution of approximately1-4 km and a temporal resolution as fine as 5 minutes. Notwithstanding the inherent uncertainties in weather radars as a remote-sensing and indirect technique, a typical coverage of a radar station can potentially provide an equivalent of a super-dense network of rain gauges. This potential advantage of weather radars raises the attention of the hydrologic and engineering communities to use their high-resolution rainfall estimates in the derivation of IDF and DDF curves. More importantly, rainfall design depths and design storms that are more representative of large areas can now be derived. Radar-rainfall estimates can also be utilized to construct Areal Reduction Factors (ARF), which have been traditionally used as a simple tool for converting point-based design depths into area-representative estimates (see Figure 5 for an example of ARF curve).

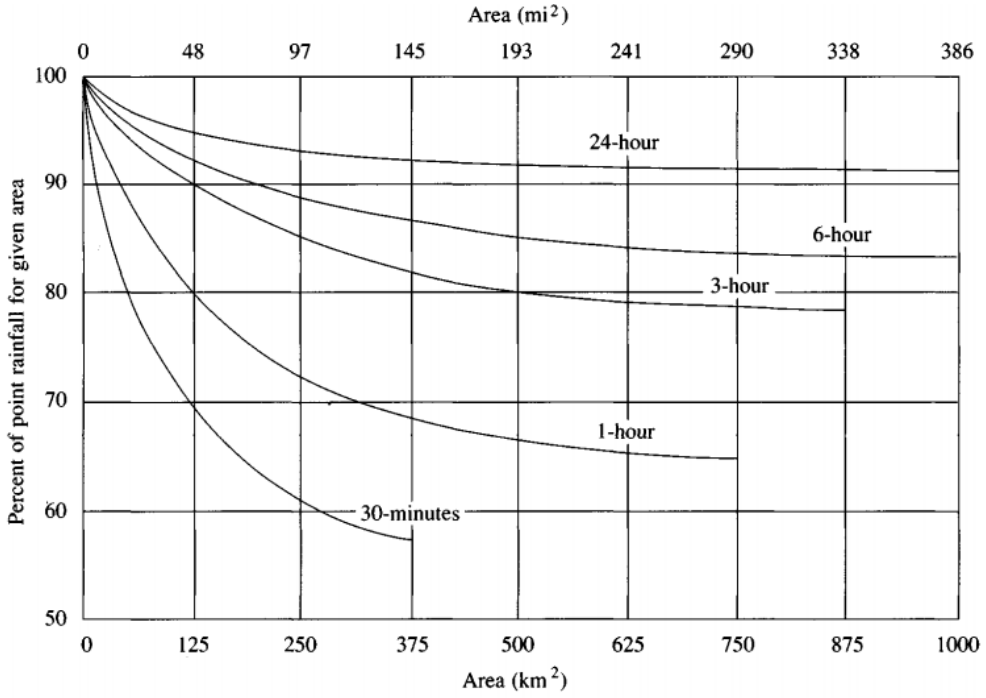

Figure 5 Depth-Area curves for reducing point rainfall to obtain areal average values (Source: *Chow, et al.,* (1988)).

1.2 Objectives

Despite the recent advances in the field of radar-rainfall monitoring and estimation, the utilization of radar QPE products for extreme precipitation analysis and the derivation of design frequency estimates are not yet capitalized on. The main limitation for the use of radar datasets for precipitation frequency estimation is their limited span of historically available data. However, with the increasing availability of radar datasets that have long archival records (>10 years), the use of radar-based information for PFE analysis is becoming more feasible. The overall objective of the current study evaluates the utility of radar-rainfall products for the derivation of precipitation frequency estimates (PFE).

The current study uses a radar-rainfall product provided by the National Weather Service (NWS) and examines two versions of such product, a real-time version (known as Stage IV),

and post-real time version with better quality control (known as RFC-MPE). The study starts by an evaluation of these two versions and selects one of them for further PFE analysis. The Following is a list of research questions addressed throughout the chapters of this thesis study:

1. What are the data quality issues associated with the use of a real-time multisensor radar-based quantitative precipitation product?

2. What are the impacts of data artifacts in radar-rainfall product on the derivation of extreme precipitation amounts?

3. How can radar-based information be used for estimating precipitation frequencies? What statistical distributions and parameter estimation methods that can be applied? What are the uncertainties associated with the estimates obtained from each method?

4. How close are radar-based PFE results to those obtained from gauge-based analysis?

5. Does a regional estimation approach, as opposed to an at-site approach, result in improved precipitation frequency estimates?

1.3 Research Plan

This study follows a systematic research plan to derive the precipitation frequencies using radar-based QPE. The procedures carried out in this study are listed as follows:

1. Assessment of the real-time Stage IV and longer-latency RFC-MPE products and choosing the appropriate product to conduct the statistical analysis required for frequency estimation.

2. Extracting extreme series representing heavy events from the radar datasets.

3. Choosing a suitable distribution for extreme rainfall analysis and estimating the parameters of this distribution using probability weighted moment approach.

4. Estimation of confidence intervals (uncertainty bounds) for the precipitation frequencies using two different bootstrap techniques.

5. Comparing the radar-based frequency estimates against those obtained from rainfall gauges.

1.4 Thesis Outline

The structure of the thesis is designed to include 7 chapters. Chapter 1 introduced the overall motivation, background, objectives, and research questions, with a brief outline of the research methodology. Chapter 2 provides an overview of rainfall monitoring and estimation techniques using weather radar and the different types of multi-sensor quantitative precipitation algorithms. Chapter 3 reviews previous studies on precipitation frequency estimates using gauge and radar-based datasets. Chapter 4 provides the assessment results of the real-time and the longer-latency radar products utilized in the current study. Chapter 5 explains the frequency analysis methodology used for deriving the precipitation frequencies. The characteristics of the extreme rainfall climatology and the results of the frequency estimates with different approaches are presented in Chapter 6. Finally, Chapter 7 summarizes the thesis, discusses its conclusions and contributions, and suggests some directions for future research that can provide next steps towards the enhancement of the radar-based QPE applications for precipitation frequency estimation.

Chapter 2 Overview of Weather Radar-Rainfall Monitoring and Estimation

2.1 Weather Radar

Weather Radars are very effective tools in detecting the precipitation and they have been used since the 1940's by the forecasters to examine the storms with more precisions. An ideal radar meteorologist should be an electrical engineer, a mathematician, a computer scientist, a meteorologist, a cloud physicist, and hopefully a hydrologist in one person to make best use of the radar system and to know the principles in order to be aware of limitations and to locate errors and uncertainties. The basic idea behind weather radars is very simple; electromagnetic waves are transmitted into the atmosphere, and after hitting any object in the atmosphere such as precipitation particles, hail stones, cloud droplets, birds, insects, or even the ground, the back scattered-waves are received by the radar as echo powers. The returned energy can be then recorded and analyzed through computers to display different products.

The basic components of the weather radar are shown in Figure 6 as described by *Meischner,* (2004). The modern weather radar consists mainly of five main subsystems: transmitter, receiver, antenna control, signal processor, control, and communication processor. First the transmitter generates microwave pulses, which are guided to the duplexer. The duplexer is a nonlinear microwave circuit which routes the signal to the antenna and the backscattered received signals to the receiver, which amplifies them and removes the microwave carrier frequency. The output signal then is digitized and processed by the signal processor, which also controls the timing of the transmitter, the transmitted pulse width, and the pulse repetition frequency (PRF). The output data are then sent to the radar product generator to convert these data into operational products.

There are no fundamental bounds on radar frequency. Any device that detects and locates a target by radiating electromagnetic energy and utilizes the echo scattered from a target can be classed as radar, no matter what its frequency. Radars have been operated at frequencies from a few megahertz to the ultraviolet region of the spectrum as shown in Table 1. The basic principles are the same at any frequency, but the practical implementation is widely different. In practice, most radars operate at microwave frequencies, but there are notable exceptions (*Skolnik,* 1970). Radar engineers use letter designations to denote the general frequency band at which radar operates. The letter bands listed in Table 1 are universally used in radar. They have been officially accepted as a standard by the Institute of Electrical and Electronics Engineers (IEEE) and have been recognized by the U.S. Department of Defense.

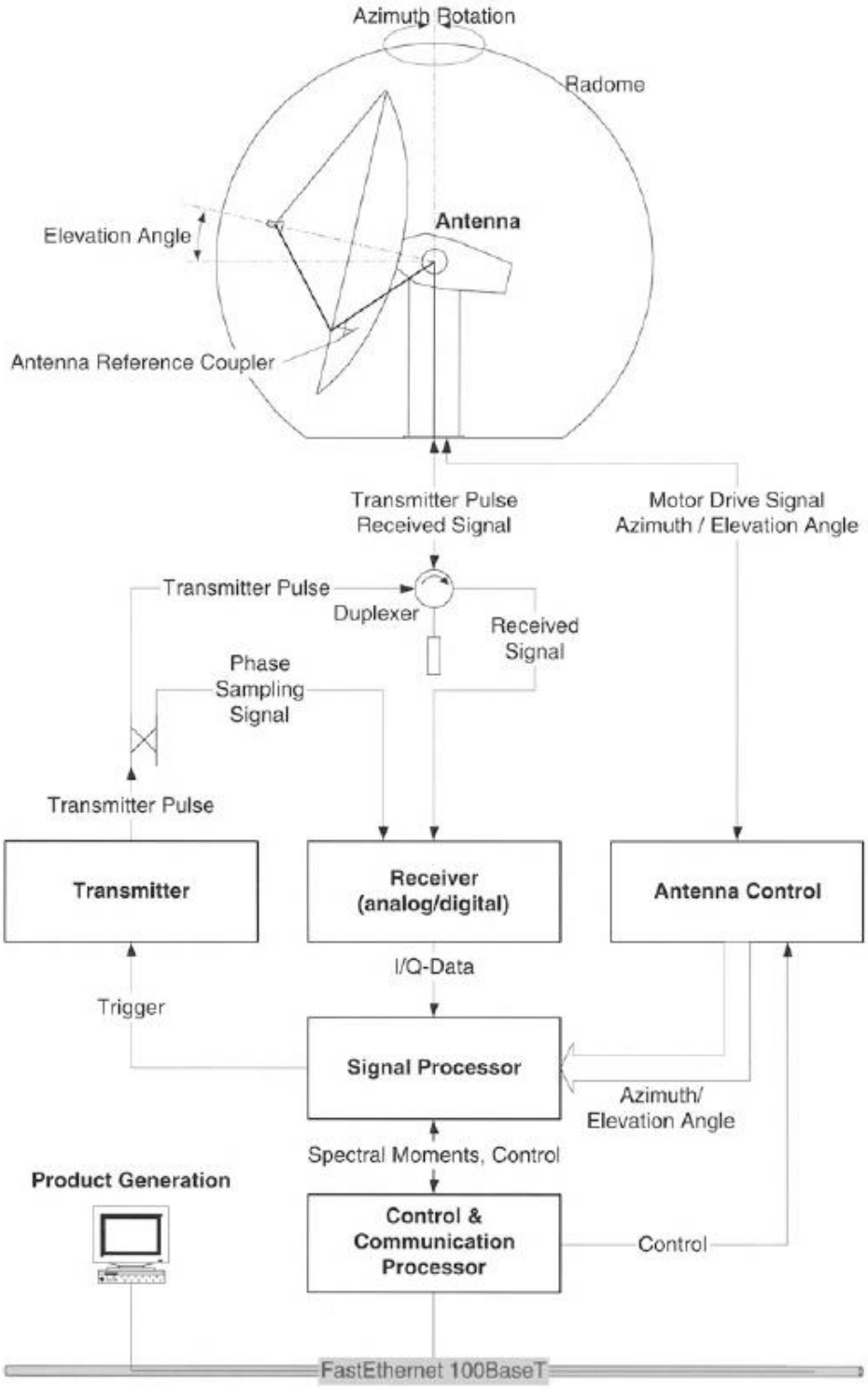

Figure 6 Basic Components of a Doppler Radar System (Source: *Meischner,* (2004)).

Table 1 Standard radar-frequency letter-band nomenclature.

Band Designation	Nominal Frequency Range	
HF	3 MHz	30 MHz
VHF	30 MHz	300 MHz
UHF	300 MHz	1000 MHz
L	1000 MHz	2000 MHz
S	2000 MHz	4000 MHz
C	4000 MHz	8000 MHz
X	8000 MHz	12000 MHz
K_u	12 GHz	18 GHz
K	18 GHz	27 GHz
K_a	27 GHz	40 GHz
V	40 GHz	75 GHz
W	75 GHz	110 GHz
mm	110 GHz	300 GHz

A Doppler radar is specialized radar that makes use of the Doppler Effect to control and measure the phases of the transmitted and received signals. The Doppler Effect or Doppler Shift is the apparent change in frequency or pitch of a wave when a sound source moves either toward or away from the listener, or when the listener moves either toward or away from the sound source. This principle, discovered by the German physicist Christian Doppler, applies to all wave motion. The measured phase shift of the received backscattered signal in the Doppler Radars, compared to the phase of the transmitted signal, allows the estimation of the mean radial or the Doppler velocity of the particles (*Chen, et al.,* 2006; *Ausherman, et al.,* 1984).

All Doppler radars rotate horizontally as they transmit energy. Not only do radars rotate horizontally, but they also can tilt vertically. In fact, depending on the volume coverage pattern (VCP), a radar may scan horizontally 360° at anywhere from four to fourteen different vertical angles. The standard elevation angle is 0.5° above the horizontal, which is referred to as a base angle. This elevation gives the name “base X” to many radar products,

where X is one of many products, such as reflectivity or velocity. When radar finishes scanning in 360 degrees at one elevation angle, it tilts up to the next elevation angle and scans 360 degrees at that angle, too. It does this until it has scanned at all elevation angles.

One of the radar products is the base reflectivity, which describes the amount of power returned back to the radar after reflecting off particles in the atmosphere. The meteorological radar equation as given by *Doviak & Zrnić,* (1993) is

$$P_r(r) = \frac{\pi^3 P_T G^2 G_R \theta^2 c\tau |K|^2 Z}{2^{10} \ln(2) \lambda^2 r^2 L_{atm}^2 L_{MF}} \tag{2.1}$$

where P_T is the transmitted peak power at the antenna, G denotes the total antenna gain, G_R is the total receiver gain, considering also path losses between antena and electronics, θ denotes the antenna 3 decibel (dB) beam width, c is the speed of light, τ is the pulse length, $|K|^2$ is a constant factor that depends on type of precipitation and it is equal to 0.93 for rain and 0.2 for ice and snow, Z is the reflectivity, λ measures the wavelength of transmitted radiation, L_{atm} is the atmospheric attenuation between antenna and target in one way, and L_{MF} is the matched filter losses. This equation is valid under the assumption that the beam formed by the antenna has a circularly symmetric shape and the resolution volume is completely filled with precipitation.

Since $c = \lambda f$, where f is frequency, equation 2.1 can be rearranged to calculate the reflectivity Z, with terms grouped according to the different radar subsystems:

$$Z = \frac{2^{10} \ln(2) c}{\pi^3 |K|^2} \cdot \frac{1}{f^2 P_T \tau} \cdot \frac{1}{G^2 \theta^2} \frac{L_{MF}}{G_R} \cdot r^2 \cdot L_{atm}^2 \cdot P_R \tag{2.2}$$

For a stable and a well calibrated radar system, all the above constant terms can be combined into one constant term C_R and and the reflectivity measured can be written as:

$$Z = C_R . r^2 . L_{atm}^2 . P_R \quad (2.3)$$

It is worth noting that the Z equation assumes Rayleigh scattering, which occurs with targets whose diameter is much smaller than the wavelength of the transmitted electromagnetic radiation (*Battan,* 1973). The WSR-88D uses a wavelength of approximately 10.7 cm, and almost all raindrops have diameters of 7 mm or less.

The reflectivity is measured in mm^6/m^3 to indicate the scattering cross section of all hydrometeors within one cubic meter (*Meischner,* 2004). Since the mm^6/m^3 units result in large dynamic range of observed reflectivities, it is more reasonable to use the logarithmic units (Decibels dBZ)

$$dBZ = 10\log[Z/(mm^6/m^3)] \quad (2.4)$$

The reflectivity and the rainfall rate are both related to the raindrop diameter (D), the reflectivity (Z) is defined as the 6^{th} moment of the diameter of the raindrop:

$$Z = \int_0^\infty N(D) D^6 dD \quad (2.5)$$

where N(D) denotes the raindrop size distribution (DSD) in a unit volume (m^3)and measured in ($mm^{-1}m^{-3}$), while (D) is the raindrop diameter in (mm). The rainfall intensity (mm/hr) is approximately propotional to the 3.67^{th} moment of the raindrop size and it is given by the following relation:

$$R = 6\pi 10^{-3} \int_0^{\infty} N(D) D^3 \nu_t(D) dD \qquad (2.6)$$

where $\nu_t(D)$ is the terminal velocity of a raindrop of diameter D, which is expressed as a power law in the form of

$$\nu_t(D) = 3.80 D^{0.67} \qquad (2.7)$$

It is obvious from the above equations (2.5 & 2.6) that both reflectivity (Z) and rain rate (R), are dependent on the raindrop diameter and hence; the drop size distribution (DSD) plays an important rule in estimating the rainfall uisng the radar refelctivity (*Seo, et al.,* 2010). According to (*Battan,* 1973), there exist an empirical evidence that the Z-R relationship follows a power form $Z=aR^b$, where a and b are empirical coefficients that depend on the season, location and type of precipitation. Based on these factors, different results were obtained by the scientists for the parameters of the Z-R relations. The different equations are summarized by *Battan,* (1973) in tables (pp.90-92) according to the geograpgical locations and the type of rainfall.

The linearity between the logarithmic (Z-R) relation was also observed between the attenuataion (A), i.e., the weakening of a radar beam as it moves downstream due to some of the energy being lost to scattering and absorption of the radar waves, and rainrate (R) by *Atlas & Ulbrich,* (1977) who studied the linear relationship between microwave attenuation (A) and rainfall rate (R) and they derived regression eqautions in the power form $A=aR^b$ for different radar wavelengths. Unlike the Z-R relations that are dependent on the DSD, they concluded that the linearity for (A-R) relation is independent on DSD. This less sensitivity to the DSD motivated *Ryzhkov, et al.,* (2014) to utilize the specific attenuation for deriving

rainfall estimates and they obtained X- and S- band estimates of rainfall in acceptable agreement with the gauges. *Watson, et al.,* (1999) investigated the capability of linking the rainfall rate (R) with both; reflectivity (Z) and attenuation (A), in the form of $R=aZ^bA^c$ and they also showed that this relation is relatively insensitive to the drop size distribution (DSD) and temperature over a wide range of rain rates.

2.2 Uncertainty in Radar Estimation

Quantitative precipitation estimates often have significant uncertainty. The error in radar measurements can be classified into three main sources of errors:

1. Measurement errors of the weather radar including all the data processing.
2. Errors inherent in the measurement method such as the scan strategy.
3. Errors caused by different meteorological conditions such as drop size distributions, attenuation, ground clutter, enhanced reflectivity in the melting (bright band), anomalous propagation, and incomplete beam filling.

These errors have to be well understood and quantified for the proper calibration and adjustment required for the use of precipitation estimates in hydrological and weather prediction models. The various sources of uncertainty have been widely explained in literature (e.g., *Anagnostou, et al.,* (1999), *Borga,* (2002), *Seo, et al.,* (2010), *Villarini, et al.,* (2010a, 2010b), *Bodine, et al.,* (2011)). Three sources of errors; ground clutter, vertical profile reflectivity, and bright band effect, are briefly explained in this section.

One of sources of contaminating the radar estimates is the ground clutter, which indicates those received signals which hit a fixed targets like mountains, buildings, or just ground. The main physical difference between ground clutter targets and meteorological objects is that they do not move and that they exist independently of any weather event (*Meischner,* 2004). To avoid the ground clutter and the beam blockage by natural or man- made obstructions, the lowest-elevation angle in the scanning strategy of a ground-based radar on a flat terrain is usually set above zero (approximately 0.5- for the Weather Surveillance Radar - 1988 Doppler (WSR-88D) version in the United States). Attenuation is the weakening in the microwave radiation when propagating through a medium like the atmosphere. The attenuation is mainly affected by the radar frequency and the gases in the atmosphere, mainly caused by oxygen and water vapor. Bright band takes place in the mid and higher latitudes where most of the formation of the precipitation occurs through the ice phase. One example of influence of ground clutter contamination on radar reflectivity is presented in Figure 7 in the study performed by *Hubbert, et al.,* (2009). Figure 7 shows the scan of reflectivity from the Denver Next Generation Weather Radar (NEXRAD) at the Denver, Colorado, Front Range Airport (KFTG) at 0.5˚ plan position indicator (PPI) clear-air surveillance. These experimental data were gathered at 2123 UTC 13 October 2006 and the large reflectivities on the left are caused by the Rocky Mountains.

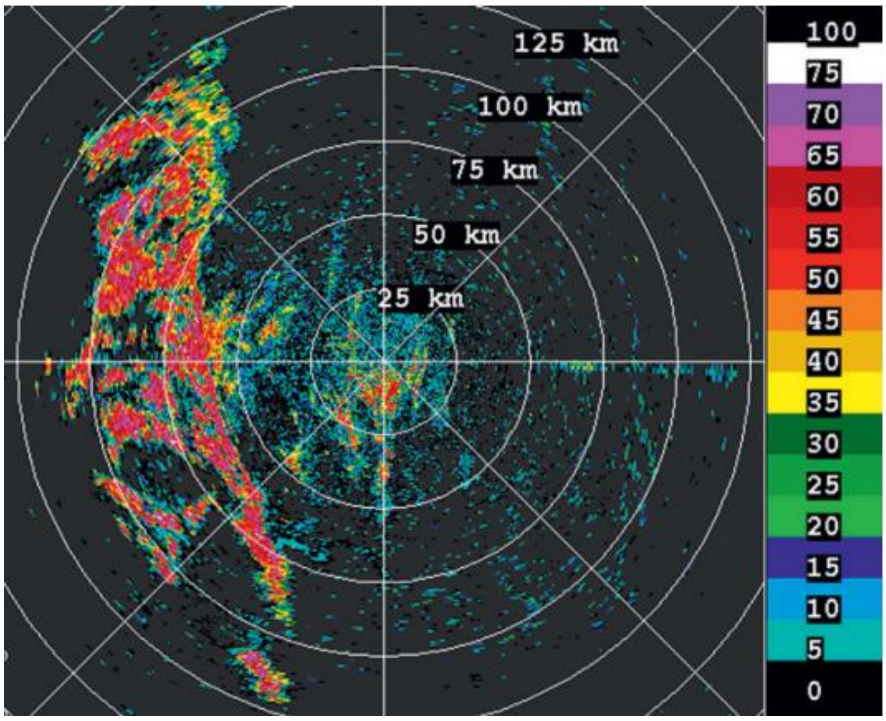

Figure 7 A KFTG clear-air PPI surveillance reflectivity scan showing ground clutter. The data were gathered at 2123 UTC 13 Oct 2006. The large reflectivities seen on the left are from the Rocky Mountains (Source: *Hubbert, et al.,* (2009).

The precipitation formation process, mainly coalescence and coagulation of liquid and frozen cloud particles and the fall of existing precipitation particles down through cloud regions, cause a significant increase of precipitation intensity from aloft down to earth. Because, with increasing distance from the radar, the measurements are taken at increased altitudes, this may cause errors in precipitation estimates at ground that significantly exceed the instrumental measurement errors of a well-calibrated radar system. This increase in the reflectivity due to the difference in the altitude is known as the vertical profile of reflectivity (VPR).

Another source of error in the radar estimates is introduced by the melting layer of precipitation on the radar observations or what is known as bright band effect which causes significant enhancement in the radar reflectivity (*Fabry & Zawadzki,* 1995). The primary

reason behind the bright band effect is the rapid increase in the dielectric constant of the hydrometeors at the top of the melting layer followed by an increase of the fall velocities of melting snowflakes toward the end of the melting process (*Battan,* 1973). Above the freezing level in stratiform clouds, the radar observes ice particles, which have much smaller effective backscattering cross section than raindrops of comparable size. As the ice particles fall past the freezing level, they begin to melt and, just below the freezing level before the ice melts completely, the radar observes water-coated ice particles, which produce significantly larger reflectivity than the resulting raindrops. The vertical extent of this layer of enhanced reflectivity, or the bright band, is quite small, typically less than 500 m (*Seo, et al.,* 2010). Figure 8 shows a schematic diagram for the VPR with illustration of the bright band layer that lies between two heights; the bottom height (h_b) and the top height (h_a), with maximum reflectivity due to bright band effect at height ($h_{m'}$).

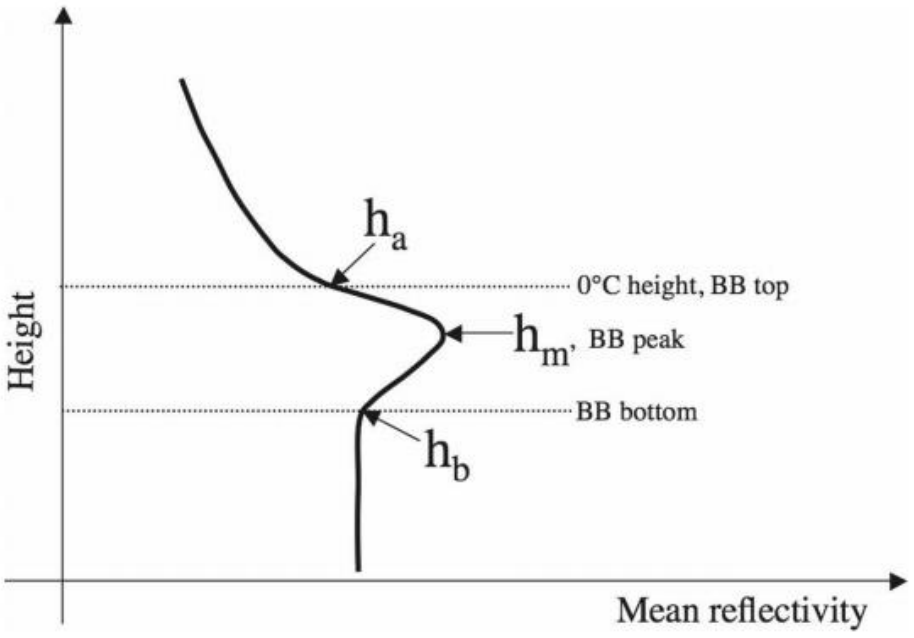

Figure 8 A schematic illustration of the conceptual model of the brightband layer in a Vertical Profile of Reflectivity (VPR) (Source: *Zhang, et al.,* (2008)).

2.3 Weather Surveillance Radar, 1988 Doppler (WSR-88D)

NEXRAD (Next-Generation Radar) is a network of about 160 high-resolution S-band Doppler weather radars operated by the National Weather Service (NWS), an agency of the National Oceanic and Atmospheric Administration (NOAA) within the United States Department of Commerce, the Federal Aviation Administration (FAA) within the Department of Transportation, and the U.S. Air Force within the Department of Defense. Its technical name is WSR-88D, which stands for Weather Surveillance Radar, 1988, Doppler.

Figure 9 shows the distribution of the radars sites over the continental United States with the coverage range of each radar. The NEXRAD system of WSR-88D radars provides high-quality, high-resolution precipitation data for the United States that meet a wide range of hydro-meteorological applications (*Smith, et al.,* 1996). The radars measure volumetric reflectivity of hydrometeors aloft rather than rainfall near the ground, hence, radar rainfall estimation is inherently subject to various sources of error (*Seo, et al.,* 2010). NEXRAD WSR-88D systems generate three basic meteorological radar quantities: reflectivity, mean radial velocity, and spectrum width (a measure of the variability of radial velocities in the resolution volume). From these base data quantities, fully automated scientific algorithms are applied to generate numerous meteorological analysis products (*Klazura & Imy,* 1993). Figure 10 shows the use rainfall estimates from radar in different quantitative hydrologic applications by the Weather Forecast Office (WFOs), the River Forecast Centers (RFCs), and the National Centers for Environmental Prediction (NCEP).

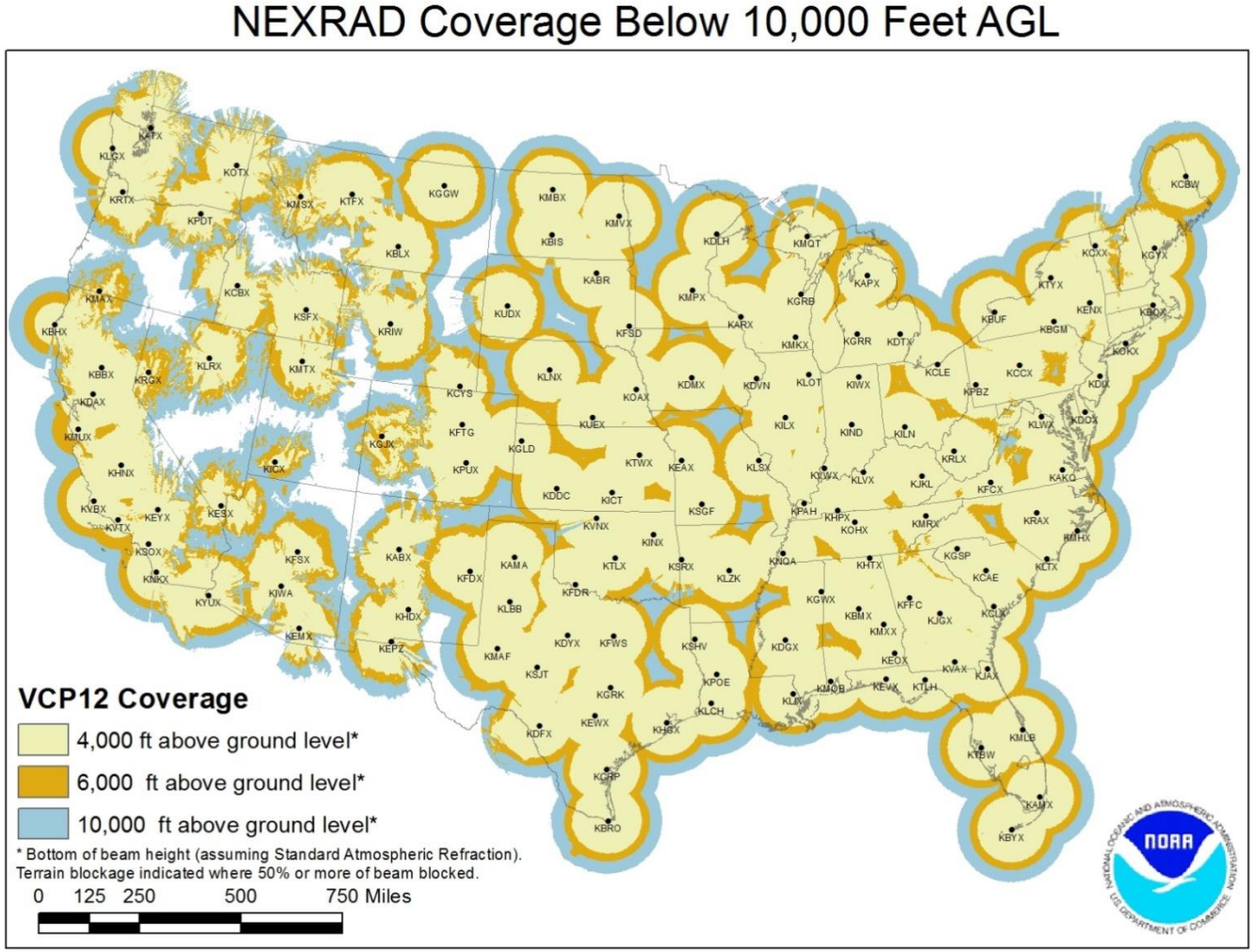

Figure 9 NEXRAD continental US sites (Source: *http://www.roc.noaa.gov/*).

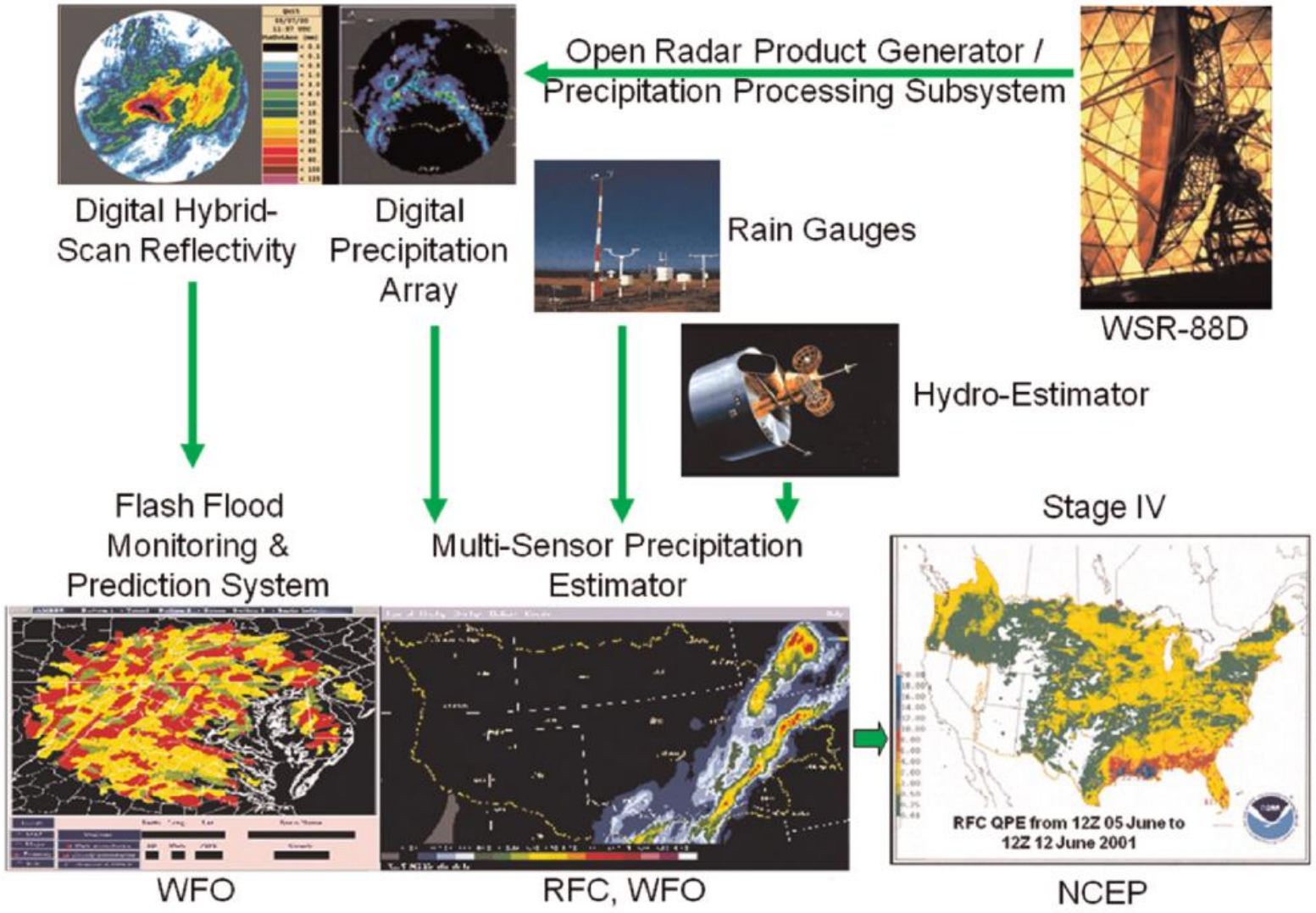

Figure 10 Use of radar rainfall data for quantitative hydrologic applications in NWS (Source: *Seo, et al.,* (2010)).

The NWS utilizes several different Z-R algorithms, depending on the rainfall characteristics, to estimate rainfall through the use of the network of NEXRAD radars (*Marshall & Palmer,* 1948). The default Z-R relationship of $Z = 300R^{1.4}$ was the primary algorithm used throughout the continental U.S. but the radar-based estimates of precipitation that used this formula suffered from over or under-estimation of rainfall. The NWS Radar Operational Center (ROC) currently adopted different Z-R relationships depending on the type of rain rates instead of using standard Z-R formula as listed in Table 2.

Table 2 List of Z-R relationships adopted by NWS/ROC for different precipitation events.

Z-R Relationship	Recommended Use	2nd Recommended Use
Palmer-Marshall $Z=200R^{1.6}$	General stratiform precipitation	
East-Cool Stratiform $Z=130R^{2.0}$	Winter stratiform precipitation- east of continental divide	Orographic Rain-East
West-Cool Stratiform $Z=75R^{2.0}$	Winter stratiform precipitation- west of continental divide	Orographic Rain-West
WSR-88 Convective $Z=300R^{1.4}$	Summer deep convection	Other non-tropical convection
Rosenfeld Tropical $Z=250R^{1.2}$	Tropical convective systems	

All the NEXRAD precipitation products are available on a 4-km resolution polar-stereographic grid (HRAP). The Hydrologic Rainfall Analysis Project (HRAP) grid, as defined by *Greene & Hudlow,* (1982), is used to define the location of each average precipitation value in a NEXRAD Stage III data set. The HRAP projection is a quasi-rectangular grid whose cell size is nominally 4 km on a side but ranges from about 3.5 km in southern contiguous U.S. latitudes to about 4.5 km in northern contiguous U.S. latitudes. This HRAP grid covers the 48 conterminous states.

2.4 Multi-Sensor Quantitative Precipitation Estimates (MQPE)

2.4.1 Remote Sensing Platforms for MQPE Analysis

Quantitative Precipitation Estimates (QPEs) are approximations for the rainfall falling over a certain location using a single sensor or multi-sensors. Rain gauges and disdrometers are examples for sensors that provide direct in situ measurements of rainfall properties at relatively high temporal resolutions (*Habib, et al.,* 2010). While rain gauges measure rainfall accumulations and intensities, disdrometers provide data on the drop size distribution that describes the rainfall microphysical structure. Although rain gauges are subjected to various sources of errors, e.g., wind effect and evaporation losses, gauge-based estimates of precipitation are considered to be the closest to ground truth, at the point-scale. However, owing to extremely large space-time variability of rainfall, point observations based on in situ sensors such as rain gauges may provide only very limited information about the spatiotemporal distribution of rainfall, depending on the spatiotemporal scale at which the analysis is desired.

The evolution of weather Radars and the observation of atmosphere by satellite instrumentation have changed the above picture dramatically by providing spatially continuous estimates of rainfall at small temporal sampling intervals, thereby filling the observation gap of rain gauges in space and time. Radar does not measure surface rainfall but the backscattered power from the hydrometeors aloft and the received power is then converted into rainfall estimates with inherent errors. To improve the quality of radar-based rainfall estimates, it is therefore necessary to understand, assess, reduce, quantify, and account for these errors. Radar data are well suited to real-time flood forecasting

applications, but they have also been used for assessing water resources and providing a basis for engineering design. This is particularly true in remote areas where rain-gauges are sparse, and satellite techniques for estimating rainfall are too inaccurate (*Meischner,* 2004).

Satellites infer the rate of precipitation from the characteristics of clouds in the infrared and visible satellite images. Satellites offer excellent coverage over mountainous areas where beam blockage restricts radar observations, and over ocean regions that are out of the range of land-based radar installations. Satellite remote sensing techniques take an important role in filling data gaps and understanding of rainfall properties and their variation. On the other hand, satellites do not observe rainfall; they only can observe the characteristics of the clouds that are producing it and therefore precipitation can only be inferred in a less physically direct fashion than in either the rain gauge or radar approaches, and this affects significantly the accuracy of the satellite-based approach (*Kuligowski,* 1997). One example of the satellite, designed to monitor and study tropical rainfall, is the U.S.-Japan Tropical Rainfall Measuring Mission (TRMM), launched in November 1997, to provide rainfall measurements over vast under-sampled oceans and data sparse continents in the tropics and sub tropics (40˚N-40˚S) (*Liu,* 2015). Figure 11 shows one example for the utility of the TRMM satellite to estimate the seasonal variation in the precipitation estimates using the TRMM research-grade product (3B42) over the entire domain of the dataset (50˚N-50˚S). Figure 12 displays the Multi-Satellite Precipitation Analysis (MPA) rainfall totals, measurements based on TRMM satellite and other satellites, tracking hurricane Katrina for the period August 23 to 31, 2005.

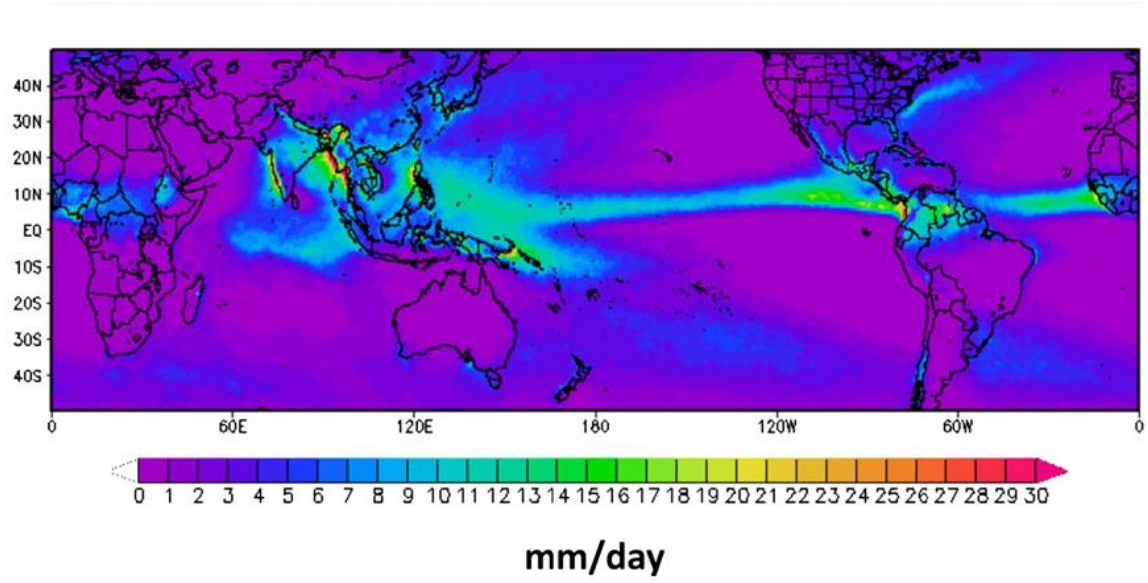

Figure 11 Mean seasonal precipitation estimates averaged during summer (June-July-August) from 2002 to 2012 from TRMM (3B42) research-grade product (Source: *Liu,* (2015)).

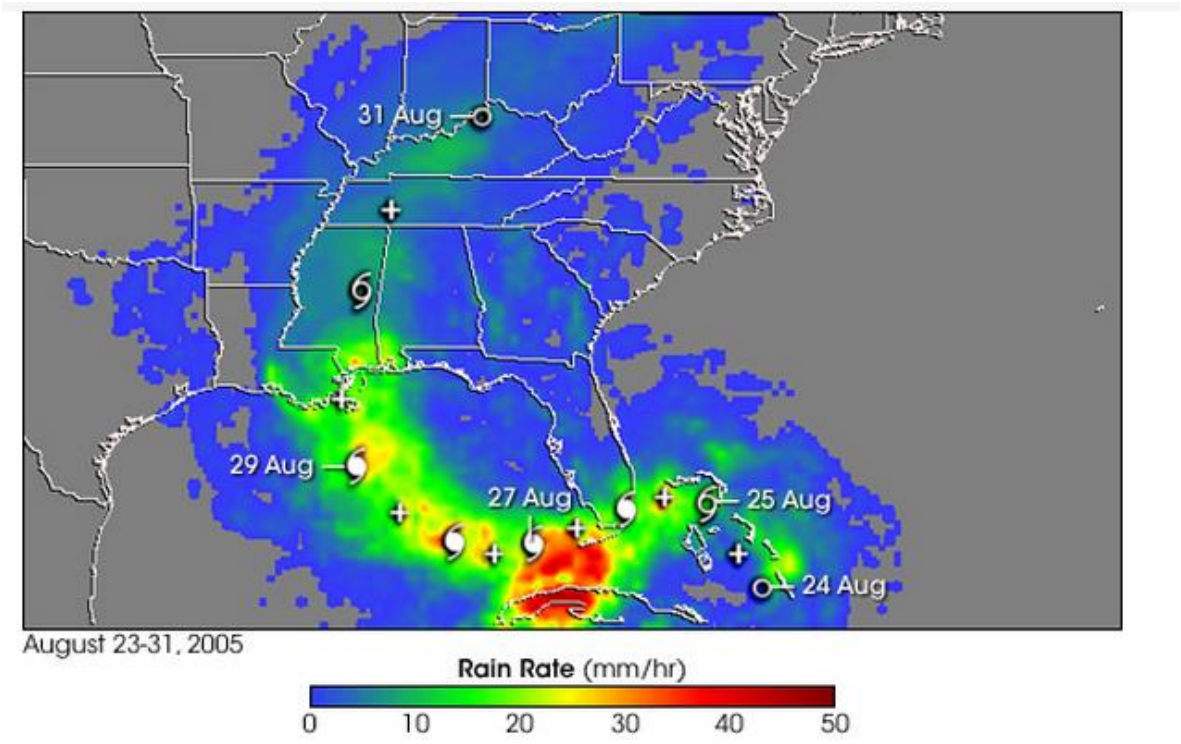

Figure 12 Multi-satellite Precipitation Analysis (MPA) rainfall totals due to the passage of Katrina for the period August 23 to 31, 2005 (Source: *http://www.earthobservatory.nasa.gov*).

Many studies have been conducted in order to quantitatively understand the utility of the satellite data sources and algorithms in estimating the precipitation amounts. *Xie & Arkin,* (1996) developed an algorithm to construct global gridded fields of monthly precipitation by merging estimates from five sources of information with different characteristics, including gauge-based monthly analyses from the Global Precipitation Climatology Centre, three types of satellite estimates and predictions produced by the operational forecast model of the European centre for Medium-Range Weather Forecasts. *Scofield & Kuligowski,* (2003) presented an overview of the satellite QPE algorithms with focus on algorithms suited for heavy precipitation required for the flash flood forecasting. *Ebert, et al.,* (2007) compared the accuracy of the daily rainfall estimates from satellite observations with the numerical weather prediction models. *Habib, et al.,* (2009) evaluated the 3-hourly 0.25˚x0.25˚ satellite-based rainfall estimates produced by the Tropical Rainfall Measuring Mission (TRMM) Multi-satellite Precipitation Analysis (TMPA) during six tropical-related heavy rainfall events over Louisiana, USA, using rain gauges and radar observations as ground reference datasets. The TMPA estimates shows reasonable level of rainfall detection especially when light rainfall rates are excluded and significant improvement in the overall and conditional bias and in correlation coefficients with slight deterioration in the probability of detecting rainfall occurrences.

Recently, the potential of using radio links from cellular communication networks to estimate rainfall was investigated. It has been proposed as a cost effective means for regional rainfall monitoring complementing existing monitoring systems such as rain gauges and weather radars. Telecommunication engineers have studied the physical relation between radio wave attenuation and rainfall intensity since the 1960s and the rain that is noise in

telecommunication engineering can be considered as signal in geophysical sciences. *Messer, et al.,* (2006) demonstrated the feasibility of environmental monitoring with wireless communication networks by estimating the surface rainfall using standard data collected from cellular network and show its improved accuracy compared with radar-based estimates. *Leijnse, et al.,* (2007) compared the rainfall intensity estimated from the signal attenuation from two cellular communication links in Netherlands with the rainfall intensities measured by a nearby rain gauge and a composite of two C band weather radars. *Chwala, et al.,* (2012) analyzed four months of continuous received signal level data from five commercial backhaul links in the alpine and pre-alpine region of Southern Germany to derive the rainfall rate and compare the results with rain gauge as well as weather radars. The microwave links have the advantage of operating much closer to the ground (tens of meters) compared to the radar (hundreds of meters to kilometers); however, there still a great bias in the rainfall estimates by the microwave links due to the uncertainty in the reference signal level as can be deduced from Figure 13, in which the bottom map compares fairly with the maps obtained using radar and gauges, while the top one deviates significantly.

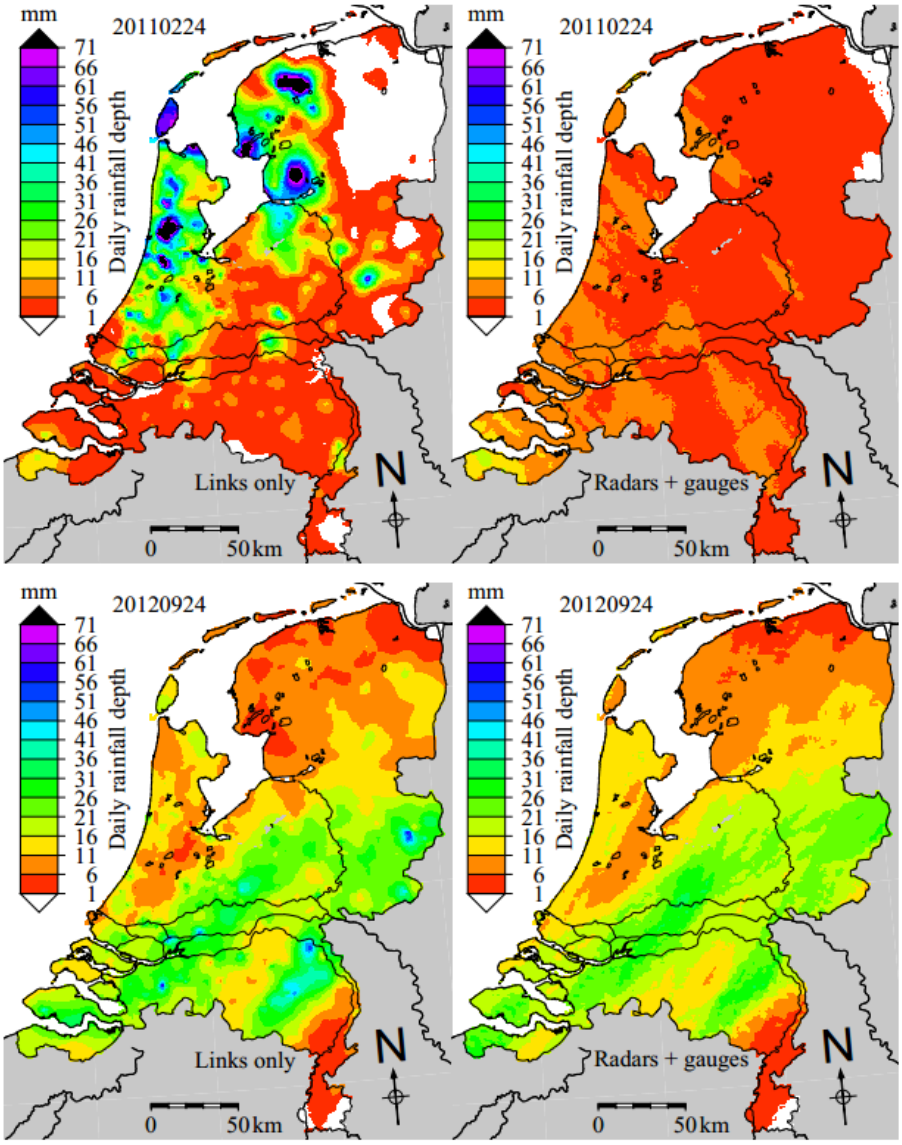

Figure 13 Daily Rainfall maps from cellular communication networks compared with merged radar-gauges estimates (Source: *Overeem, et al.,* (2014)).

Although rain gauges are subjected to various sources of errors, the gauge-based estimates of precipitation are considered to be the ground truth for hydrologic forecasting by which all other measurements are calibrated. The optimum combination of information from multiple sensors is known as Multi-sensor Quantitative Precipitation Estimates or (MQPEs), for example, Radar precipitation estimates can be grossly inaccurate, so radar-based precipitation values are calibrated with the routinely available hourly surface gages. The combined

product provides the spatial resolution of radar with the increased accuracy of surface gage networks. The merging of the available rainfall rates from gauges, radar, satellites or link measurements may provide the opportunity to obtain improved spatio-temporal distributions of rainfall for all kinds of hydrological analyses. It is worth noting that MPEs are still vulnerable to some inaccuracies due to different sources of uncertainties in each sensor that are not completely captured in the bias corrections and quality control processing algorithms.

2.4.2 Algorithms for Radar-Based Quantitative Precipitation Estimates

For improving the estimation of precipitation, the rain gauges observations are merged with radar estimates using precipitation estimation algorithms. These algorithms help reduce the uncertainties accompanied with the radar measurements and produce Multisensor Quantitative Precipitation Estimates (MQPEs) that can be used for operational purposes. MQPEs are created by the NWS River Forecast Centers (RFCs) at near–real time during river and flash flood forecasting operations. The primary bases of MQPEs are precipitation gauge reports and observations of WSR-88 Doppler radars (*Seo,* 1998). The NWS precipitation estimation algorithms can be divided into radar-only and multisensor components (the latter include a gauge-only component). Stage I radar only products are real time estimates of liquid only precipitation at ground level derived from radar reflectivities, while in the legacy multisensor algorithms, stage I estimates underwent bias correction to produce stage II estimates which were quality assured and mosaicked on a regional basis to come up with stage III product. These legacy multisensor algorithms were replaced by new multisensor precipitation estimator (MPE) algorithms in which stage II and III algorithms were updated to incorporate the new algorithms for mean-field and local bias correction in

the products as well as provisions for creating gauge-only and gauge-radar merged products (*Zhang, et al.,* 2011).

The NWS precipitation estimation algorithms can be divided into radar-only and multisensor components (the latter include a gauge-only component). Stage I radar only products are real time estimates of liquid only precipitation at ground level derived from radar reflectivities. The algorithm that produces rainfall estimates, called the Precipitation Processing System (PPS), is actually a set of subalgorithms that execute in series (*Fulton, et al.,* 1998). The Precipitation Processing System (PPS) algorithm computes rainfall estimates from reflectivity measurements collected on a polar grid centered on the radar with a fixed spatial resolution of 2.0 km in range by 1.0 degree in azimuth. The PPS algorithm transforms the radar-centered polar grid onto a polar stereographic projection (HRAP) projection and produces an Hourly Digital Precipitation Array (called HDP or DPA) product which is a digital one-hour rainfall accumulation product (*Fulton,* 1998). A complete explanation for the derivation of how polar rainfall estimates are mapped to the HRAP grid within the PPS is discussed in (*Fulton,* 1998). In the legacy multisensor algorithms, stage I estimates underwent bias correction to produce stage II estimates which were quality assured and mosaicked on a regional basis to come up with stage III product. These legacy multisensor algorithms were replaced by new multisensor precipitation estimaor (MPE) algorithms in which stage II and III algorithms were updated to incorporate the new algorithms for mean-field and local bias correction in the products as well as provisions for creating gauge-only and gauge-radar merged products (*Zhang, et al.,* 2011). The MPE algorithm improves the quality control of the radar-rainfall estimates to produce multi sensor precipitation estimates

in real time for forecasters in support of the National Weather Service's warning and forcast missions.

In late 2001 the National Centers for Environmental Prediction (NCEP) began to routinely generate national multi-sensor analysis, the NCEP Stage IV based on the MPE algorithm and mosaicked from the regional multi-sensor 1h and 6h analyses produced by the 12 CONUS RFCs (*Lin & Mitchell ,* 2005). Stage IV MPE based product is the same as the product resulted from Stage III MPE algorithm but mosaicked into a national product at NCEP. Stage IV benefits from the manual quality control at the local RFCs and therefore it is better than the MPE-based Stage II, which has no manual quality control; however, Stage IV hourly real-time estimates do not catch the later manual corrections performed at each RFC.

Each NCEP stage IV precipitation analysis is initiated 35 min after the end of each hourly collection period and may be updated over a period of several hours with new data coming from the 12 U.S. regional centers. A first inflow of automatically generated precipitation data is available within a few hours after the accumulation time, while a second inflow of updated manually quality-controlled data becomes available later (with a delay of up to 12 h) (Lopez, 2011). Table 3 and Table 4 summarize the NWS precipitation estimation algorithms and the NWS/MPE algorithm radar-based multisensor precipitation products, respectively.

Table 3 NWS precipitation estimation algorithms.

Algorithm	**Radar Only Algorithm**	**Multisensor Algorithm**				
		Old (Legacy) Algorithms		**New (Current) Algorithms (MPE-MM-P1)***		
Stage	**Stage I**	**Stage II**	**Stage III**	**Stage II**	**Stage III**	**Stage IV**
Data Sources	Radar only	(Radar + Gauges)	(Radar + Gauges)	(Radar + Gauges)	(Radar + Gauges)	(Radar + Gauges)
Duration	1hr	1hr	1hr / 6hr	1hr	1hr / 6hr	1hr / 6hr
Corrections	--	Bias Correction	Bias Correction	Mean-field & Local Bias Correction	Mean-field & Local Bias Correction	Mean-field & Local Bias Correction
Quality Control (QC)	--	--	Manual QC	--	Manual QC	Manual QC for some hourly files
Regional Mosaic	--	--	RFC	National	RFC	National
Domain	RFC	RFC	RFC	CONUS	RFC	CONUS
Product	Digital Precipitation Arrays (DPAs)	Merged Radar and Gauges product	Merged Radar and Gauges product	Merged Radar and Gauges product	Regional Multi-Sensor Precipitation Analysis (RMPA) product	Mosaicked Regional Multi-Sensor Precipitation Analysis (RMPA) product
Remarks			Stage III is the product of stage II with Manual QC and Regional Mosaic	Prior to 2000 (Before Stage IV Mosaicked product) the names Stage II/Stage IV are used interchangeably	Stage III is the product of stage II with Manual QC and Regional Mosaic instead of National Mosaic	Stage IV is the product of stage III with National Mosaic

* MPE is Multisensor Precipitation Estimator algorithm used for most RFCs, MM is Mountain Mapper algorithm used for Western RFCs and P1 (Process 1) is the precipitation processing algorithm developed and implemented by ABRFC.

Table 4 NWS/MPE algorithm radar-based multisensor precipitation products.

Product	Description
Gauge-Only Analysis (GAGEONLY)	Interpolation of hourly rain gauge observations within the service area of the RFC with adjustment, if necessary, for spatially nonhomogeneous precipitation climatology
Radar-Only Mosaic (RMOSAIC)	Mosaicking the DPA products without any use of gauge observations.
Mean-Field Bias-Adjusted Radar Mosaic (BMOSAIC)	Correction for systematic, spatially uniform biases that may result from inappropriate Z-R relationships or radar calibration problems by applying a radar-specific, time-varying but spatially uniform multiplicative adjustment factor to each pixel within the effective coverage of the radar in the DPA product
Multisensor Analysis Based on BMOSAIC and Rain Gauge Data (MMOSAIC)	Local merging of the mean-field bias adjusted radar mosaic (BMOSAIC) and the point rain gauge observations
Local Bias-Adjusted Radar Field (LMOSAIC)	Correction of spatially non-uniform biases in the RMOSAIC field (e.g., biases owing to bright band and the vertical profile of reflectivity effects).
Multisensor Analysis Based on LMOSAIC and Rain Gauge Data (MLMOSAIC)	Merging the local bias-adjusted product (LMOSAIC) with the rain gauge observations.
RFC-Selected Product for Hydrologic Operations, NEXRAD MERGED (XMRG)	Selected product by RFC forecasters in real time by introducing manual corrections to generate the best multisensor product.

2.5 Hydrologic Applications of QPEs

The NEXRAD systems provide highly sensitive fine-resolution measurements of reflectivity, mean radial velocity and spectrum width data and generate up to 39 categories of analysis products derived from the base data every volume scan. NEXRAD (QPEs) have been used for a long time in different applications including weather prediction models, flash floods prediction and monitoring systems and it is expected that the use of radar will spread more widely and play an even more important role in quantitative rainfall estimation and related applications (*Seo, et al.,* 2010). Numerous studies have been performed to make use of the NEXRAD QPE in hydrological modeling and flash flood prediction systems (e.g. *Bedient, et al.,* (2000), *Neary, et al.,* (2004), *Zhang, et al.,* (2004), *Krajewsk, et al.,* (2007) and *Seo, et al.,* (2011)).

Bedient, et al., (2000) used NEXRAD to estimate the areal and spatial distribution of rainfall for three storms over the Brays Bayou watershed in Houston for hydrologic modeling purposes. *Neary, et al.,* (2004) used Stage III radar-derived precipitation data to investigate possible improvement of spatially lumped continuous hydrologic modeling in two subbasins of the Cumberland River basin in Middle Tennessee. *Zhang, et al.,* (2004) investigated how to effectively use the high spatial and temporal resolution provided by NEXRAD data to enhance river-forecasting capabilities using six years of continuously simulated hydrographs from an eight-subbasin model and compared to those from a single-basin (or lumped) model, both applied to the Blue River basin in Oklahoma. *Fang, et al.,* (2008) used 5-min NEXRAD rainfall data as input to hydrologic models to develop a flood warning system in the Brays Bayou Watershed of southwest Houston. Recently, NEXRAD radar rainfall products have been involved into Hydro-NEXRAD project, which allows ordering customized radar-

rainfall maps (products) for hydrologic studies based on NEXRAD data (for more details see *Krajewsk, et al.,* (2007) and *Seo, et al.,* (2011)).

The NCEP Stage IV merged Weather Surveillance Radar-1988 Doppler (WSR-88D) radar and surface rain gauge dataset is often considered to be the best long-term gridded dataset of precipitation observations covering the contiguous United States (*Smalley, et al.,* 2014).

NCEP Stage IV QPE data have been involoved in many hydrological and mteorological applications. *Lopez & Bauer,* (2007) studied the potential impact of assimilating NCEP stage-IV analyses of hourly accumulated surface precipitation over the U.S. mainland using the one- plus four-dimensional variational data assimilation (1D+4DVAR) method currently run in operations at ECMWF with rain-affected radiances from the Special Sensor Microwave Imager. *Kursinski & Mullen,* (2008) examined the spatiotemporal variability of precipitation events from hourly stage IV analyses for the eastern United States during the cool [December–February (DJF)] and the warm [June–August (JJA)] seasons for the four years of 2002–2005 and they estimated anisotropic statistics that should provide useful guidance for diagnosing and improving the spatiotemporal variance characteristics of precipitation for downscaling algorithms and numerical models of hydrometeorological prediction systems. *Zhang, et al.,* (2011) presented different methodologies for mitigating temporally inconsistent biases in National Weather Service (NWS) real-time (MQPEs) through rain gauge–based readjustments, and examines their effects on streamflow simulations. *Hou, et al.,* (2012) introduced a methodology to generate a new precipitation dataset by adjusting the Stage IV 6-hour accumulations based on available joint samples with the Climate Prediction Center (CPC) Unified Global Daily Gauge Analysis to take advantage of both datasets. They applied a simple linear regression model to the archived historical

Stage IV and the CPC datasets after the former is aggregated to the CPC grid and daily accumulation. *Zagrodnik & Jiang,* (2013) compared rainfall estimates from versions 6 (V6) and 7 (V7) of the Tropical Rainfall Measuring Mission (TRMM) precipitation radar (PR) 2A25 and Microwave Imager (TMI) 2A12 algorithms with the NEXRAD MQPEs stage-IV hourly rainfall product, they performed a detailed statistical analysis for the rainfall estimates and Stage IV estimates are used as reference for comparison between V6 and V7 estimates at low and high rainfall rates. *Smalley, et al.,* (2014) compared hourly Stage IV observations of precipitation occurrence to collocated observations from the 94-GHz CloudSat Cloud Profiling Radar, which provides excellent sensitivity to light and frozen precipitation and statistics from 4 yr of comparisons show that the skill of Stage IV for precipitation detection is found to decline rapidly when the near-surface air temperature falls below 0°C. As a result, agreement between Stage IV and CloudSat tends to be best in the southeast, where radar coverage is good and moderate-to-heavy liquid precipitation dominates.

Many studies have evaluated NEXRAD products and the issues associated with the estimates resulted from these produtcs. *Johnson, et al.,* (1999) compares the Mean areal precipitation values derived from NEXRAD stage III data with mean areal precipitation (MAP) values derived from a precipitation gauge network. *Young, et al.,* (2000) used the NEXRAD products to examine the issues involved in these products through an assessment of a 5.5-yr record of multisensor estimates from the Arkansas–Red Basin RFC and recommendations are made to help to facilitate routine verification of NEXRAD products. *Jayakrishnan, et al.,* (2004) performed an accuracy assessment of Stage III precipitation data from the WSR-88 network over the Texas-Gulf Basin for the period from 1995 to 1999 using 24-hr accumalations from 545 raingages. They observed significant variation in radar performance

over the years, however, a general improvement in the radar performance was detected which is consistent with the on-going developments in the WSR-88D data processing algorithms. They also recommended to evaluate the quality of WSR-88D precipitation data and make appropriate corrections to the Stage III data before their application in hydrologic studies. *Young & Brunsell,* (2008) presented an evaluation of NEXRAD Stage III and MPE precipitation estimates for the Missouri River Basin River Forecast Center (MBRFC) using daily gauge data from the National Weather Service cooperative network. NCEP Stage IV precipitation estimates are evaluated with Stage II estimates by *Boyles, et al.,* (2006) over the Carolinas for accuracy at several time scales using NWS Cooperative observer gages, which are not included in the MPE estimation process to verify the NCEP gridded radar estimates and to investigate the accuracy of NCEP precipitation estimates over areas with diverse topographic regimes. They concluded, according to several comparative statistics, that Stage II and Stage IV products compare well with the gages observations.

Boyles, et al., (2006) used their conclusions, that Stage II and Stage IV products compare well with the gages observations, to apply the gage-corrected radar estimates to develop a heavy precipitation mapping and alert system for storm water quality management at the State Climate Office of North Carolina and to to investigate mesoscale precipitation patterns in coastal, central and mountainous regions of North Carolina.

As mentioned above, many authors have used Stage IV in different precipitation analysis applications; however, few studies have been directed towards the assessment the Stage IV when used with the heavy precipitation as extreme events. Although Stage IV benefits from the automated quality control performed at each RFC, the precipitation estimates do not currently incorporate the manual quality control procedures performed later , not in real-time,

by the RFC. This limitation in Stage IV real time product is one of the restrictions that should be considered when dealing with Stage IV product.

Chapter 3 Literature Review on Precipitation Frequency Analysis

In the hydrological applications, it is of particular interest to study the heavy precipitation events accompanied with radar rainfall estimates for the hydrologic analysis and design purposes like the design of flood protection structures and the development of roadway drainage systems. Moreover, the statistics of extremes as heavy precipitation have played an important role in engineering practice for water resources design and management (*Katz, et al.,* 2002). The extreme rainfall rate setting also raises special challenges for development of radar-rainfall estimation algorithms, validation of rainfall algorithms and design of radar-rainfall estimation experiments (*Krajewski & Smith,* 2002).

The purpose of the frequency analysis of the precipitation is to find the frequency at which excessive rates of precipitation which are fundamental for the adequate and economical design farm terrace system, farm drainage system, highway and railway culverts, municipal storm sewer systems, small and large dams with the spillways provided to control the flow and other engineering works that must care for storm run-off (*Yarnell,* 1935). The precipitation frequency analysis requires dealing with the statistics of the extreme events. *Buishand,* (1989) and *Katz, et al.,* (2002) explained the use of extreme value theory procedures and applications in the field of climatology and hydrology.

The radar QPE estimates have an important advantage, which is the high temporal and spatial resolution compared with the sparse coverage of the rain gauges network. The weather radars provide spatially continuous estimates of rainfall while rain gauges measure rainfall in-situ at the surface but only at the points where the gauges are located (*Seo, et al.,* 2010). This advantage raises the attention to the hydrologists to use these high resolution estimates in the

derivation of the Intensity-Duration-Frequency (IDF) curves or the Depth-Duration-Frequency (DDF) curves. Moreover, the radar estimates are applied in the calculation of areal reduction factor (ARF) to obtain spatial information about the precipitation distribution in the area of interest. Although the evolution of the radar estimates and their contributions in different applications, the utilization of the QPE in the extreme precipitation statistical analysis and the derivation of the frequencies estimates is not widely employed.

3.1 Gauge-Based Studies

Many studies have been conducted to estimate the precipitation frequencies based on the gauge observations and most of them relate the frequency with both the duration and intensity, or depth to develop the IDF, or DDF, curves. The availability of NEXRAD QPE in a high temporal and spatial resolution covering the United States is currently stimulating the researchers to study the applicability of the radar-based QPE in deriving the precipitation frequencies. However, all the current available studies released officially by the NWS for the frequency analysis of the precipitation are based on rain gauges. This subsection focuses only on the official studies of the NWS and outlines the historical development of the publications released by the NWS for the precipitation frequency analysis and the estimation methods applied in these studies.

The first study for the rainfall extremes in the United States was undertaken by *Yarnell,* (1935) who provided isohyetal charts for the maximum rainfall depth in periods of 5 minutes to 24 hours that may be expected to occur with average frequencies of 2 to 100 years. He studied only the storms with high rainfall intensity and short duration, which are usually the

most destructive, using the records of excessive short-time precipitations at the Weather Bureau stations in continental United States.

In 1953, the Weather Bureau published a technical paper 24 (TP24) (*Bureau,* 1953; *Bureau,* 1954) including the rainfall intensities and frequencies required for design criteria in estimating required capacities of drainage systems for various types of military installations. The study was prepared in two parts; the first part is for the portion of the United States that lying west of the 115th meridian, while the second part is for the portion lying between 105˚ W and 115˚ W. The two parts estimated the rainfall depths for the durations of 5 minutes to 240 minutes and 2, 5, and 10 year return period. The frequency analysis of the rainfall rates in this study was simply performed using the plotting position formula to compute the return period of each rainfall amount by dividing the period of record by the serial number of the rainfall amounts arranged in decreasing order.

The Weather Bureau published a new Technical Paper 25 (TP) (*Bureau,* 1955) in 1955 that contained IDF curves for 203 locations in the United States, Alaska, Hawaii, and Puerto Rico for different durations from 5 minutes to 24 hours and for 2 to 100 year return periods. The IDF curves developed in his study by fitting the annual maximum precipitation to extreme distribution type I (Gumbel). TP25 appears to be the first publication to model the extreme precipitation using extreme value distribution. In 1956, the U. S. Weather Bureau expanded the two parts of TP24 to Technical Paper 28 (TP28) that encompassed longer durations and wider range of return periods, prepared for the Soil Conservation Service (SCS), by extending the durations to 24 hours and using return periods from 1 to 100 years. While in TP 24, only the partial duration series were used for the frequency analysis, in TP28, both partial duration series and annual maximum series are considered in this paper.

TP 28 was followed by a series of five parts of Technical Paper 29 (TP29) (*Bureau,* 1957; *Bureau,* 1958; *Bureau,* 1958; *Bureau,* 1959; *Bureau,* 1960) covering eastern portion on the United States. In these series, the area-depth relations were first studied and the areal/point ratios were calculated to generate areal reduction curves that permit point rainfall values represented by IDF curves to be converted to spatially averaged values.

The US Weather Bureau published Technical Paper (TP40) in 1961 as a convenient summary of empirical relationships, working guides, and maps, useful in practical problems requiring rainfall frequency data by applying the at-site frequency analysis for the extreme series extracted from the rainfall data available in the stations across the United States (*Hershfield,* 1961). TP 40 presents isohyetal maps and seasonal variation diagrams for rainfall durations from 30 min to 24 h and for return periods from 1 to 100 years (Figure 14). Several studies were conducted after TP 40 that made use of more number of gauges and longer records and extended longer durations (e.g. TP49 (*Bureau,* 1964)).

By the middle to late 1970s, the growing environmental awareness had increased the demand for hydrologic planning and design for small area drainages having very short times of concentration. It was also observed that for storm durations of less than 1 h, ratios of sub-hourly to hourly rainfall values that had been published in TP 40 were in need of revision as they had a discernible geographic pattern. These issues led to the publication of the NOAA Technical Memorandum NWS HYDRO-35 in June 1977 (*Frederick, et al.,* 1977a) for estimation of 5- to 60- minute precipitation frequency for the eastern and central United States (see for example Figure 15). HYDRO-35 utilized the Gumbel frequency distribution for modeling the extreme precipitation series and estimated the parameters using the method of moments.

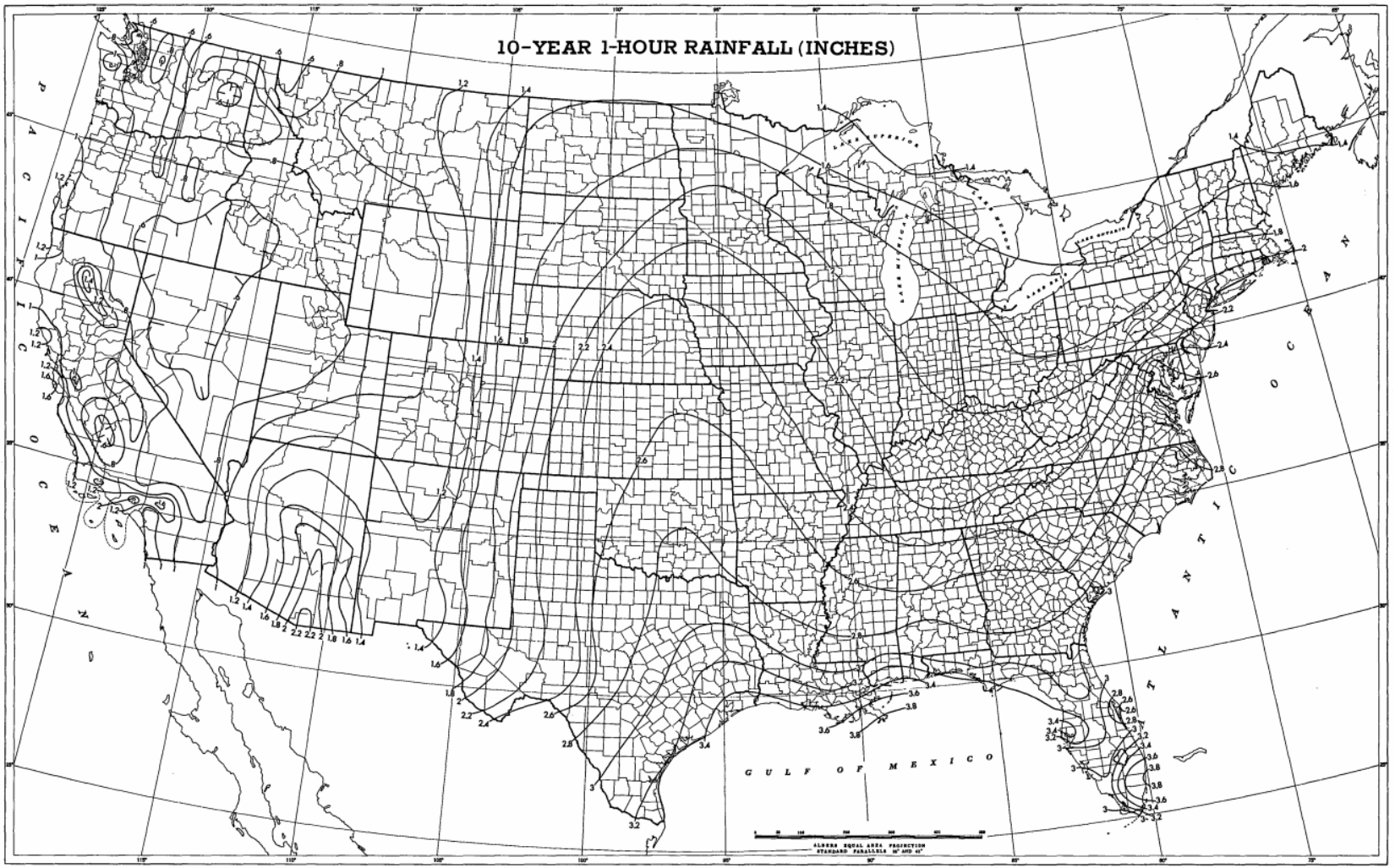

Figure 14 The 10-year 1-hour rainfall (inches) for the United States (Source: *Hershfield,* (1961)).

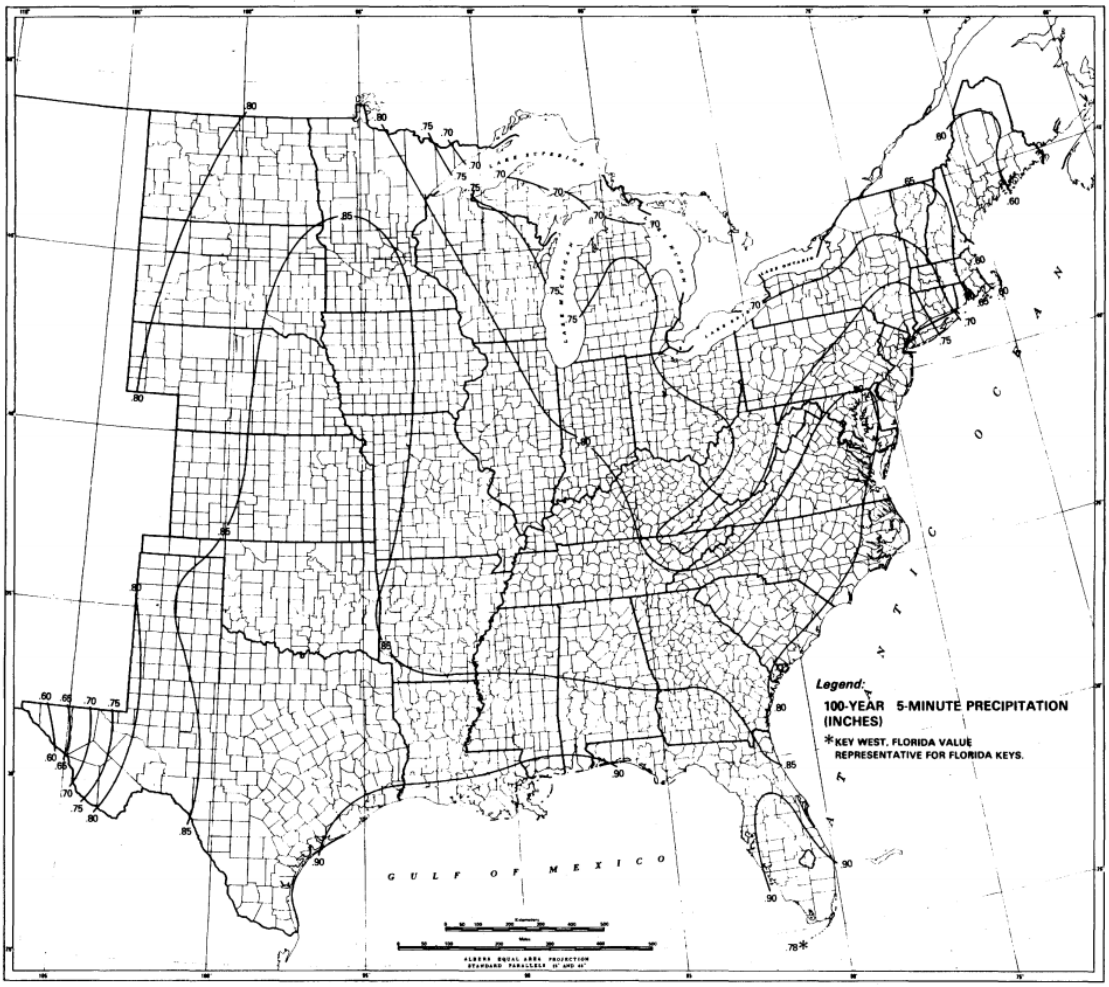

Figure 15 The 100-year 5-minute rainfall depth for the eastern and central United States (Source: *Frederick, et al.,* (1977a)).

Since the previous studies had considered the topography in only a general sense and due to the orographic effects caused by the high mountain ranges in the western United States, the National Weather Service (NWS) published the NOAA Atlas 2 (*Miller, et al.,* 1973) in 11 volumes, with each volume being applicable to one of the western states. This Atlas studied the relation between the precipitation frequency values and the topography both objectively and subjectively. The relation was studied objectively through the use of the multiple regression screening techniques which develop equations used to assist in interpolating values between stations in regions of sparse data.

The National Weather Service is currently conducting rainfall frequency studies on a regional basis to update TP 40, HYDRO-35, and the NOAA Atlas 2 and is publishing the results of the new studies as the NOAA Atlas 14 (*Durrans,* 2010). For example, the NOAA Atlas 14 Volume 9 (*Perica, et al.,* 2013) provides precipitation frequency estimates for durations of 5-minutes through 60-days at average recurrence intervals of 1-year through 1,000-year for six southeastern states: Alabama, Arkansas, Florida, Georgia, Louisiana, and Mississippi. The estimates and associated bounds of 90% confidence intervals are provided at 30-arc seconds resolution (Figure 16). The Atlas also includes information on temporal distributions for heavy precipitation amounts for selected durations and seasonal information for annual maxima data used in the frequency analysis. In addition, the potential effects of climate change as trends in historic annual maximum series were examined. The information in NOAA Atlas 14 Volume 9 supersedes precipitation frequency estimates for of Alabama, Arkansas, Georgia, Florida, Louisiana, and Mississippi contained in *Hershfield,* (1961), *Bureau,* (1964), and *Frederick, et al.,* (1977a). Precipitation frequency estimates, in NOAA Atlas 14 have been computed for a range of frequencies and durations using a regional frequency analysis approach based on L-moment statistics calculated from annual maximum series.

The Hydrometeorological Design Studies Center (HDSC) is providing a complete list of all studies performed by the National Weather Service (or its predecessor, the Weather Bureau) and the publications, e.g., technical and hydrometeorological reports, technical papers, technical memoranda, and atlases, released for the precipitation frequency analysis; The studies are organized by state and duration and some of the publications are digitized and available for downloading from the HDSC website.

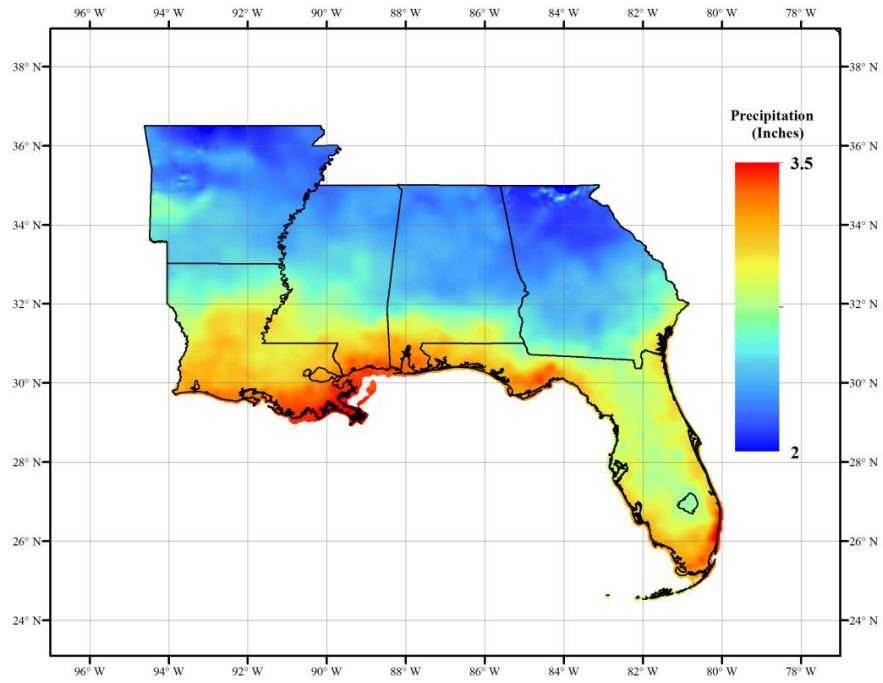

Figure 16 The 10-Year 60-minute rainfall depth over the domain covered by NOAA Atlas 14 Volume 9 (Source: *NOAA ATLAS 14, Precipitation Frequency Data Server*).

3.2 Radar-Based Studies

Frederick, et al., (1977b) used the converted digitized radar data into precipitation to derive depth-area reduction curves by averaging precipitation thus estimated over discrete area sizes. The prototype ARF curves were developed for watershed areas up to 1500 km^2 and accumulation periods ≤ 1 h. *Durrans, et al.,* (2002) evaluated the potential of NEXRAD radar-rainfall data for development of geographically fixed depth-area relationships and to identify potential obstacles that might hinder use of such data. The data analyzed for this study are those recorded for the Arkansas-Red Basin River Forecast Center (ABRFC) and span the period of time from May 1993, to September 2000. They concluded that data heterogeneities and shortness of data records are major factors limiting development of depth-area relationships on the basis of radar-rainfall data. *Allen & DeGaetano,* (2005)

explored the feasibility of radar-based extreme precipitation climatologies in the development of prototype radar areal reduction factor (ARF) curves and their comparison to those based on traditional rain gauge networks. *Lombardo, et al.,* (2006) studied the areal reduction factor using radar reflectivity maps and the results obtained are compared with the most important relations of the ARF reported in the literature. *Olivera, et al.,* (2008) calculated the average precipitation areal reduction factors (ARFs) for the 685,000 km^2 of Texas using NEXRAD rainfall estimates of years 2003 and 2004 and by studying 18,531 storms of different durations that took place in different seasons and regions of Texas. *Overeem, et al.,* (2009) applied the extreme value theory to estimate the depth-duration-frequency curves using weather radar data covering the entire land surface of the Netherlands for the period from 1998 to 2008. They derived the extreme rainfall statistics and their uncertainties by applying regional frequency analysis approach. *Overeem, et al.,* (2010) used the same 11 year high-quality radar rainfall data set to derive Radar-based areal reduction factors (ARFs) and these ARFs were shown to be comparable to those based on high-density rain gauge networks and it is concluded that radar data, after careful quality control, are suitable to estimate extreme areal rainfall depths. *Villarini, et al.,* (2010b) used rainfall estimates from two WSR-88 weather radars, located 150 km from the urban core of Charlotte in the analysis of the 23 July 1997 storm and flood occurred in this basin. This study provided an assessment for the accuracy of radar rainfall estimates for extreme, flood-producing rainfall and it showed that bias-corrected radar rainfall estimates for the 23 July 1997 storm are quite accurate and provide the capability for resolving the fundamental rainfall forcing associated with regional variation in extreme flood response in urban landscapes. *Wright, et al.,* (2013) presented an alternate framework for rainfall frequency

analysis that couples stochastic storm transposition (SST) with storm catalogs developed from a ten-year high-resolution (15-min, 1-km^2) radar rainfall dataset for the region surrounding Charlotte, North Carolina, USA. The SST procedure involves spatial and temporal resampling from these storm catalogs to reconstruct the regional climatology of extreme rainfall. SST-based intensity–duration– frequency (IDF) estimates are driven by the spatial and temporal rainfall variability from weather radar observations and they are compared to curves computed using conventional (rain gage-based) methods.

3.3 Frequency Analysis Approaches

Two main approaches for the frequency analysis of the rainfall have been discussed in the literature; one is the at-site estimation of frequencies which simply uses the data at each station for the statistical analysis, while the second method is a regional estimation approach that makes use of observations from gauges that share a homogenous region with similar climatological and physical characteristics.

Svensson & Jones, (2010) reviewed the estimation methods in the rainfall frequency analysis in nine different countries and each country's method is different, but most use some form of regionalization to transfer information from surrounding sites to the target point. Several of the methods are variations of a regionalization method that combines a local estimate of an index variable (typically the mean or median annual maximum rainfall) with a regionally-derived growth curve to obtain a design rainfall estimate. Although radar QPE provides estimates at each pixel with a high spatial resolution, these regionalization techniques might be very advantageous to reduce the variability in the radar PFEs resulted from the short record of samples. *Naghavi & Yu,* (1995) applied a regional frequency analysis approach to

precipitation data in Louisiana using AMS extracted from 25 synthesized stations with long periods of record. The climatologically homogeneous regions in Louisiana are identified using the mean annual precipitation, geographical locations, and the synoptic generating mechanisms. The results showed that the regional procedure can substantially reduce the Relative root-mean-square error (RRMSE) and relative bias (RBIAS) in quantile prediction. *Sveinsson, et al.,* (2002) analyzed short duration annual maximum precipitation (AMP) for Northeastern Colorado and developed regional frequency curves that may be useful for that part of Colorado. *Fowler & Kilsby ,* (2003) used regional pooling of 1-, 2-, 5- and 10-day annual maxima for 1961 to 2000 from 204 sites across the UK and they produce generalized extreme value growth curves for long return-period rainfall events for nine defined climatological regions. *Trefry, et al.,* (2005) applied a regional approach based on L-moments on the Annual Maximum Series (AMS) and Partial Duration Series extreme precipitation extracted from 76 hourly recording stations and 152 daily recording stations in order to update rainfall IDF estimates in the state of Michigan. They considered the entire state as one homogenous region and applied two regional index flood models: a generalized Pareto distribution fit to PDS data (PDS/GPA model), and a generalized extreme value distribution fit to AMS data (AMS/GEV model). *Lin, et al.,* (2006) provided an overview of NOAA Atlas 14, the updates of the rainfall frequency atlases and technical papers published by the National Oceanic and Atmospheric Administration's National Weather Service for the Semiarid Southwest United States and the Ohio River Basin and surrounding states. They discussed an L-moments based regional rainfall frequency approach with focusing on technical/statistical aspects during the application of this approach.

3.4 Addressing Statistical Uncertainty

The statistical estimates are associated with sampling variability, i.e., the sample statistics like the mean and quantiles differ in samples derived from same population, since these samples do not include the whole population. Quantifying this variability in the estimates is very crucial in any statistical studies because only the estimates may lead to inexact conclusions. Therefore, addressing the uncertainty in the precipitation frequencies simply refers to draw an inference about the confidence limits with which any estimate can be accepted as representing the true result of the precipitation. These confidence limits give an indication of the range of values in which quantiles can be expected to lie because in the absence of an infinitely long rainfall record consistent with the current climate to represent the population, the true quantiles estimates are unknown. There are many methods in the literature to account the sampling uncertainty, for example, the bootstrap resampling different techniques and the Monte Carlo simulations.

The Bootstrap methods, first introduced by *Efron,* (1979), enable the derivation of confidence limits and the use of significance tests in situations where the underlying statistical population is unknown or where an analytical solution is impractical. Bootstrapping is based on the generation of many resamples, which are selected from the original sample. This original sample is used as the distribution from which the resamples are chosen randomly with replacement, i.e. with each value being returned to the original sample after it has been chosen, so that it may be chosen again (*Faulkner & Jones,* 1999). It is a computer-based method, which substitutes considerable amounts of computation in place of theoretical analysis (*Efron & Tibshirani,* 1986; *Efron & Tibshirani,* 1994). Efron's insight was that we can simulate replication. After all, we have already fitted a model to the data,

which is a guess at the mechanism which generated the data. Running that mechanism generates simulated data which, by hypothesis, have the same distribution as the real data. Hence, Bootstrapping is simply the estimation of the population distribution by using the information based on a number of resamples from the sample. The bootstrap can be used as a nonparametric time series model by simply resampling, with replacement, from the historical record. The challenge is to resample the records, in such a way as to assure that the temporal and spatial covariance structure of the original time series is preserved (*Vogel & Shallcross,* 1996).

In precipitation frequency analysis, there are many approaches suggested for using the bootstrapping methods. *Athreya, et al.,* (1999) studied the asymptotic properties of bootstrap methods for the maximum of a stationary process and they concluded that the Efron's bootstrap provides a valid approximation to the distribution of the maximum for a class of stationary processes, but it does not in general, while the moving block bootstrap provides a valid approximation in a wider class of stationary processes. *Lall & Sharma,* (1996) proposed a nearest neighbor bootstrap scheme for resampling hydrologic time series, in which the dependence structure of the time series is preserved while bootstrapping. *Vogel & Shallcross,* (1996) applied the moving blocks bootstrap resampling algorithm to estimate the storage capacity of a surface water reservoir and compared this approach with the use a parametric time series model. They concluded that using the bootstrap techniques is very advantageous and always produces estimates with lower root-mean-square-error than the parametric alternative. *Sharma & Tiwari ,* (2009) combined neural networks analysis with the bootstrap techniques, named Bootstrap based artificial neural network (BANN) analysis, for the prediction of monthly run-off in Upper Damodar Valley Catchment in India. *Ebtehaj, et al.,*

(2010) introduced an approach to improve the robustness of hydrologic parameter estimation by the use of moving block bootstrap resampling. *Hailegeorgis, et al.,* (2013) used the balanced bootstrap resampling, suggested by *Davison, et al.,* (1986) for more efficient bootstrapping, to estimate the confidence intervals for the sampling uncertainty in the estimation of quantiles using the regional frequency analysis techniques. The confidence limits are provided in NOAA Atlas 14, for the first time in the NWS precipitation frequency atlases, to quantify the uncertainty in the estimates (*Lin, et al.,* 2006). Monte Carlo Simulation was used to generate samples from the parameters estimated at each site using the statistical distribution fitted to the site sample. The confidence limits of the estimates can be then estimated either by assuming normal distribution of the estimates or by sorting the estimates and use any appropriate plotting positions formula.

Chapter 4 Assessment of Heavy Precipitation Real-time Stage IV Product over CONUS Domain

Radar-based quantitative precipitation estimates (QPE) have been widely used in many hydrological and meteorological applications; however, these estimates are inherently imperfect which could introduce significant uncertainties to their applications. As mentioned earlier, many authors have used Stage IV in different precipitation analysis applications; however, few studies have been directed towards the assessment the Stage IV when used with the heavy precipitation as extreme events. Although Stage IV benefits from the automated quality control performed at each RFC, the precipitation estimates do not currently incorporate the manual quality control procedures performed later , not in real-time, by the RFC. This limitation in Stage IV real time product is one of the restrictions that should be considered when dealing with Stage IV product. This chapter explores quality issues in the real-time Stage IV QPE product and examines their impacts on the analysis of hourly heavy precipitation amounts over the period from January 2002 to June 2013. To discern the causes of the quality issues, the real-time, i.e., Stage IV, and longer-latency radar multisensory QPEs, i.e. MPE products, are compared for the largest precipitation amounts derived from the Stage IV data. Stage IV QPE data were provided by National Center for Atmospheric Research/Earth Observing Laboratory (NCAR/EOL) under sponsorship of the National Science Foundation (http://data.eol.ucar.edu)

4.1 Artifacts in Stage IV Product

The national NCEP Stage IV (QPE) is mosaicked from individual RFC's multi-sensor precipitation analyses and it covers the domain over the Continental United States (CONUS).

The Stage IV QPE is available from 2002 to real-time data and in this study, the 1-hourly precipitation estimates are used from January 2002 to June 2013 (note that: we do not consider some hourly data that have problems, either missing or corrupted. For more details, see log of problem hours on http://www.emc.ncep.noaa.gov). The extreme precipitation is represented by fields of the maximum precipitation estimate for each pixel sorted in descending order, for instance, the first field is the highest precipitation estimate for each pixel for the period of study. The extraction of the maximum precipitation in this manner has been widely used in the frequency analysis of precipitation and it is known as Partial Duration Series or PDS as discussed in the next chapter.

The hourly extreme precipitation amounts extracted from real-time Stage IV data show a number of artifacts in precipitation estimates (upper panel in Figure 17). The artifacts are mostly dominant in the form of circular patterns, or rings, formed around some pixels. Most of these rings show suspicious, very high rainfall rates that are surrounded with lower values. While these artifacts are spread throughout the entire CONUS domain, they are more dominant in the western southeastern, northeastern and northern regions. These artifacts in the southeastern regions seem to be associated with the largest values in the PDS series and diminish gradually beyond the first few largest fields. They are mostly absent in the fifth largest PDS field (Figure 17, lower panel). Unlike the case in southeastern US, artifacts in the western regions are more persistent through most of the PDS series (Figure 17). In the central and northeastern regions, occurrences of such ring-like feature are also evident; however, a close examination of the fifth largest PDS field shows a northeast-southwest strip of suppressed extreme rainfall values that is somewhat aligned with the Central Appalachians.

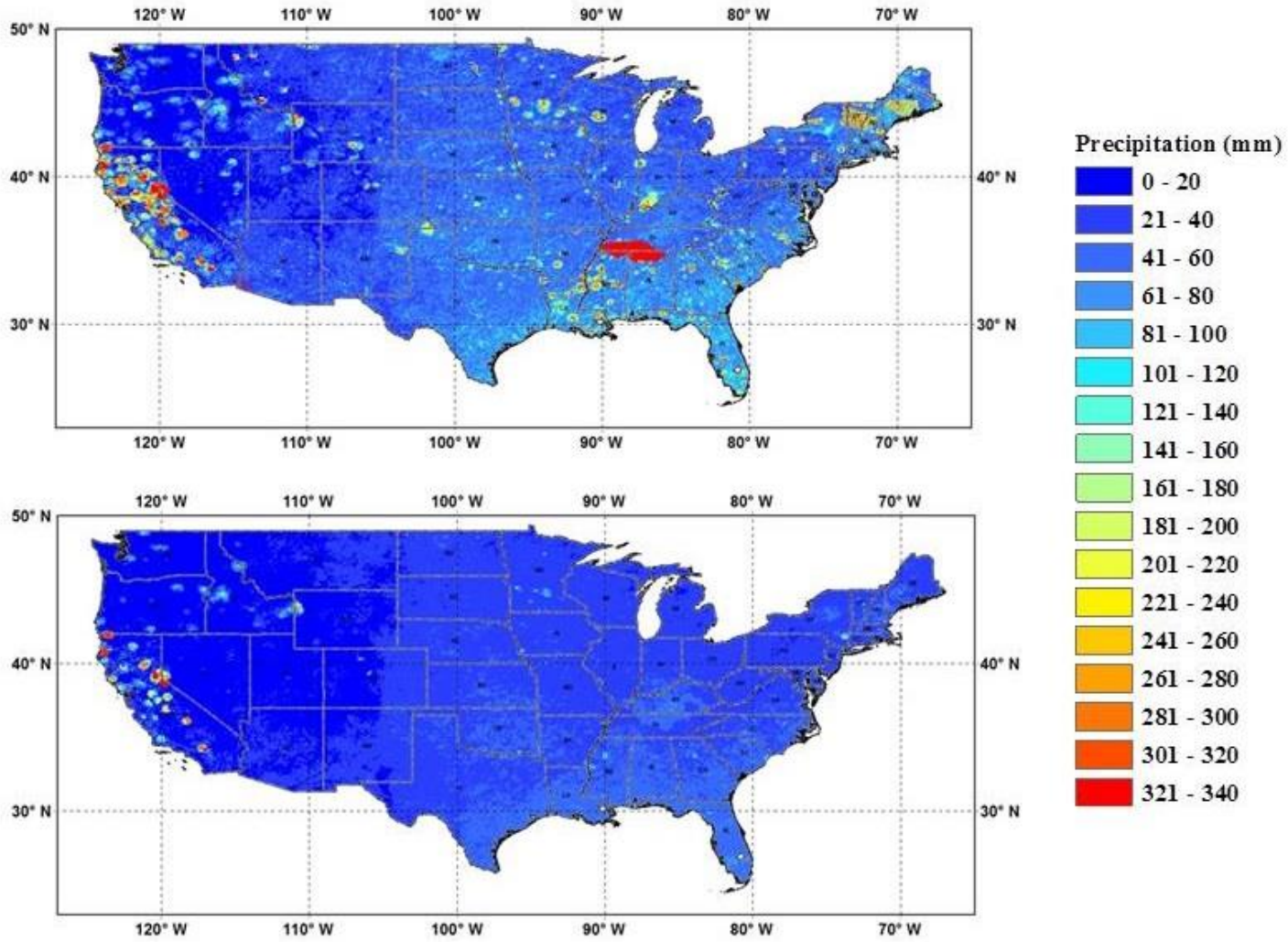

Figure 17 Maximum Fields (PDS) of hourly precipitation over the CONUS for the period of study January 2002- June 2013. Upper Panel: first field of PDS (i.e., maximum value at each individual pixel); Lower Panel: fifth field of PDS (i.e., fifth maximum value at each individual pixel).

The suppressed extremes feature in the PDS spatial fields is not necessarily a data processing artifact, but is probably due to radar estimation problems in regions of complex terrains. To further inspect any possible regionally specific patterns in the PDS artifacts and suspicious features, and to examine whether they are associated with specific dates or hours of the day, the year and hour of occurrence of each of these cases were extracted for the first PDS field and plotted for the southeastern (Figure 18), western (Figure 19), and northeastern (Figure 20) regions.

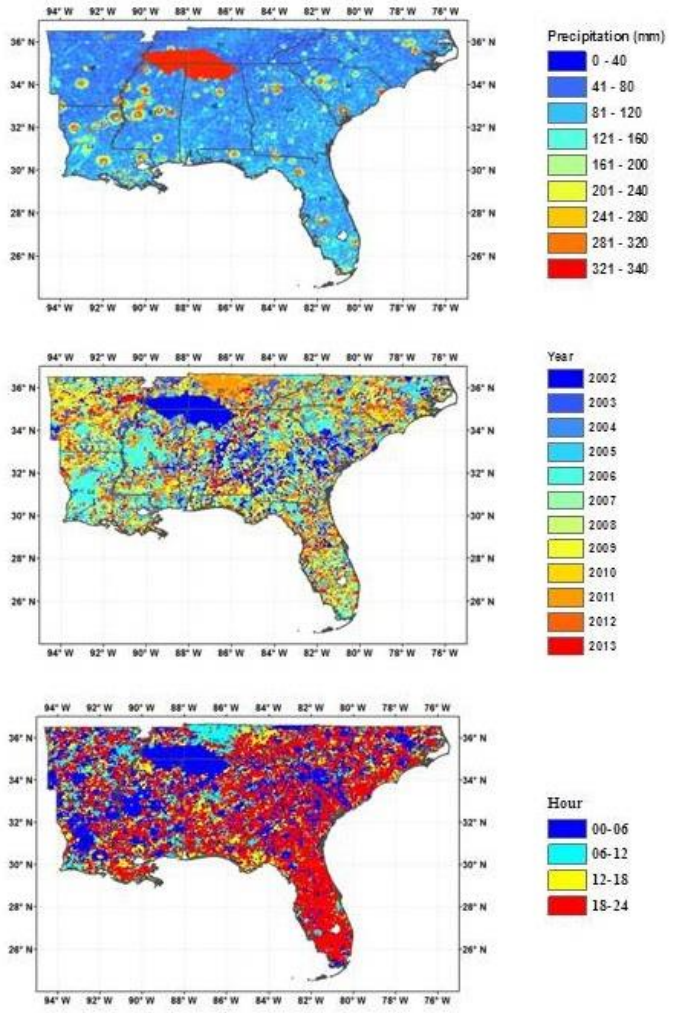

Figure 18 Upper Panel: Artifacts detected in the first field of PDS in the Southeastern coast. Middle Panel: The year of occurrence of each extreme estimate in the first field of PDS. Lower Panel: The hour of occurrence of each extreme estimate in the first field of PDS.

It is obvious form Figure 18 that most of the ring-like artifacts in the southeastern US occurred in 2006 and in the time between 00:00 UTC and 00:06 UTC. Further examination of these occurrences did not show that they were associated with any certain days in the year. Another feature in Figure 18 is a polygon with a constant value of very large hourly precipitation value (> 300 mm/h) observed in 2002 in the Tennessee, Mississippi and Alabama border area. This polygon is often drawn by a forecaster to remove anomalous propagation from the radar by setting all the grids in the polygon to zero. However, it appears here that the grids in this polygon were accidentally set to a very large value instead of zero and thus caused the artifact to appear.

In the western US, the ring-like features are more noticeable (Figure 19) and dominate the entire region in central and northern California. These are not associated with specific years or times of the day as they occurred in different years and at different hours of the day. Radar-rainfall estimation problems in the western US are well-known to the operational community due to significant terrain blockage, shallow precipitation, and low freezing levels. For these reasons, only one-fourth to one-third of the land surface in the region has sufficient radar coverage for precipitation estimation. Although improvements to the WSR-88D PPS algorithm have undoubtedly improved radar-derived quantitative estimates near the radar site, the extensive blocking and bright band effects in the western coast will continue to considerably limit the extent and usefulness of radar-based precipitation measurements in the region. As such, rain gauges will continue to be the principal instrument for determining the extent and quantity of precipitation throughout a significant portion of the western US, particularly over mountainous regions (*Westrick, et al.,* 1999). The heavy use of rain gauges

in this region is the main reason for such artifacts that can dominate the identification of heavy rainfall.

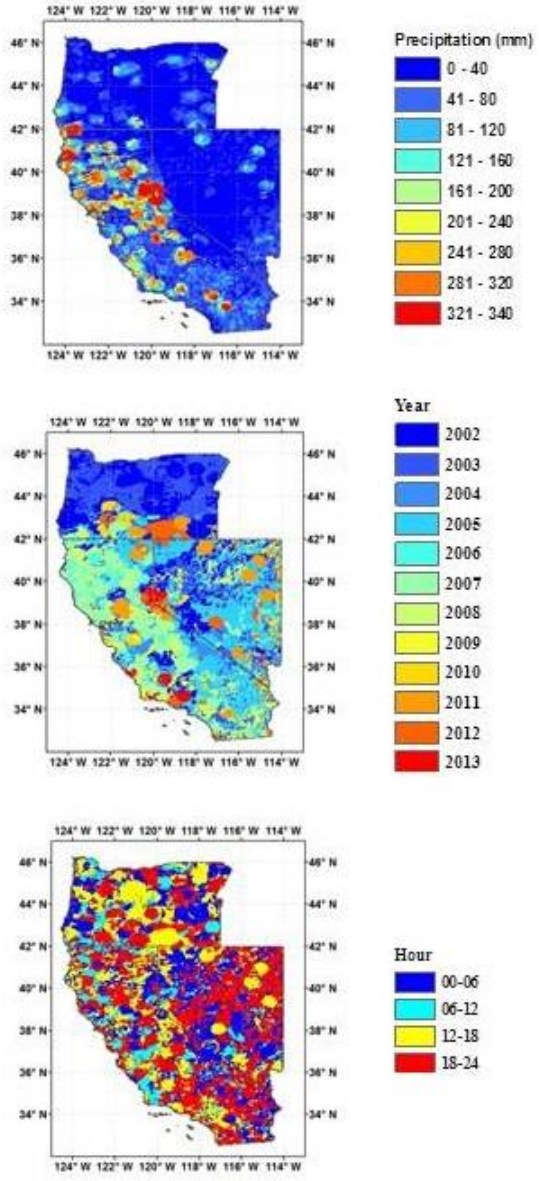

Figure 19 Upper Panel: Artifacts detected in the first field of PDS in the Western Coast. Middle Panel: The year of occurrence of each extreme estimate in the first field of PDS. Lower Panel: The hour of occurrence of each extreme estimate in the first field of PDS.

The northeastern states (e.g. Maine, New Hampshire, and Vermont) show some peculiar non-ring, polygon-like features in their PDS fields (Figure 20) that do not necessarily have pre-set fixed values. These features are associated with the year 2008 and in the hours between 00:00 UTC and 06:00 UTC (Figure 20). Other apparent artifacts in the region are more scattered spatially and temporally. The most northeastern part of the region shows some linear features in the PDS fields that are associated with hours 12-18 UTC and the earlier years of the Stage IV record (2002-2003). Other pockets of lower PDS are noticed in some parts of the states of Maine and New York.

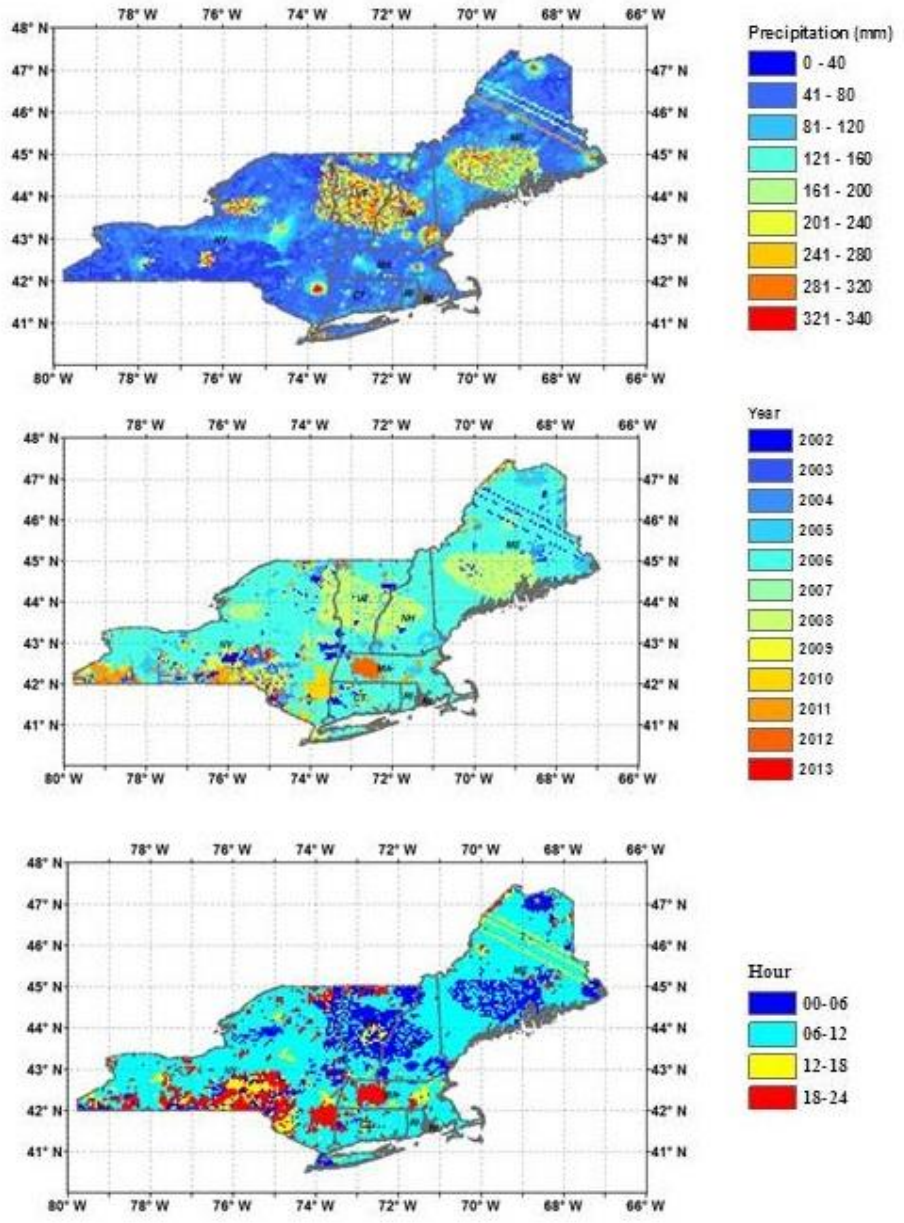

Figure 20 Upper Panel: Artifacts detected in the first field of PDS in the Northeastern coast. Middle Panel: The year of occurrence of each extreme estimate in the first field of PDS. Lower Panel: The hour of occurrence of each extreme estimate in the first field of the PDS.

4.2 Inter-comparison of Stage IV and MPE Products

In this section we will inspect the MPE products developed by the NWS RFC's for the same artifacts that we observed in the Stage IV product. The reader is reminded that while the Stage IV product is basically a national mosaic of the final regional product (XMRG) produced at each RFC, it doesn't take advantage of the forecaster's manual interventions and quality control measures that are performed post real-time. For space limitations, we will perform and present such analysis for one of the RFC's only, namely the Lower Mississippi River Forecast Center (LMRFC). The hourly PDS series was developed for LMRFC XMRG product in a similar manner to the Stage IV analysis but for the period from January 2002 to December 2012 (the data for 2013 were not available while performing this study). The first (largest) PDS field for the LMRFC XMRG product is shown in Figure 21 and, as expected, the problematic artifacts that were evident in the Stage IV are now absent.

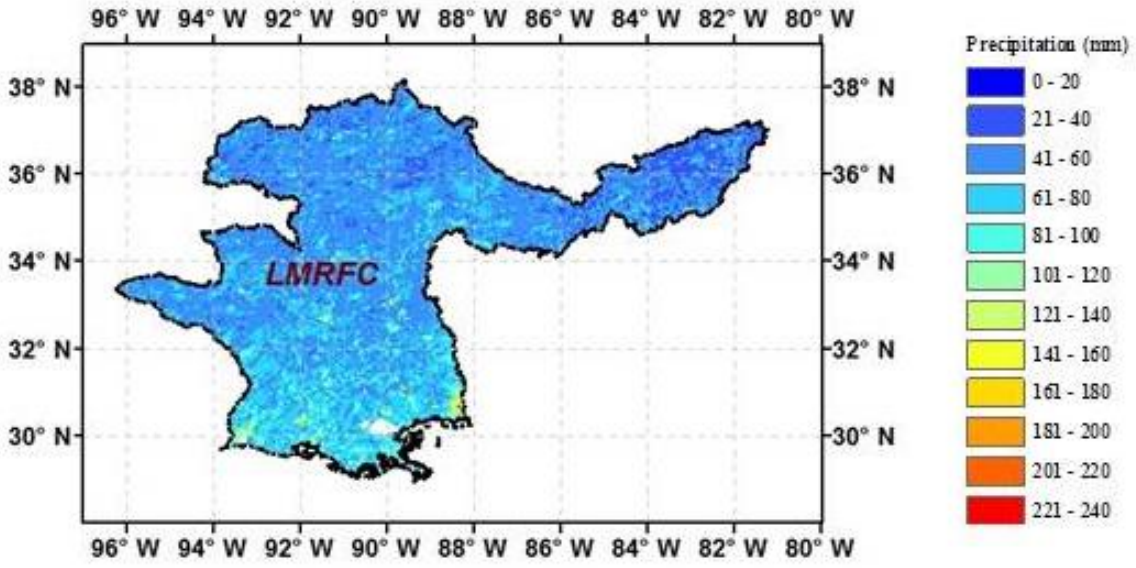

Figure 21 First field of maximum precipitation over the LMRFC Domain extracted for each pixel during the period of study January 2002- December 2012.

To track the possible sources of the Stage IV artifacts, we analyzed each of the six intermediate RFC products (summarized earlier in Table 4) from which the XMRG was eventually selected. For each of these products, the PDS fields were extracted in a similar manner to the Stage IV analysis. To get a closer look at some of the problematic ring-like features, we used three representative examples, which we refer to as R1, R2 and R3 (Figure 22).

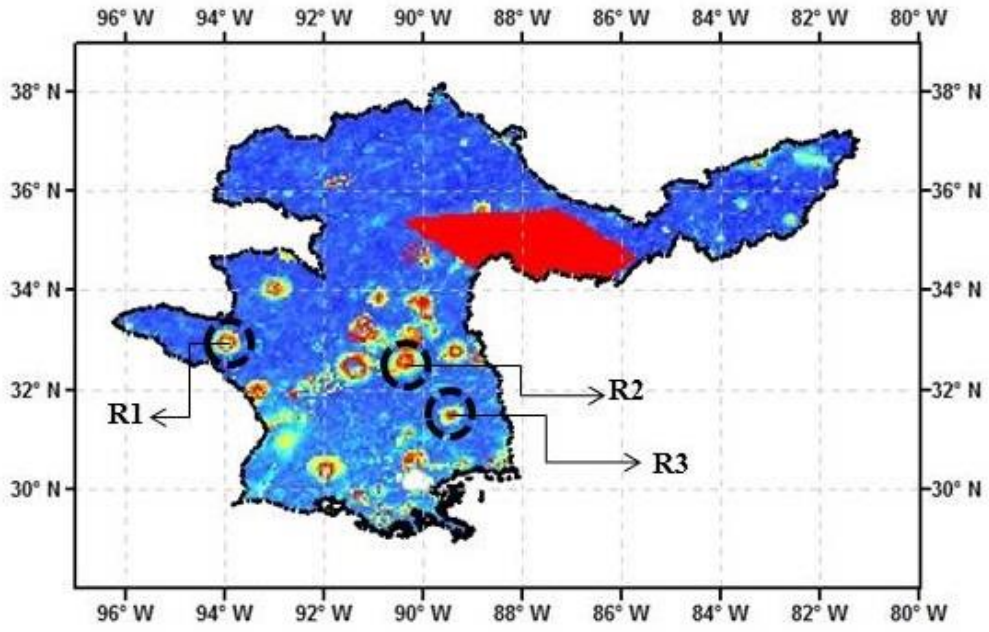

Figure 22 The location of three rings detected in Stage IV and used in the comparative study with the LMRFC products.

For each of these three cases, we identified the specific date and hour on which the case was reported and plotted the actual hourly precipitation field (i.e., not the PDS field) for the RFC suite of products (Figure 23, Figure 24, and Figure 25). We also show the corresponding fields from the Stage IV 1-hourly and 6-hourly products. As expected, it is clear that the XMRG field does not show any of the Stage IV artifacts. However, it is noted that the GAGEONLY field shows ring features similar to those in the Stage IV hourly field, at least

for the two cases of R1 and R2, indicating that the sources of such artifacts are malfunctioning gauges. These bad gauges were apparently identified during later quality control procedures at the river forecast center and therefore the final product (XMRG) does not show the same artifacts. In the case of ring (R3), the GAGEONLY field does not show the Stage IV problematic artifacts, and neither does the final product, XMRG. We still believe that the source of the R3 case in Stage IV is due to a malfunctioning gauge. The reason behind this is that the RFC forecasters sometimes, when quality controlling the data, use a polygon and set all grids in the XMRG field to zero to remove bad data and therefore the underlying gage-only field would not benefit and would still show the bad gauge as in the case of (R1) and (R2). In other instances, forecasters might set a bad gauge to missing and re-run the fields to remove their effects, thus benefiting all of the other fields, such as the case in R3. The NCEP also produces a 6-hourly product, which apparently does not show the same artifacts in the 1-hourly product indicating that this product captures the quality control done later by the forecasters in the RFC. It is noted here that the 6-hourly NCEP analyses are not simple summations of the hourly fields. The RFCs send NCEP both hourly and 6-hourly analyses for their respective local domains, and typically, the RFC 6-hourlies have better quality control (QC). Some of the hourlies received by the NCEP are only the automated runs (no manual QC), while the 6-hourlies almost always receive the manual QC adjustments. Actually, one of the RFC's (Northwest River forecast center, NWRFC) does not produce an hourly analysis, and produces only a 6-h product. In addition, NCEP may not always receive an hourly analysis for an RFC (in that case the analysis from a neighboring RFC will contribute to the Stage IV values in the missing RFC domain), which is another factor contributing to the differences in quality of 1-h and 6-h products (*NCEP/EMC/NOAA,* 2013).

The Stage IV 24-hour product was also analyzed (not shown) and similar conclusions were made since this product is summed from the four 6-hourly Stage IV analyses.

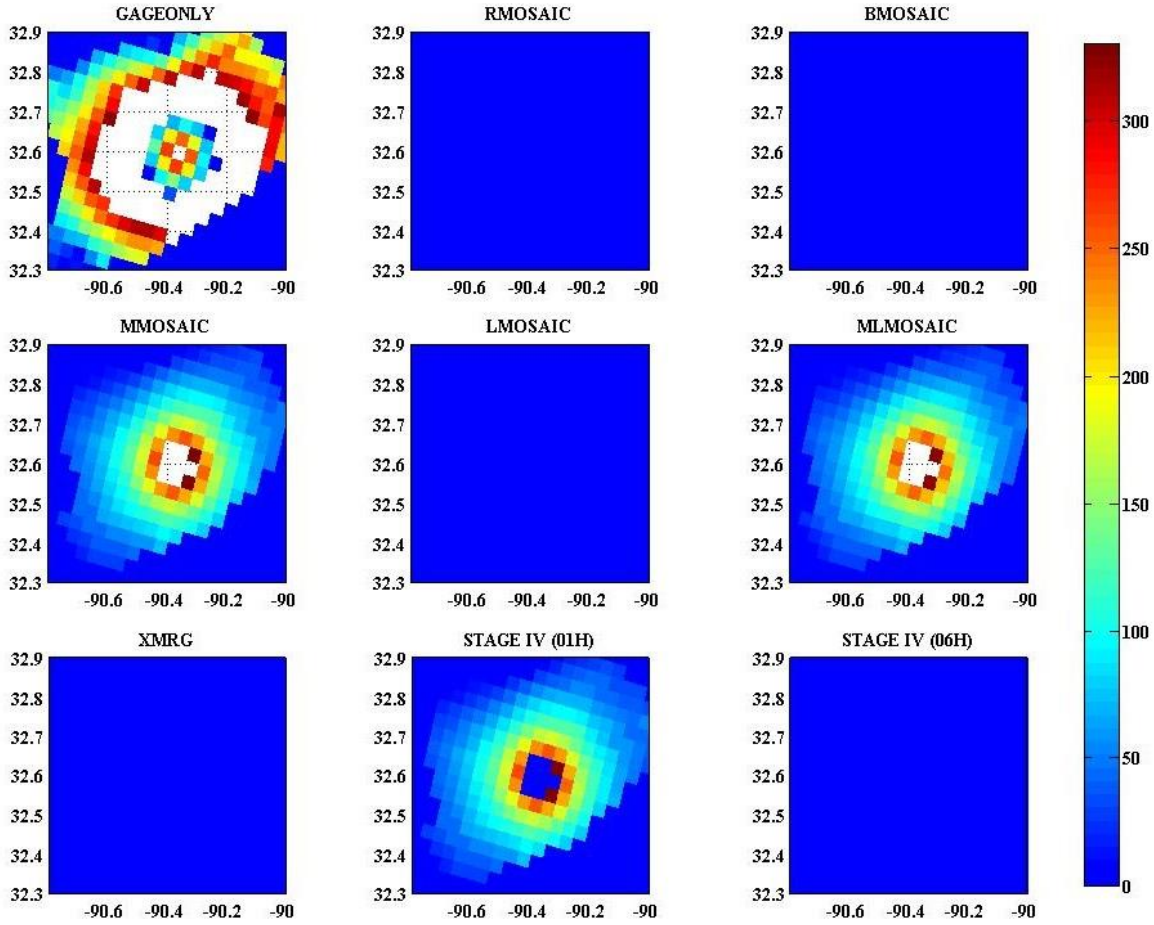

Figure 23 Comparing precipitation estimates from StageIV (R1) with LMRFC different products in 8th of October 2006 at 06 UTC.

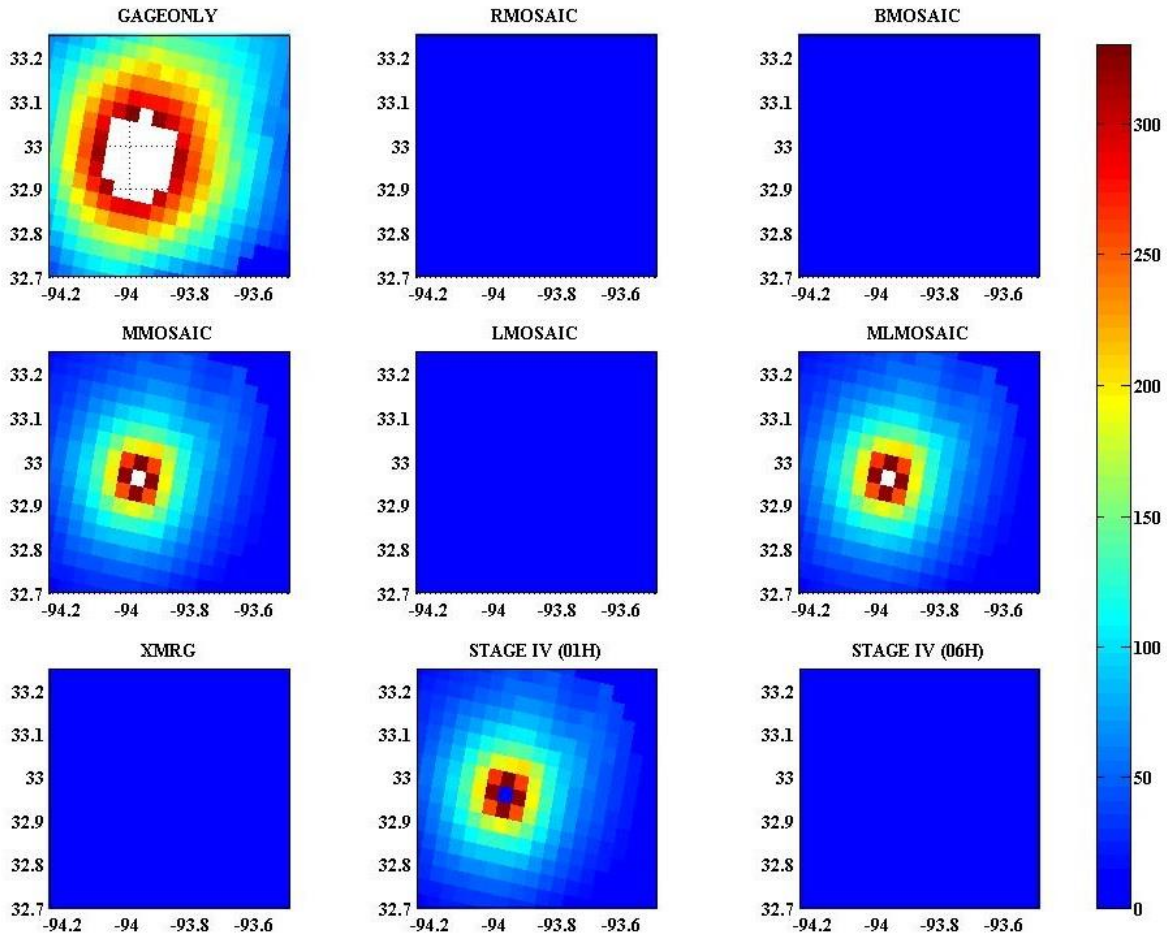

Figure 24 Comparing precipitation estimates from StageIV (R2) with LMRFC different products in 19th of April 2006 at 05 UTC.

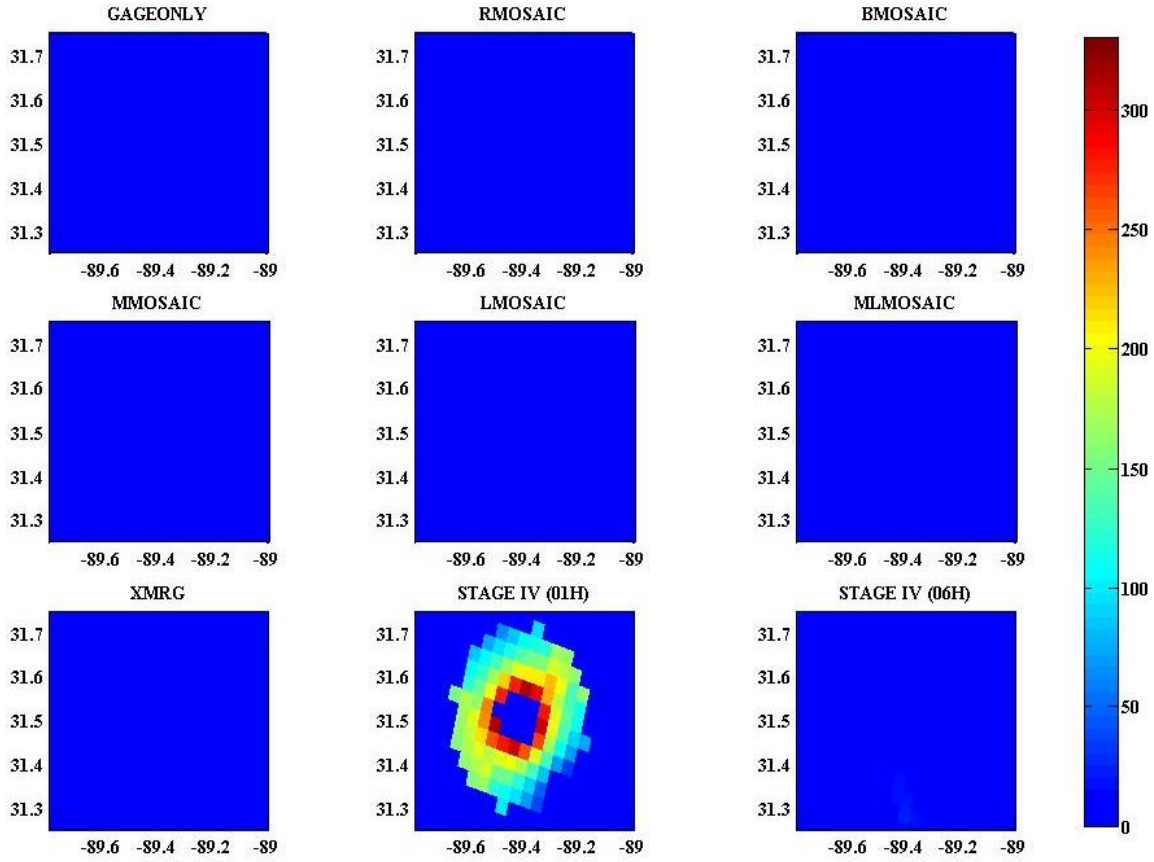

Figure 25 Comparing precipitation estimates from StageIV (R3) with LMRFC different products in 23rd of July 2006 at 06 UTC.

4.3 Application of an Outlier Detection Test

Grubbs-Beck (GB) outlier detection test is used to evaluate whether the artifacts in Stage IV product could be removed statistically by considering them as outliers or not and thus, the Stage IV product can be used for the purpose of frequency analysis of extreme precipitation. Outliers are data points which depart significantly from the trend of the remaining data and the purpose of a statistical study of outliers is to assess whether our subjective declaration of outliers in a sample has important objective implications for an analysis of the sample (*Barnett,* 1978). The identification of the outliers requires judgment involves both mathematical and hydrological consideration (*USGS,* 1982).

There are different methods suggested for the outlier detection in the statistical literature, (e.g. Z-scores, Box Plot, Generalized Extreme Studentized Deviate (ESD) test, Sample Kurtosis, The Shapiro-Wilk W Test, Dixon Tests, Moving Window Filtering Algorithm and Grubbs-Beck Test). *Iglewicz & Hoaglin,* (1993), *Barnett & Lewis,* (1994) and *Garcia,* (2012) provide an extensive discussion of the outlier tests mentioned above (as well as other tests not mentioned).

The GB test (explained by *Grubbs,* (1950), *Grubbs,* (1969) and *Grubbs & Beck,* (1972)) is used to detect a single outlier in a univariate data set that follows an approximately normal distribution. GB test follows the same procedures suggested by *Pearson & Sekar,* (1936) for testing the significance of the largest observation, hence, it is sometimes referred to as the maximum normed residual test or extreme studentized deviate (ESD) test when used to test for up to a specified number of outliers. Procedures described by *Grubbs & Beck,* (1972) given for determining statistically whether the highest observation, the lowest observation,

the highest and lowest observations, the two highest observations, the two lowest observations, or more of the observations in the sample are statistical outliers.

GB test is defined for the hypothesis:

H_0 (Null Hypothesis): There are no outliers in the data set.

H_1 (Alternative Hypothesis): There is exactly one outlier in the data set.

The GB test procedures can be summarized as follows: first, the observations are arranged in an ascending order $x_1 \leq x_2 \leq x_3 \leq x_4 \leq \ldots\ldots\ldots\ldots \leq x_n$. Second, Grubbs' test statistic is estimated depending on the observation required to be tested and the ratio of the deviation of this observation to the sample standard deviation. The test statistic (T) is defined, for testing whether the largest observation (x_n) is too large, as:

$$T_n = \frac{(x_n - \bar{x})}{S} \tag{4.1}$$

where $\bar{x}$ and S are the sample mean and standard deviation respectively.

The sample standard deviation is estimated using:

$$S = \left[\sum \frac{(x_i - \bar{x})^2}{(n-1)}\right]^{\frac{1}{2}} \tag{4.2}$$

Third the value of the test statistic (T) is compared with critical values given in tables by *Grubbs & Beck,* (1972) to decide whether observation (x_n) is significantly large and can be treated as an outlier or not. In case of testing the significance of the two largest observations

(x_n & x_{n-1}), a $S^2_{(n-1,n)}/S^2_o$ criterion is computed and compared with the critical values given in tables by *Grubbs & Beck,* (1972), where:

$$S_o^2 = \sum_{i=1}^{n} (x_i - \bar{x})^2 \tag{4.3}$$

and

$$S^2_{(n-1,n)} = \sum_{i=1}^{n-2} (x_i - \bar{x}_{(n-1,n)})^2 \tag{4.4}$$

and

$$\bar{x}_{(n-1,n)} = \sum_{i=1}^{n-2} \frac{x_i}{n-2} \tag{4.5}$$

Similar procedures can be followed to test for the lowest value as well as the lowest two observations by simply substituting (x_n) by (x_o) and ($S_{n-1,n}$) by ($S_{1,2}$). *Grubbs & Beck,* (1972) provided tables of percentage points for significance tests concerning the highest or the lowest observation in normal samples, or the two highest or the two lowest observations in normal samples. The critical values given these tables are based on the results obtained by *Thompson,* (1935) which indicate that the expression $\frac{T\sqrt{n-2}}{\sqrt{n-1-T^2}}$ follows a Student's t-distribution with degrees of freedom (f) = n – 2. Considering this result and other comprehensive studies done by *Pearson & Sekar,* (1936) on this expression, Grubbs was able to estimate the critical values of (T) using the following formula for two sided test at a given significance level α :

$$T_{critical} = \frac{n-1}{\sqrt{n}} \sqrt{\frac{t^2_{\alpha/2n,n-2}}{n-2+t^2_{\alpha/2n,n-2}}} \quad (4.6)$$

with $t_{\alpha/(2n),n-2}$ denoting the upper critical value of the t-distribution with n − 2 degrees of freedom and a significance level of α/(2n). For the one-sided tests, α/(2n) is replaced with α/n.

Although the normality assumption for the GB test, it has been widely used in the field of precipitation frequency estimates and flood frequency analysis. The GB test is recommended by the federal guidelines for detection of low outliers in flood flow frequency computation in the United States. *Cohn, et al.,* (2013) presented a generalized Grubbs-Beck test statistics for normal data that can provide a consistent standard for identifying multiple potentially influential low flows. In addition, The GB test is used in NOAA Atlas 14 for AMS screening and removing of annual maxima which depart significantly from the trend of the corresponding remaining maxima (*Perica, et al.,* 2013). *Lee & Maeng,* (2003) used the GB test for the identifying of the outlier data on annual maximum daily rainfall in 38 Korean rainfall stations.

In this study, the GB test is applied to the Stage IV extreme series fields (PDS) in each pixel with various sample sizes by using different r-largest events for constructing PDS. For instance, the GB test was applied for PDS resulted from r=11, 20, 50 largest events. The rationale of using different sample sizes is avoiding removing some precipitation estimates that are not artifacts but can be considered as statistical outliers with respect to other events in case of small sample sizes. The GB test successfully removes most of the circular ring-like patterns (Figure 26) when increasing PDS sample at each pixel, for instance, the GB results

from PDS of sample size of 50 extreme events are shown in (Figure 26). Moreover, the test effectively removes the polygon with constant value drawn by the forecaster in 2002 in the Tennessee, Mississippi and Alabama border area. In general, the GB test can statistically remove the overestimated precipitation estimates which form the ring patterns and consider them as outlier observation compared with the rest of the sample; however a predefined threshold should be established to set the value of (r) required to construct PDS sample. This threshold is important to avoid removing some actual extreme events that might be flagged by the test as outliers For example the window in South Louisiana in Figure 26 shows the GB test removed artifacts detected in PDS; though some of the actual extremes in the surrounding pixels were also indicated as outliers and removed.

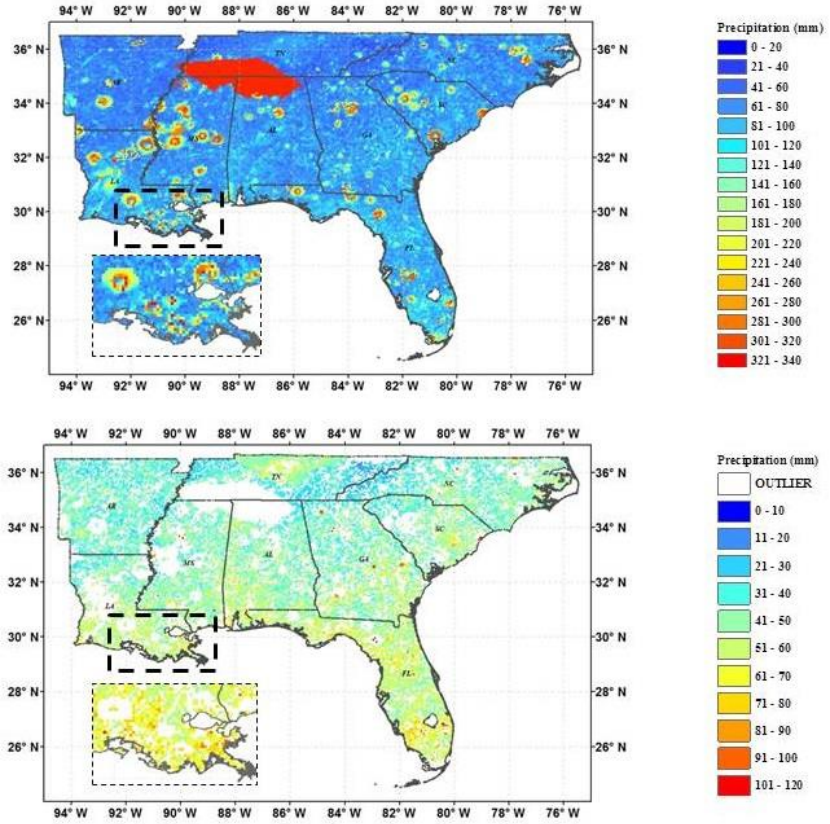

Figure 26 Upper Panel: The first field in PDS in the Southeastern Coast. Lower Panel: The first field in PDS after removing the artifacts using the Grubbs-Beck statistical test.

Chapter 5 Methodology for Precipitation Frequency Analysis

In this chapter, the methodology for deriving Precipitation Frequency Estimates (PFE) for different return periods based on the hourly radar QPE dataset is presented. The precipitation quantiles are estimated using two different frequency analysis approaches; pixel-based and region-based approaches. Section (5.1) briefly describes the dataset and the study area selected to apply the frequency analysis procedures. Section (5.2) defines the statistical series that are used to best describe the extreme events. The statistical distribution used to model the extreme events and the estimation of the distribution parameters are explained in section (5.3) and section (5.4) respectively. Finally, Section (5.5) presents the two approaches used for estimating the precipitation frequencies.

5.1 Datasets and Study Area

Based on the assessment of the NWS real-time Stage IV product explained in the previous chapter, the Stage IV product can't be used directly for the frequency analysis until manual quality control performed. Therefore, for the purpose of frequency estimates, the longer-latency MPE/XMRG product which received the manual quality control at the LMRFC is employed. The MPE/XMRG, radar data used in this study, is not a new product in itself, but represents what the RFC forecaster decided to choose in real time among the different MPE products after introducing various additional corrections (*Habib, et al.,* 2013). Only the 1-hourly MPE/XMRG is utilized for the period from January 2002 to December 2012.

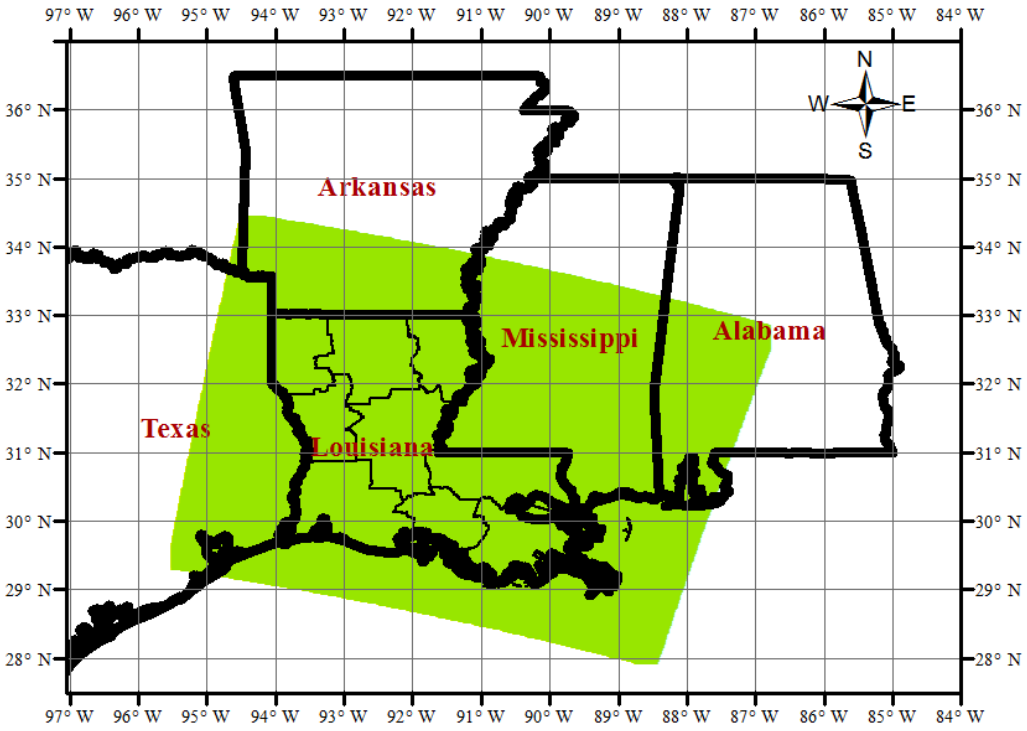

Figure 27 The 180x140 HRAP domain covering Lousiana.

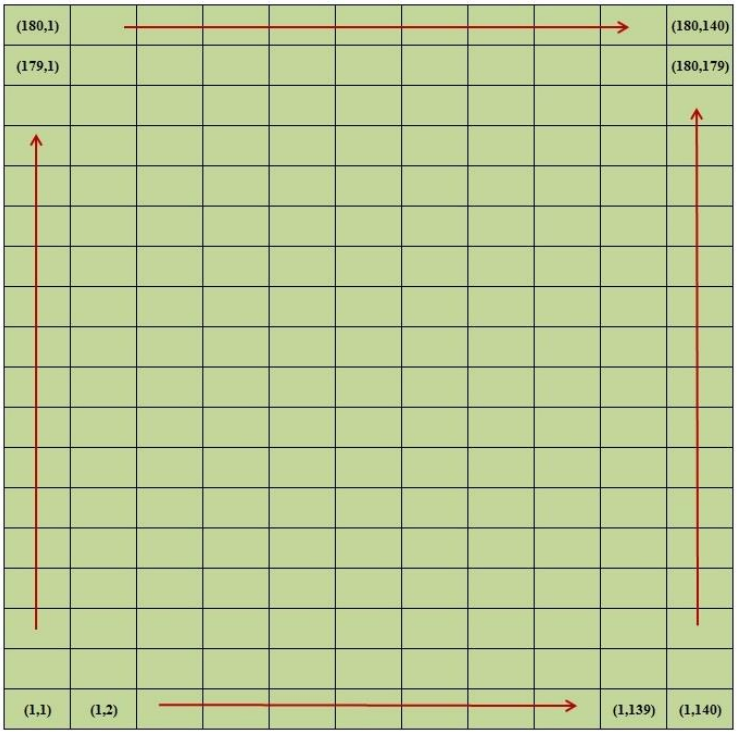

Figure 28 Numbering of Pixels in the study area.

Figure 29 Radars covering the study area in Louisiana.

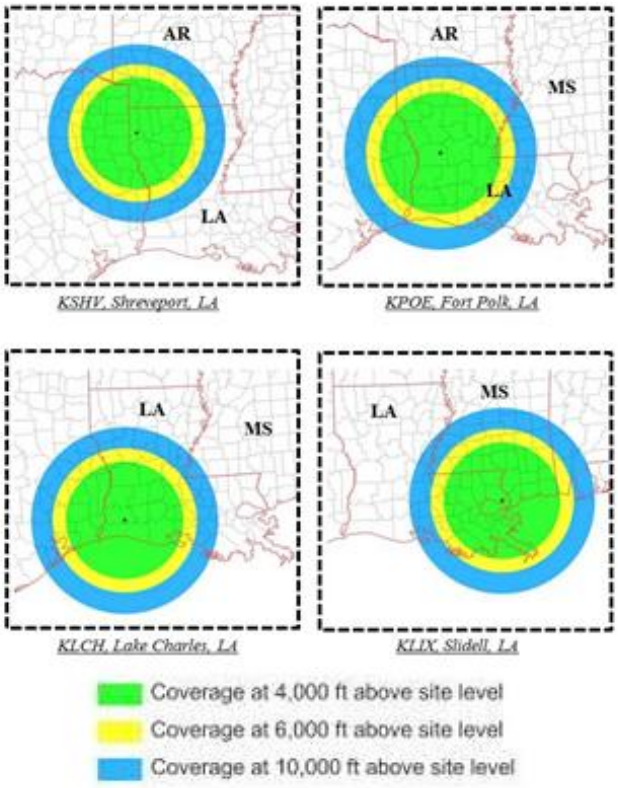

Figure 30 Area Scanned by radars in Lousiana (LA) (Source: *NOAA/NWS Radar Operations Center (ROC)* http://www.roc.noaa.gov).

Table 5 Radars deployed in Louisiana.

City	County	Site Name	Site ID	Radar ID	ICAO	Latitude	Longitude	Elevation (Feet)	Tower Height (Feet)	Agency
Shreveport	Caddo	SHREVEPORT	SHV	SHV	KSHV	32.450˚	-93.841 ˚	273	30	NWS/DoC
Fort Polk	Vernon	FORT POLK	POE	POE	KPOE	31.155 ˚	-92.975 ˚	408	15	AFWA/DoD
Lake Charles	Calcasieu	LAKE CHARLES	LCH	LCH	KLCH	30.125 ˚	-93.215 ˚	13	20	NWS/DoC
Slidell	ST. Tammany	SLIDELL	LIX	LIX	KLIX	30.336 ˚	-89.825 ˚	24	30	NWS/DoC

Although the complete dataset for the whole LMRFC domain is available (419 x 419 pixels), we are focusing only on the pixels covering Louisiana (180x140) to reduce the computational effort required for the frequency analysis (Figure 27). The pixels are numbered using transformed HRAP, i.e., local grids, by considering the lower left corner pixel as first pixel with transformed HRAP (1, 1) and the pixel at the upper right corner as the last pixel with transformed HRAP (180,140) (Figure 28). There are four radars deployed in Louisiana (Figure 29), three of these radars are operated by the National Weather Service, Department of Commerce (NWS/DoC), while the radar in Fort Polk is operated by Air Force Weather Agency, Department of Defense (AFWA/DoD) (see Table 5 for more identification information about the four radars). The area scanned by the radars in Louisiana at different elevations above site level is shown in (Figure 30).

5.2 Extreme Precipitation Series

Extreme precipitation events are rare events that are infrequent to occur and they are either heavy precipitation that causes floods or prolonged shortage in precipitation that may lead to drought. Studying these extremes and their statistics is very important in hydrological studies to describe the magnitude and probability of occurrence of such events. The rarity of precipitation events or climatological events in general, can be described in different ways and there is no one unique criterion to define an extreme event. For instance, in hydrological frequency analysis, series, which is a convenient sequence of data, hourly, seasonal, or annual observations of hydrological variables, is used to construct the statistical sample representing the heavy precipitation.

The extreme precipitation series are used in this study as a way to represent heavy precipitation. The two most common approaches to extract extreme for modeling series in hydrological applications are using the annual maximum or minimum series (AMS) and the partial duration series (PDS). The latter is also known as peaks over threshold (POT) approach. The AMS is a special case of the block maxima or minima model, which selects the largest or smallest events within each time block, e.g., each year. The PDS approach studies exceedances over an upper limit or predefined threshold as compared to maxima over fixed time periods in the AMS (*Chow, et al.,* 1988). A third and less common alternative, which partly combines the classical AMS and the PDS approach, is to select the r-largest events in each time interval of equal size (block) and it is possible to consider the whole time series as one block and extract r events from the total series. If r equals the number of observation years, it is referred to as annual exceedance series (AES) (*Tallaksen & van Lanen,* 2004). The AES is a special case of the PDS where the threshold is selected such that the number of values in the series (r) is equal to the number of years of the record. Figure 31 explains the difference between extracting annual exceedances and annual maxima for a 20-year record of hydrologic data. In this figure, only 16 of the 20 annual maxima appear in the annual exceedance series; the second largest value in several years outranks some annual maxima in magnitude. However, in the annual maximum series, these second largest values are excluded, resulting in the neglect of their effect in the analysis.

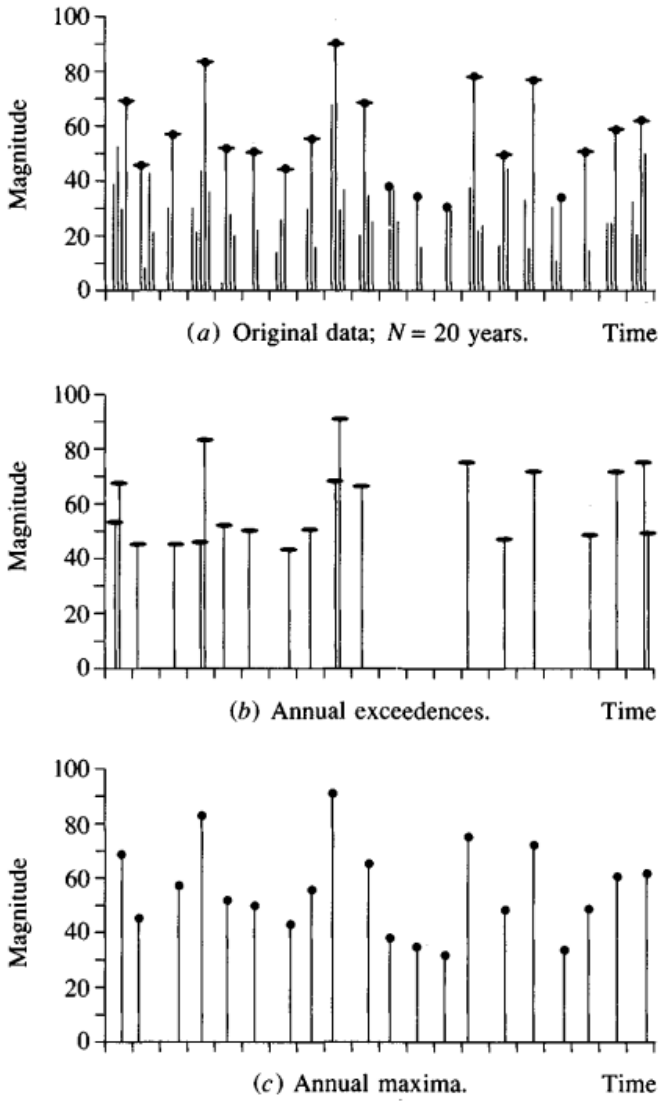

Figure 31 Hydrologic data series arranged by time of occurrence (Source: *Chow, et al.,* (1988)).

Various studies have been conducted to compare the use of AMS and PDS in modeling extreme hydrologic and the statistical distribution associated with each approach (e.g. *Martins & Stedinger,* (2001), *Madsen, et al.,* (1997), *Wilks,* (1993)). The AMS and PDS models have been widely used in modeling of extreme flow series and flood frequency analysis (e.g. *Bhunya, et al.,* (2012), *Cunnane,* (1973), *Franchini, et al.,*(2005)). In general, as the return period of the event being considered becomes large, the results from the two

approaches become very similar because the chance that two such events will occur within any year is very small (*Chow, et al.,* 1988).

In this study, the annual maximum series (AMS) is extracted for each pixel to construct a sample of 11 observations representing the maximum precipitation estimate in each year from 2002 to 2012. The use of AMS is chosen as it is very common in probabilistic analysis because of the availability of the data and the theoratical basis for extrapolating beyond the range of the observations (*El Adlouni & Ouarda,* 2010). On the other hand, the PDS model lacks the independence of consecutive events required for applying the classical extreme value theory and a criteria must be set to identify only independent peaks without considering multiple peaks that may belong to the same event. In general, the PDS model is considered more complicated to be applied in frequency analysis as opposed to the AMS model (*Stedinger, et al.,* 1993).

The hourly radar-rainfall observations used in this study are the clock-hour data, i.e., the observation once every hour at fixed time (this is also known as constrained observations). It is expected that the extracted (constrained) annual maxima will be lower than the unconstrained maxima. A factor to adjust statistical clock-hour data to 60-min values was determined empirically by NWS several years ago (*Bureau,* 1953; *Bureau,* 1954). It was found that, on the average, the N-yr 60-min value derived from the series of annual maximum 60-min events is 1.13 as great as the N-yr clock-hour value estimated from the series of annual maximum clock-hour values. This does not mean that a clock-hour annual maximum multiplied by 1.13 will give the maximum annual 60-min event in a particular case. This adjustment applies only to the results of a statistical analysis of a series of events. This factor was reduced in the NOAA Atlas 14 Volume 9 for the Southeastern States to 1.09

(*Perica, et al.,* 2013). Since this factor is very small and it may not affect the conclusions drawn from the statistical analysis of the precipitation data, we focus throughout this study on the results of the constrained AMS.

Although the results in this study are based only on AMS, conversion factors can be used to find the PDS estimates corresponding to the same return period. For instance, NOAA Atlas 14 frequency analysis is based on the AMS, and the PDS results are obtained using conversion factors that convert AMS estimates to PDS estimates. *Chow, et al.,* (1988) derived a mathematical formula to relate the return period in terms of both AMS and PDS:

$$T_{PDS} = \left[\ln\left(\frac{T_{AMS}}{T_{AMS} - 1}\right)\right] \quad (5.1)$$

5.3 Probability Distribution of Precipitation Annual Maximum Series (AMS)

The classical probabilistic extreme value theory deals with the stochastic behavior of the maximum and the minimum of independent and identically distributed (i.i.d) random variables. The distributional properties of extremes (maximum and minimum), extreme and intermediate order statistics, and exceedances over (below) high (low) thresholds are determined by the upper and lower tails of the underlying distribution (*Kotz & Nadarajah,* 2000). In climate applications and estimation of precipitation frequencies, many distributions have been suggested for modeling the extreme events, including the Generalized Extreme Value distribution (GEV), Generalized Pareto distribution (GP), gamma distribution, lognormal distribution and others. The GEV distribution was recommended for flood frequency analysis in the U.K. Flood Studies Report (*Madsen, et al.,* 1997). Moreover, according to the gauge-based Precipitation-Frequency Atlas of the United States, NOAA

Atlas 14, Volume 9 (*Perica, et al.,* 2013), the GEV distribution provided an acceptable fit to data more frequently than any other distribution and was chosen to model the annual maximum series of all the stations covering the US southeastern states (Alabama, Arkansas, Florida, Georgia, Louisiana and Mississippi). These conclusions were obtained using a goodness-of-fit test based on L-moment statistics for 3-parameter distributions along with the results of $\chi 2$ and Kolmogorov-Smirnov tests and visual inspection of probability plots. The reader is referred to *Hosking & Wallis,* (1997); *Chowdhury, et al.,* (1991) for more details on goodness of fit tests for different distributions (Generalized Logistic; Generalized Normal; Generalized Pareto; Pearson Type III; Kappa; Wakeby and Generalized Extreme Value distributions). *Naghavi & Yu,* (1995) studied extreme precipitation in Louisiana for regional frequency analysis purposes, and they conducted procedures suggested by *Hosking,* (1990) to identify the statistical distribution that best fits the data. They examined six different distributions: (1) normal; (2) Generalized Pareto; (3) Extreme Value type (I) (Gumbel); (4) Logistic; (5) Generalized Logistic; (6) Generalized Extreme Value (GEV), using L-moment ratio curves, i.e., L-Skewness and L-Kurtosis. They concluded that GEV distribution outperforms other distributions. For the current study, and based on prior results and recommendations, we will proceed with using the generalized extreme value distribution (GEV) to represent the annual maximum series (AMS).

The GEV distribution is a three parameter distribution developed within the extreme value theory to combine three different models. These models are Gumbel, Frechet and Weibull distributions, which are often referred to as Types (I), (II) and (III) distributions respectively. The probability density function of the GEV distribution, in terms of the three parameters: Location parameter (α), Scale Parameter (β), and Shape Parameter ($\kappa \neq 0$), is given by:

$$f_X(x) = \frac{1}{\beta}[1 - \frac{\kappa}{\beta}(x - \alpha)]^{(1/\kappa - 1)} F_X(x) \qquad (5.2)$$

where $F_X(x)$ is the cumulative distribution function (CDF) and given by:

$$F_X(x) = \exp\{-[1 - \frac{\kappa}{\beta}(x - \alpha)]^{1/\kappa}\} \quad \kappa \neq 0 \qquad (5.3)$$

The parameters space for the GEV distribution is $-\infty < \alpha$ (Location) $< \infty$, β (Scale) > 0 and $-\infty < \kappa$ (Shape) $< \infty$. It is worth noting that for $\kappa < 0$, then $\alpha+\beta/\kappa \leq x < \infty$ and the GEV distribution corresponds to the Type (II) Frechet distribution whose tails decrease at such a slow (i.e. power law) rate (heavy-tailed), such as Student's t and its moments are infinite for all orders greater than $1/\kappa$ (e.g., the variance is infinite if $\kappa > 0.5$; the mean is infinite if $\kappa > 1$). While for $\kappa > 0$, x is bounded by $\infty \leq x < \alpha+\beta/\kappa$ and the distribution in this case corresponds to the Type (III) Weibull distribution whose tails have a finite upper bound at $x = \alpha+\beta/\kappa$ (bounded tail), such as the beta. For $\kappa = 0$, the GEV distribution is reduced to the Gumbel distribution in which tails decrease at a relatively rapid (i.e., exponential) rate (light-tailed), such as the normal (*Katz, et al.,* 2005). The Type (I) extreme value distribution is also known as "double exponential" distribution due to the structure of the distribution function where there are two exponential functions (presence of right and left tails) (*Pal, et al.,* 2006).

Figure 32 shows how the probability density function changes with the variation in the distribution parameters. The upper left panel displays the three different types of extreme value distribution and how the tails look like for each type. The three distributions are constructed for the same location and scale parameters ($\beta=1$ & $\alpha=0$), while the shape parameter varies according to the distribution type, i.e., $\kappa=0$ for Gumbel distribution, $\kappa=-1$ for Frechet distribution and $\kappa=1$ for Weibull distribution. The upper right panel shows the

change in the distribution function with changing the shape parameter and keeping the other two parameters constant. The shape parameter affects the range of the random variable x and identifies how the tail of the distribution is decaying. The change in location parameter is simply shifting the distribution by a value proportional to the value of the location parameter as shown in the lower left panel. In the lower right panel the scale parameter is stretching or shrinking the distribution to describe its dispersion.

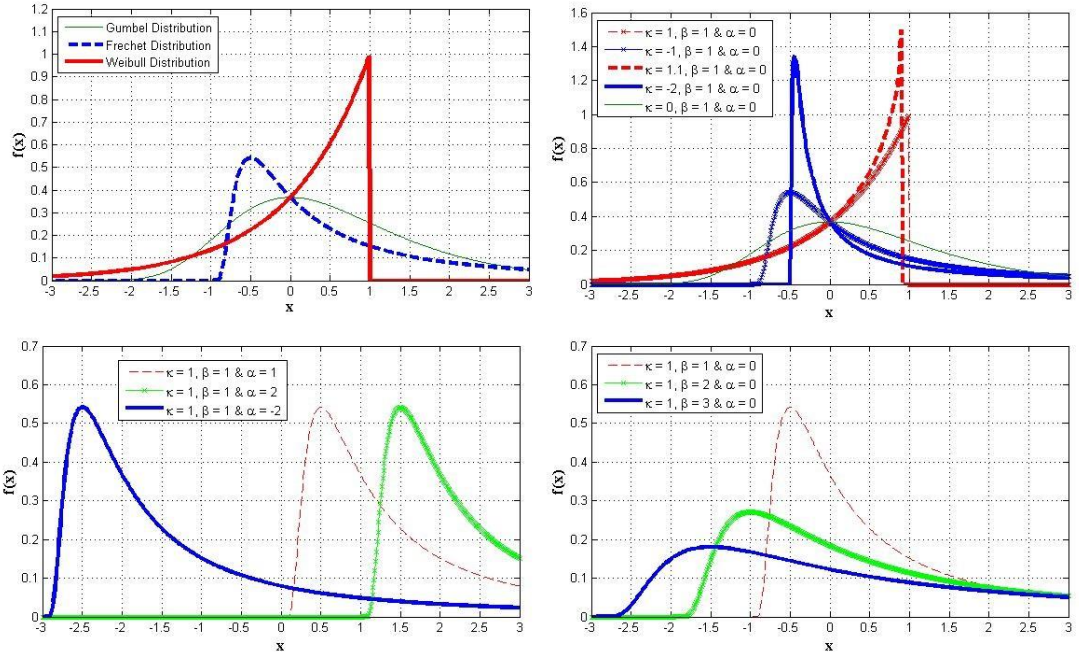

Figure 32 The three GEV distributions and the effect of changing parameter values on the distribution shape.

The quantiles of the samples modeled using the GEV distribution are estimated using the inverse of the CDF equation:

$$\xi(q) = \alpha + \frac{\beta}{\kappa}[1 - (-\ln q)^{\kappa}] \tag{5.4}$$

where $\xi(q)$ is the quantile estimator and q is the cumulative probability F(x) that can be described in terms of the return period (T) by the Annual Exceedance Probability (AEP):

$$\mathrm{AEP} = \frac{1}{\mathrm{T}} \tag{5.5}$$

$$\mathrm{F(x)} = 1 - \frac{1}{\mathrm{T}} \tag{5.6}$$

5.4 Parameter Estimation

The use of probability-weighted moments (PWM) has gained popularity in hydrologic frequency analysis since the late 1970 (*Sveinsson, et al.,* 2001). In this study, the method of linear moments (LMOM) is used for the estimation of the GEV distribution parameters. There are many advantages of using the method of L-moments over using the conventional method of moments. For example, L-moments are able to provide more information about the shape of the distribution even with using small samples as opposed to the method of moments that sometimes fails to describe the distribution shape. L-moments are more robust to the presence of outliers in the data and the parameter estimates obtained are sometimes more accurate in small samples than even the maximum likelihood estimates (*Hosking,* 1990). The performance of maximum likelihood can be extremely erratic for small samples ($n \leq 25$) in the estimation of extreme quantiles of the GEV distribution. This is mainly attributed to the theoretical basis of ML method in which the primary justification for ML arises from its asymptotic properties (i.e., for large samples) (*Katz, et al.,* 2002). Using Monte-Carlo simulations, *Martins & Stedinger,* (2000) compared the performance of different estimation methods, including the method of moments, method of maximum

likelihood and the method of L-moments, for the quantile estimators for the GEV distribution for small samples. They concluded that the ML estimations for the GEV distribution can result in unreasonable shape parameter (κ) estimates in small samples and poor performance for quantile estimators. For instance, they generated a small sample of 15 observations from a GEV distribution with κ=-0.2 and the true value for the 0.999 quantile is 14.9; however, the ML estimators are -2.48 and order of 6 x 10^6 for the shape parameter and the 0.999 quantile respectively (Figure 33). This biased estimators led to the use of Bayesian prior distributions to restrict estimated values to a statistically/physically reasonable range in a generalized maximum likelihood (GML) estimators. Although the GML quantile estimators should be preferred for at-site analysis, L-moments are still useful to compute unbiased estimators of κ for use in regionalization (provided that κ is not too negative), to describe characteristics of data, and to provide a good basis for goodness-of-fit tests (*Martins & Stedinger,* 2000).

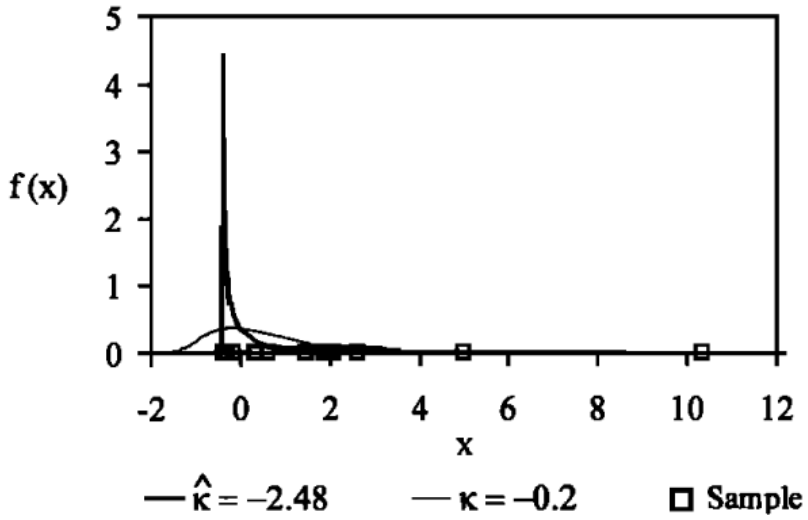

Figure 33 True (κ=-0.2) and estimated ($\hat{\kappa}$=-2.48) distribution for a small sample (N=15) (Source: *Martins & Stedinger,* (2000))

The probability-weighted moments of a random variable X with distribution function F(x) = P(X < x) are:

$$M_{p,r,s} = E[X^p\{F(X)\}^r\{1 - F(X)\}^s] \qquad (5.7)$$

where p, r, and s are real numbers (*Greenwood, et al.,* 1979). Probability- weighted moments are likely to be most useful when the inverse distribution function x(F) can be written in a closed form:

$$M_{p,r,s} = \int_0^1 \{x(F)\}^p F^r (1 - F)^s dF \qquad (5.8)$$

When r and s are integers, $F^r(1 - F)^s$ may be expressed as a linear combination of either powers of F or powers of (1 - F). As such, it is possible to summarize a distribution either by the moments $M_{l,r,0}$ (r = 0, 1, 2, ...), or by $M_{l,0,s}$ (s= 0, 1, 2, ...) (*Hosking, et al.,* 1985). Considering the moments $\beta_r = M_{l,r,0} = E[X\{F(X)\}^r]$ (r = 0, 1, 2, ...) and given a random sample of size n from the distribution F, estimation of β_r is most conveniently based on the ordered sample $x_l < x_2 <\ldots\ldots.< x_n$. An unbiased estimate of β_r, when r is a non-negative integer, is given by

$$\hat{\beta}_r = \frac{1}{n}\binom{n-1}{r}^{-1} \sum_{j=r+1}^{n} \binom{j-1}{r} x_j \qquad r=0, 1, 2,..... \qquad (5.9)$$

where the x_j, j = 1, ... , n, have been ordered from x_j, the smallest, to x_j, the largest (*Landwehr, et al.,* 1979). These PWMs can be expressed as linear combinations of L-moments, so procedures based on PWMs and on L-moments are equivalent. L-moments are more convenient, however, because they are more directly interpretable as measures of the scale and shape of probability distribution (*Hosking,* 1990).

In terms of probability weighted moments, L-moments are defined by

$$\lambda_1 = \alpha_0 = \beta_0 \tag{5.10}$$

$$\lambda_2 = \alpha_0 - 2\alpha_1 = 2\beta_1 - \beta_0 \tag{5.11}$$

$$\lambda_3 = \alpha_0 - 6\alpha_1 + 6\alpha_2 = 6\beta_2 - 6\beta_1 + \beta_0 \tag{5.12}$$

$$\lambda_4 = \alpha_0 - 12\alpha_1 + 30\alpha_2 - 20\alpha_3 = 20\beta_3 - 30\beta_2 + 12\beta_1 - \beta_0 \tag{5.13}$$

In general, the $(r + 1)^{th}$ L moment, λ_{r+1}, is defined as

$$\lambda_{r+1} = \sum_{k=0}^{r} (-1)^{r-k} \binom{r}{k} \binom{r+k}{k} \beta_k \tag{5.14}$$

For example, λ_1 is the mean of the distribution, and λ_2 is a measure of the scale or dispersion of the random variable. L-moment ratios are standardized (dimensionless) L moments that measure the shape of a distribution independently of its scale ad they are defined by:

$$\tau_2 = \frac{\lambda_2}{\lambda_1} \tag{5.15}$$

$$\tau_r = \frac{\lambda_r}{\lambda_2} \quad r=3, 4..... \tag{5.16}$$

where τ_2 (L CV), τ_3 (L skewness), and τ_4 (L kurtosis) are alternative measures of coefficient of variation, skewness, and kurtosis, respectively. The L-moment estimators for the GEV distribution parameters are given as follows:

$$\hat{\kappa} = 7.8590c + 2.9554c^2 \tag{5.17}$$

$$c = \frac{2}{(3 + \hat{\tau}_3)} - \frac{\log(2)}{\log(3)} \tag{5.18}$$

$$\hat{\alpha} = \hat{\lambda}_1 - \frac{\hat{\beta}}{\hat{\kappa}}[1 - \Gamma(1 + \hat{\kappa})] \tag{5.19}$$

$$\hat{\beta} = \frac{\hat{\lambda}_2 \hat{\kappa}}{(1 - 2^{-\hat{\kappa}})\Gamma(1 + \hat{\kappa})} \tag{5.20}$$

5.5 At-site and Regional Precipitation Frequency Estimation

Frequency analysis is the estimation of how often a specified event will occur. It is of particular importance to study the frequency of extreme events because there are numerous sources of uncertainty about the physical processes that give rise to these events (*Hosking & Wallis,* 1997). Estimated quantiles corresponding to various return periods or frequencies and for different durations are usually summarized in the form of IDF curves from which design storm hyetographs can be derived. This information is then useful for the design and management of urban drainage infrastructure, bridges, spillways, and risk analysis for landslide hazards, among many other applications (*Hailegeorgis, et al.,* 2013).

In this section, two approaches for the frequency analysis of extreme precipitation are described; pixel-based and region-based estimation methods. The uncertainties in the estimates due to sampling effect will be assessed using bootstrap techniques and quantified in terms of confidence bounds. The results of each method will be for the different quantiles will be compared to the corresponding gauge-based estimates that are reported in the NOAA Atlas 14 Precipitation Frequency Estimates (*Perica, et al.,* 2013).

5.5.1 Pixel-Based Frequency Analysis

This approach is mainly analogous to at-site frequency analysis of extreme precipitation extracted from rain gauge observations at a certain station. For the entire domain, each 4-km x 4-km HRAP radar pixel is treated as a single station. This is equivalent to considering the domain of study as a dense network of "stations" that are located 4 km apart from each other. At each pixel, the Annual Maximum Series (AMS) is extracted from the 11-year radar dataset to yield an AMS sample with a size N=11. The AMS at each pixel is fitted to the GEV model and the parameters of the distribution are estimated at each pixel using the L-moment method as described in section (5.4). The quantiles corresponding to different return periods (1, 2, 5, 10, 20, 25, 50, 100, 500, & 1000 years) are estimated at each pixel using the parameters estimated for each AMS sample. This approach was applied in the technical reports published earlier by the National Weather Service (NWS), formerly Weather Bureau, to establish the rainfall frequency isohyetal maps for the United States (See section 3.1for NWS studies).

The confidence limits for the parameters and quantiles estimates are constructed using bootstrap techniques. The classical scalar bootstrap procedure suggested by *Efron,* (1979) is usually employed in single-site analysis (i.e., at-site estimation). The bootstrap procedures can be used to make inference on the estimates without making assumption on its distribution. The basic idea behind the non-parametric bootstrap is to replicate the original sample many times, sampling it with replacement, and to analyze the behavior of the statistic of interest calculated on these replicates. Many aspects of the behavior of the selected statistic can be measured with bootstrap, for example its confidence intervals. This bootstrap

procedure is used to generate a large number of samples (500 in our case) for each individual pixel.

5.5.2 Region-Based Frequency Analysis

For sites with sufficient record length with respect to the return period of the extreme precipitation quantile of interest, at-site frequency analysis can be considered as an adequate approach. However, for some sites data may not be available at all (i.e., un-gauged sites), or the historical records may not be long enough to be able to make reliable prediction of extreme quantiles especially for larger return periods. Hence, data augmentation may be performed by using extreme precipitation records from other sites within a representative region (*Hailegeorgis, et al.,* 2013). For example, a regional frequency analysis approach was adopted by the NOAA Atlas 14 (*Perica, et al.,* 2013). *Cunnane,* (1988) explained twelve different regional frequency approaches used in the literature and discussed the accompanying choice of distribution. These regional analysis techniques have been shown to offer the ability to reduce the uncertainties in quantile estimation of extreme events relative to the conventional at-site analysis (*Pilona, et al.,* 1991).

A Spatial Bootstrap Technique for Regional-Based Estimation:

In this study, a probability weighted regional sample approach is employed to estimate the precipitation frequencies. This method was recently proposed by *Uboldi, et al.,* (2014) as a resampling approach for estimation of parameters of rainfall annual maximum series statistical distribution. It can also be used to construct uncertainty bounds for the parameters estimated and for the rainfall depths at assigned return periods. This technique incorporates the generation of a regional sample at any desired location by taking into account all data

observed at surrounding stations with decreasing importance when distance increases. As such, the probability of contribution of a certain station decreases as it goes far away from the station at the desired location. The probability of sampling also takes into consideration the length of the time series at each station, and as such, the possibility of over sampling can be avoided and the use of short time series is enabled. This method is basically a spatial bootstrap technique in which a regional sample is generated repeatedly from the surrounding locations (pixels) based on the randomness produced from the probability of data extracting.

The procedures of this approach involves formation of a homogenous region, construction of regional sample, estimation of statistical distribution parameters, repeating of the regional sampling and parameter estimation several times as in any bootstrap technique, and finally obtain a distribution of estimates for each parameter. The mean of such distribution is finally used as the actual estimate, while the standard deviation measures its associated uncertainty, due to sample variability.

The regional synthetic sample of size (N) is constructed by extracting (N) observations randomly from all of the available data (M) in a homogenous region. The probability of extraction of each observation is assumed to be proportional to a prescribed Gaussian function (γ_m) of the distance between the station at the desired location (X) and any other station (K_m). Therefore, for each pixel at a desired location X, and by prescribing distance-dependent extraction probabilities, observations from nearby pixels are selected more often than observations from stations located far away. The probability of extraction of the m^{th} observation located at a pixel (K_m) is given by the following relation:

$$\gamma_m = \exp\left\{-\frac{1}{2}\left[\frac{d_h(X,k_m)}{D_h}\right]^2\right\}.\exp\left\{-\frac{1}{2}\left[\frac{d_v(X,k_m)}{D_v}\right]^2\right\} \qquad (5.21)$$

where $d_h(X,K_m)$ and $d_v(X,K_m)$ are the horizontal and vertical distance between pixel K_m and the pixel at the desired location (X). The D_h and D_v are scale parameters that are selected to impose some degree of smoothing and were chosen in this study to be close to the standard deviation of the available distances between (X) and (K_m).

The probability of extraction of each observation is then normalized by the sum of probabilities of all the observations (M):

$$\Gamma = \sum_{m=1}^{M} \gamma_m \qquad (5.22)$$

Therefore, the probability of extraction of each observation from N set of available observations becomes:

$$\bar{\gamma}_m = \frac{\gamma_m}{\Gamma} \qquad (5.23)$$

By sorting the (M) observations in a descending order according to their probability of extraction $\overline{\gamma_m}$ and assigning each observation a number (m) from 1 to M, a series of sequential ordered dataset is obtained. The cumulative normalized probability of extraction $\overline{\Gamma_m}$ of each observation $\overline{\gamma_m}$ ranges between [0,1] and the probability of extraction of this cumulative probability $\overline{\Gamma_n}$ is assumed to be uniformly distributed, i.e. $\overline{\Gamma_m} \sim U(0,1)$. A continuous random variable (ρ) can be used to implement a random number generator for a discrete random variable (m) with any prescribed (non-uniform) probability distribution on positive integers up to a generic M. By generating a random number (ρ), the corresponding

cumulative probability $\overline{\Gamma_m}$ is equal to the generated random number (ρ) and realization number (m) is equal to the first observation that has cumulative probability greater than or equal to the generated probability (ρ).

Selection of Homogeneous Regions:

The spatial bootstrap region-based approach requires the formation of a homogenous region surrounding each pixel, from which a regional sample can be constructed. The identification of homogenous regions is usually the most difficult stage in the regional frequency analysis and it requires the greatest amount of subjective judgement (*Hosking & Wallis,* 1997). The term homogeneity is predominantly used in statistics to describe the connection between samples from different populations which may, or may not, exhibit identical behavior or display similar characteristics (*Heiser & Meulman,* 1992).

Homogenous region is the area including a group of sites, or pixels as in the case of radar fields, that share similar site physical characteristics and at-site statistics. Regionalization, in the context of flood frequency analysis, refers to identification of homogeneous regions and selection of appropriate frequency distributions for the identified regions. The advantages of working with a homogeneous region is that the historical data available within the region can be pooled to get an efficient estimate of parameters of a chosen distribution and hence a more robust quantile estimate (*Kachroo , et al.,* 2000). (*Hosking & Wallis,* 1997) strongly prefered to base the formation of homogenous regions on site characteristics (e.g. geographical delineation, cluster analysis, principle components analysis) and to use the at-site statistics only in subsequent testing of the homogeneity of the proposed set of regions. Moreover, the convenetional regionalization techniques identify a fixed set of sites to form a contiguous

region and hence, fixed boundary regions will be constructed without smooth transition across these boundaries. *Burn,* (1990a, 1990b) presented Region of Influence (ROI) approach for defining homogenous region, in which every site can have a potentially unique set of gauging statations for use in the estimation of at-site extremes.The ROI technique is recommended as it avoids the transition problems across fixed boundaries by introducing smooth change in the estimates across the boundaries of the regions. The selection of the radius of influence is a trade-off problem, in which larger radius R values will increase the number of sites included in the ROI, but the homogeneity of a set of sites can be expected to decrease. Conversely, a smaller radius R will result in an increase in the homogeneity of the sites included, but the information transfer will be decreased due to the smaller number of pixels.

The questions involoved in identifying the homogenous regions when using radar estimates with uniform gridded pixels can be summarized as follows:

1. Define a region with similar climatic and physical characteristics.

2. Define a region with similar at-site statistics.

3. Specify a radius of influence that encompass the similar pixels to allow smooth transition.

4. Looking for a unique radius of influence that is appropriate for all the pixels in order to reduce the computationl effort required.

Although *Durrans, et al.,* (2002) estimated the precipitation frequencies using radar-based QPEs, the conventional regionalization approaches were not utilized in this study. They

applied a smoothing algorithm to the estimates of the sample L-moments to reduce the effects of sampling variations caused by the short time series and this smoothness technique implements a form of regionalization to the estimates.

In this study, the region of influence (ROI) approach is applied by assuming same number of pixels (Radius of influence R) surrounding the pixel of interest from all directions. The region bounding each pixel forms a square window of area $(2R+1)^2$ as shown in Figure 34. The window is moving on each pixel to construct the regional sample from the pixels lying inside this window (Figure 35). The window crosses each pixel is expected to form a homogenous region surrounding this target pixel (central pixel).

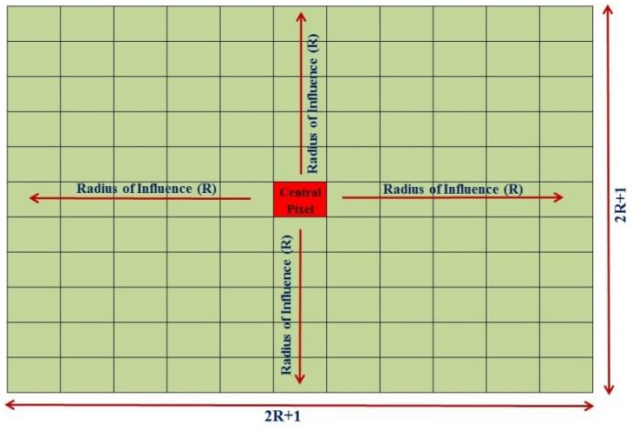

Figure 34 The Radius of Influence approach applied on radar pixels.

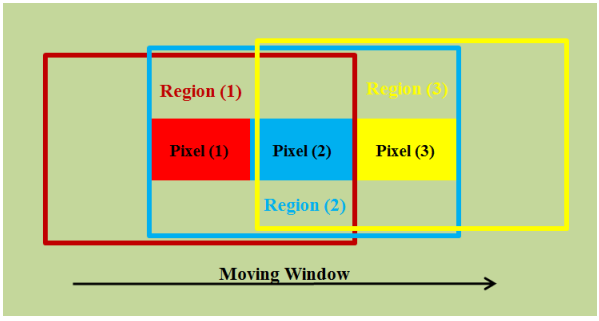

Figure 35 The moving widow forming homogenous region for each pixel.

As mentioned above, the choice of a homogenous region, or the window size, has to be based on climatic and physical characteritics. The U.S. Climate Divisions are used in this study to give an indication for the reasonable range of the radius of influence (R) that can be applied. Each of the 48 contiguous U.S. states has been subdivided into as many as 10 climate divisions, depending upon the size of the state (see for example Figure 36). The divisional boundaries are structured such that they often coincide with county boundaries and always cover the total area of the state (*Guttman & Quayle,* 1996).

Figure 36 Louisiana Climate Divisions (Source: *NWS/Climate Prediction Center*).

While climate divisions might not be the best representation for depicting regional climate anomalies, especially for extreme precipitation, it can be used to give some insight into the range of radius of influence (R) that can be applied. Louisiana parishes are clustered into nine Climate Divisions and the average surface area of each climate division is approximately covering a window with side length of about 31 pixels, which corresponds to R=15 pixels. Therefore, based on these preliminary results, R=15 is chosen as a threshold for homgenous climatic region. *Hosking & Wallis,* (1997) presented statistical procedures to estimate

homogenity measures based on the variations in the L-moment ratios ,i.e., L-CV and L-Skewness. These measures can be used to identify one radius of influence and forms homogenous region around each pixel. This approach can be highly inefficient compuationally due to the large number of pixels within the domain of interest. In this study, instead of using homogenity statistics, two different square windows (R=5, 10) will be tested to study the effect of the region size on the uncertainty of the estimates. As shown in Figure 37, using radius of 5 pixels will result in a window of 11x11 pixels with the potential to extract observations from 121 different pixels, each with record length of 11 years (M=11 observations x 121pixels). Increasing the window size to 21x21, by using radius of influence=10 pixels, will allow for many more pixels (441 pixels and M=11observations x 441 pixels) to be included in the region of each target pixel. The scale parameters in equation (5.21), i.e., D_h and D_v, are chosen equal to approximately the standard deviation of of each radius of influence (for R=5, D_h=D_v=1pixel and for R=10, D_h=D_v=3pixels). The regional sample size is chosen to be the same as the actual number of years available in the radar dataset, i.e., N=11.

In order to reduce the likelihood of extracting annual maxima that might be come from the same event, a constarint is added to the observation when extracted. This constraint implies that the gap in the time stamp of any two annual maxima must be greater than 6 hours. This criteria is evaluated using the Julian Date (continuous count of days and fractions of day since the beginning of the Julian Period used primarily by astronomers) in which the 6 hours represent 0.25 day. For instance, if one annual maxima extracted occurs with a certain Julian Date (JD), then any new annual maxima must be checked that it occurs with new Julian Date greater than (JD+0.25) or smaller than (JD-0.25). This restriction to the extraction of annual

maxima might not be very useful in case of gauges since the gauges are scattered without any uniform distribution and usually with relatively large distances in between and therefore it is less probable to have annual series in two gauges that share exactly the same events magnitude. On the other hand, the application of this conditioned extracted annual maxima is very critical to the radar-based annual maxima, since they are provided on a uniform grid with very high spatial resolution of 4x4 km.

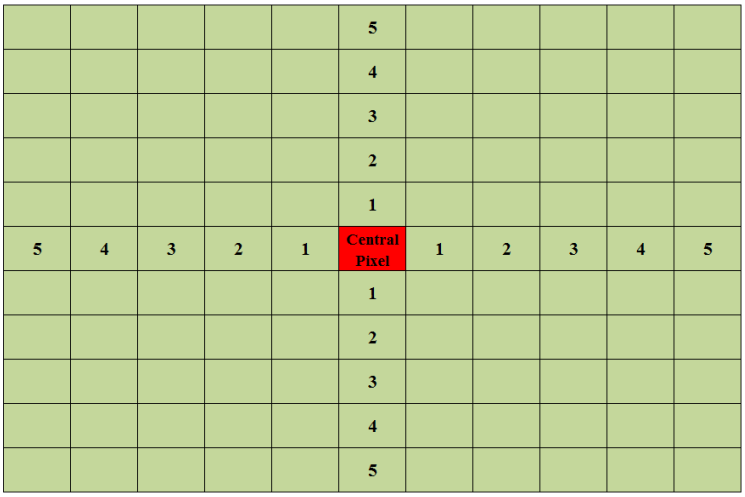

Figure 37 The moving window with radius of influence R=5 pixels.

Some remarks on the spatial bootstrap technique are stated as follows:

1. The distance-dependent function given above could encompass other factors that might affect the probability of extraction, for instance (*Uboldi, et al.,* 2014) used the elevations above mean sea level as one more aspect to calculate the probability of extraction (γ_m). In addition to considering site characteristics such as location and elevation, this technique can be developed by introducing some physical properties associated with each site like the mean annual precipitation (MAP) that has been widely involved in cluster analysis procedures for formation of homogenous regions.

2. Distance-dependent probabilities (γ_m) are assigned to individual observations, rather than to stations, to avoid oversampling from "short" time series located near the target point (X).

3. Oversampling from nearby stations with only few data is effectively avoided by assigning distance-dependent probabilities to individual observations, rather than to stations, and normalizing with the sum of probabilities of all observed values, therefore, all observations from the same station still have the same probability, but the probability of extracting from a particular station depends both on distance and on the size of its observation set, i.e. the length of its time series.

4. This technique uses the stationarity hypothesis, where the actual order in time of the sampled observations is not important, and as such the time coordinate is not used in the parameter estimation. On the contrary, if stationarity is an issue, sampling could be performed by prescribing extraction probabilities that effectively ensure uniformity in time (for example, by extracting one observation, or a fixed number of them, for each year). In that case nonstationary extreme value analysis should be applied by using time coordinate in the estimation (see for example *Sugahara, et al.,* (2009), *Hanel, et al.,* (2009) & *Gregersen, et al.,* (2013)) to consider assumed time dependent patterns for some of the distribution parameters.

Chapter 6 Results on Precipitation Frequency Estimates

6.1 Characteristics of Annual Maxima

The Radar precipitation estimates provide new possibilities to investigate the climatology of extreme rainfall at high spatial resolutions and over large areas (*Overeem, et al.,* 2009). Lousiana is considered the wettest of the contiguous 48 states with extreme events that are generated by several rainfall mechnaisms. The extreme events in the Southeastern United States are typically generated from different synoptic weather patterns, for example, tropical storms, fronts, and convective airmass thunderstorms. *Faiers, et al.,* (1994) analyzed the differences in the different synoptic weather type frequencies of the three-hour extreme events in four different locations in Louisiana (Shreveport, Lake Charles, Baton Rouge and New Orleans) for the period from 1948 to 1991. They concluded that there are no significant differences in synoptic weather type frequencies between the different locations, mainly due to the dominance of the frontal events. Moreover, the Gulf Tropical Disturbance (GTD) and airmass events are very frequent in New Orleans which is a good evidence for the occurrence of tropical storms and hurricanes in this area. All of these conclusions are consistent with the proximity of Louisiana to the Gulf of Mexico.

Figure 38 shows the maximum annual hourly rainfall depth for each pixel in the domain of the study area. Most of the pixels maxima are in the range between 20 mm and 100 mm with a significant increase in the annual maxima towards the gulf coastal zone. The Mean Annual Maxima (MAM) displayed in Figure 38 shows a gradual increase moving from areas in northern Louisiana towards the southern part of the state close to the Gulf Coast.

Maddox, et al., (1979) examined the meteorological conditions associated with more than 150 intensive convective precipitation events that cause flash floods over the conterminous United States (CONUS) excluding the heavy tropical events. They reported that the monthly distribution of extreme events reveals the predominance of July where 25 % of the sample was located, simply due to the convective nature of the studied events. These results agree with Figure 39 which depicts the spatial distribution of average month of occurrence for annual maximum rainfall and shows dominance of the summer season (June – July – August) throughout most of the state. This is also shown from the histogram in Figure 40 of the percentage of occurrence of AMS in each month. The highest frequency of AMS is reported in the warm season (April-September), which again indicates that most of these extreme events are of convective nature.

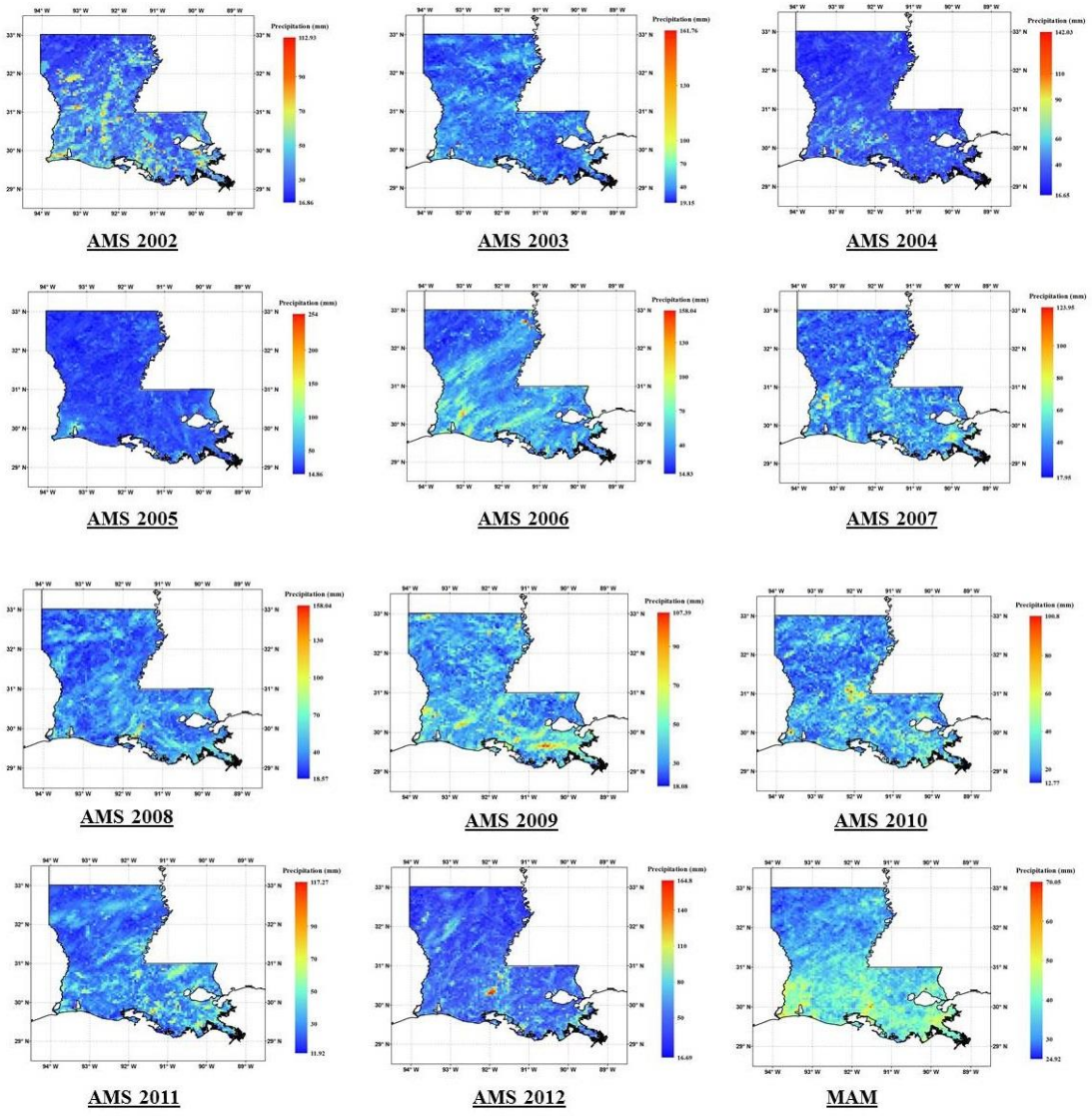

Figure 38 The annual maximum rainfall estimate for each pixel extracted for the years from 2002 to 2012.The last panel shows the mean annual maximum (MAM) for each pixel.

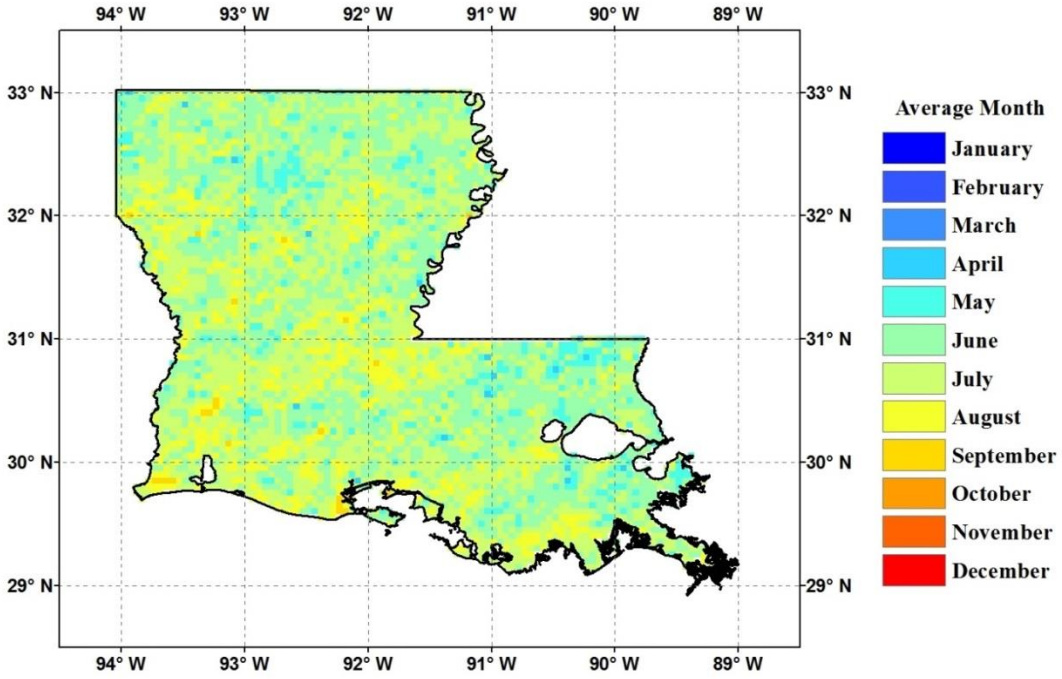

Figure 39 The average month of occurrence for the AMS in each pixel during the period of study (2002-2012).

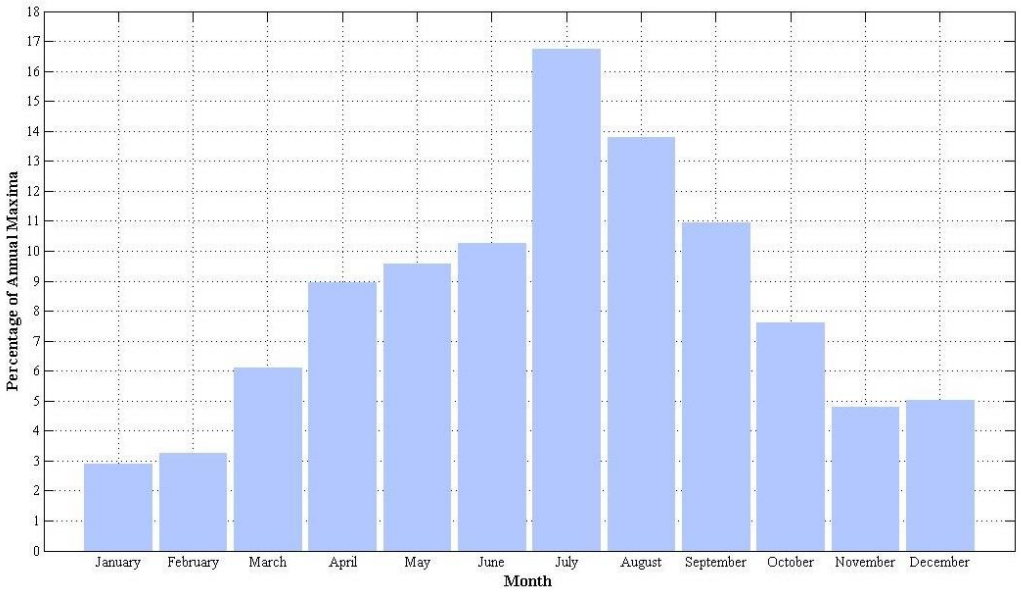

Figure 40 Frequency of occurrence (histogram) of the AMS in each month of the year during the period of study (2002-2012).

The diurnal distribution of the annual maxima is explained through the studying the average 6-hour of annual maxima occurrence (Figure 41 and Figure 42). The two figures show the spatial distribution and the frequency of occurrence of AMS for each hour of the day during the period of study. The results indicate that most of the annual maxima occured between 18:00 UTC and 00:00 UTC, fewer number of events ocuured in the two intervals (00:00 UTC – 06:00 UTC) and (12:00 UTC- 18:00 UTC), while nearly no events occured in the hours between 06:00 UTC and 12:00 UTC. The histogram in Figure 42 shows that the maximum extreme events occcurs more frequently at hour 21:00 UTC. A similar conclusion was reported by *Schumacher & Johnson,* (2006) who studied the characteristics of a large number of extreme rain events over the eastern two-thirds of the United States and found that the diurnal distribution has an average peak time at 21:00 UTC.

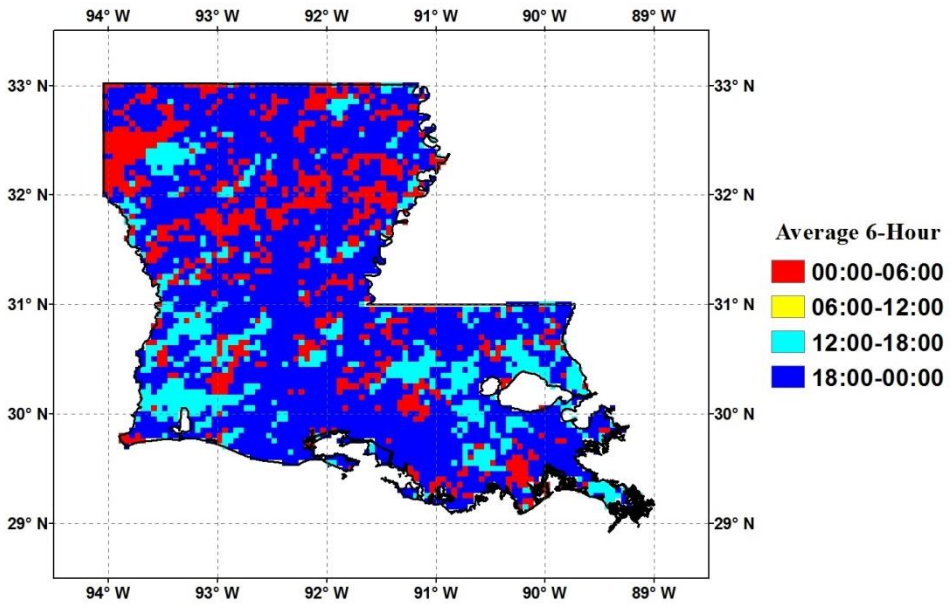

Figure 41 The average 6-hour of occurrence for the AMS in each pixel during the period of study (2002-2012).

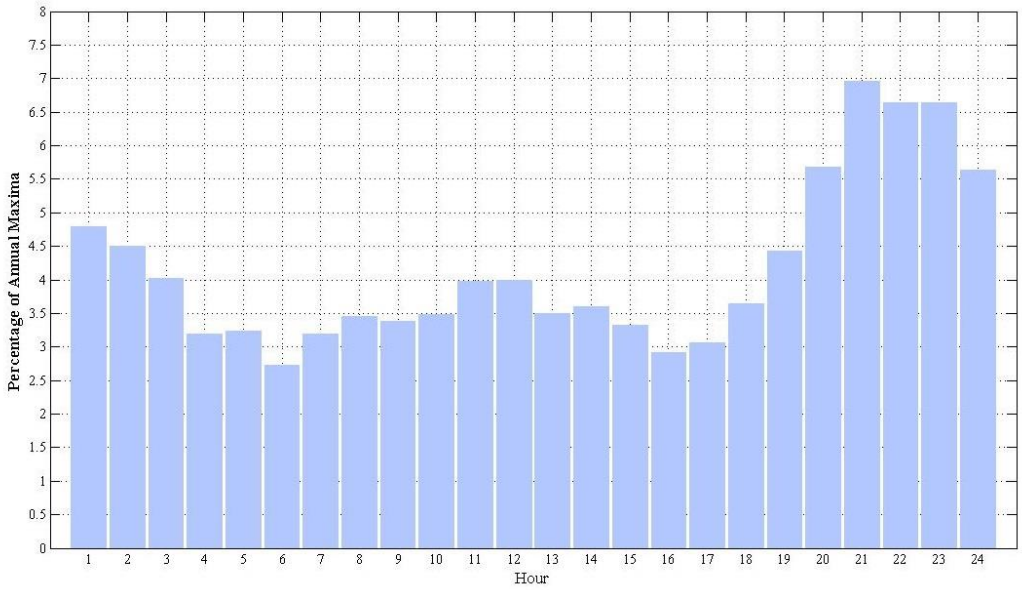

Figure 42 Frequency of occurrence (histogram) of the AMS in each hour of the day during the period of study (2002-2012).

The average occurrence of the extreme events during the 11 years of the study period is studied in each decade of the month, i.e. every ten days of the month, and for each day of the month. The variation in the average occurrence of the extreme events is given in the spatial map shown in Figure 43 and the frequency of AMS in the 36 decades of the year is given in Figure 44. As expected, these results don't show the dominance of a certain day or decade of the month.

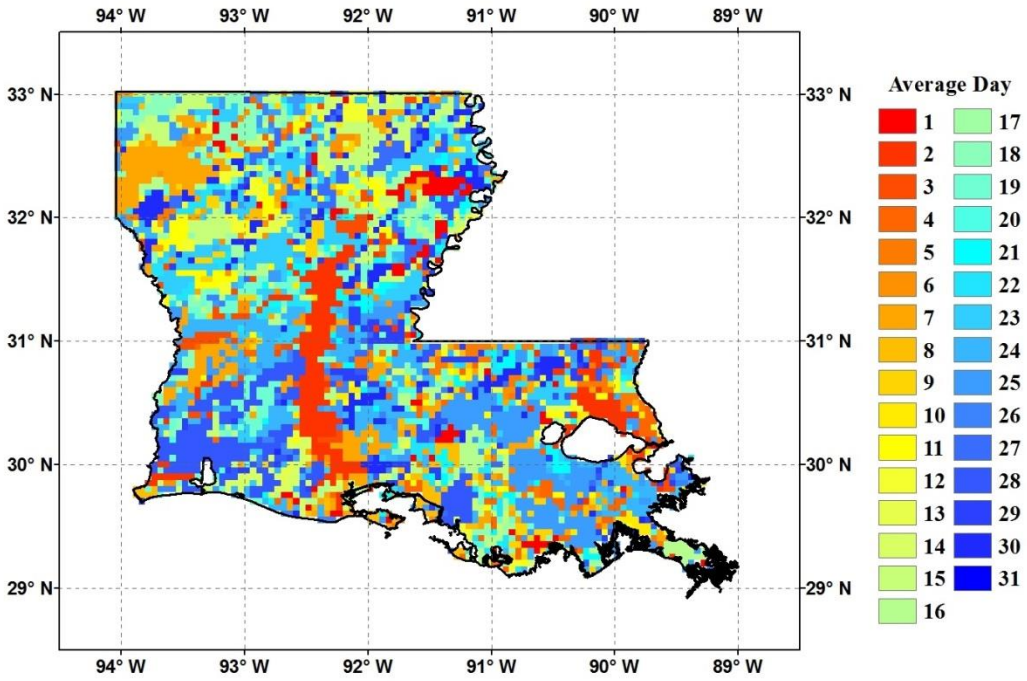

Figure 43 The average dates of occurrence for the AMS in each pixel during the period of study (2002-2012).

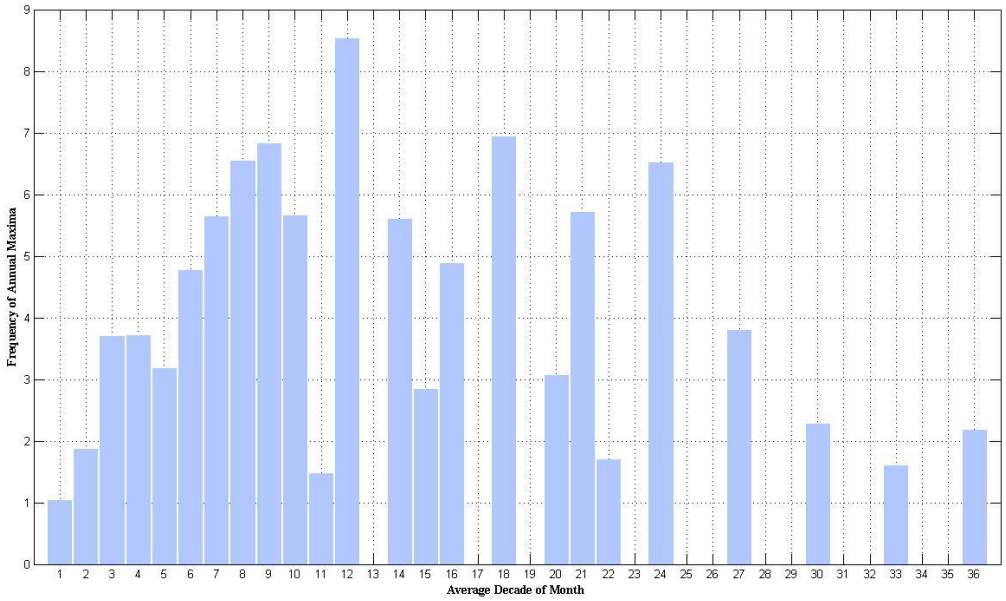

Figure 44 The frequency of the annual maxima corresponding to the decade of the month during the year.

6.2 Pixel-Based Precipitation Frequency Estimates (PFEs)

The pixel-based estimation procedure described in Section (5.5.1) was applied to the radar dataset to estimate the GEV distributional parameters and the corresponding quantiles (PFE) at different return periods ranging from 2 to 100 years. The bootstrap technique was also applied at each pixel to construct the confidence intervals for the estimated parameters and quantiles. The parameters and the precipitation frequency estimates for each pixel are represented using the mean of the 500 runs of bootstraps. The lower 5% and upper 95% quantiles of the bootstrap samples are used to assess the uncertainty in the estimates. The upper and lower quantiles can be calculated in different ways, some are parametric that assume normal distribution for the estimates obtained from bootstrap runs, while others are non-parametric methods which don't pre-assume any kind of distribution (*Langford ,* 2006). The method used in this study is a non-parametric method, in which a probability is initially assigned to the sorted values of the sample ((0.5/n), (1.5/n), ..., ([n – 0.5]/n)), where n is the sample size, i.e., n=500 runs. The quantiles are then computed as the probability equal to the confidence limit required, e.g. 0.95, 0.90, 0.05, or 0.1. Quantiles for intermediate values are calculated using linear interpolation. The first and last value in the bootstrap sample are assigned to the quantiles for probabilities less than (0.5/n) and greater than ([n – 0.5]/n), respectively.

Figure 45 shows the GEV parameters estimated at each pixel for the domain of study (180x140 pixels) covering Louisiana. The mean shape parameter, estimated from the average of 500 bootstrap runs, varies between positive and negative values mostly between [-0.5, 0.5]. The 5% and 95% confidence of the shape parameter can have values below -0.5 and above 1 due to the sampling variability. Compared to the width of the confidence interval, it

appears that the mean of the shape parameter does not deviate from the value of zero, which corresponds to the case of Gumbel distribution (see Section 5.3), suggesting that it the shape parameter may not be statistically different from zero. The mean scale parameter, in most pixels, falls in the range of [5, 20], with some subtle spatial gradients. The location parameter has noticeable spatial gradients similar to those of the mean annual maxima (MAM) (Figure 38) where the parameter increases from north to the south and as we get closer to the Gulf boundary. The sampling effect on both parameters is evident in the 5% and 95% confidence limits.

The corresponding Precipitation Frequency Estimates (PFE) are displayed for six representative return periods of 2, 5, 10, 25, 50 and 100 years (Figure 46 and Figure 47). The maps of these PFE's show significant variability in space with clear gradients from north to south. The uncertainty associated with these estimates as reflected in the confidence bounds is fairly large especially for large return periods (e.g., 50 and 100 years). The spatial maps also show clear signs of graininess and noise in the spatial variability of the estimated quantiles, which are most noticed for large return periods.

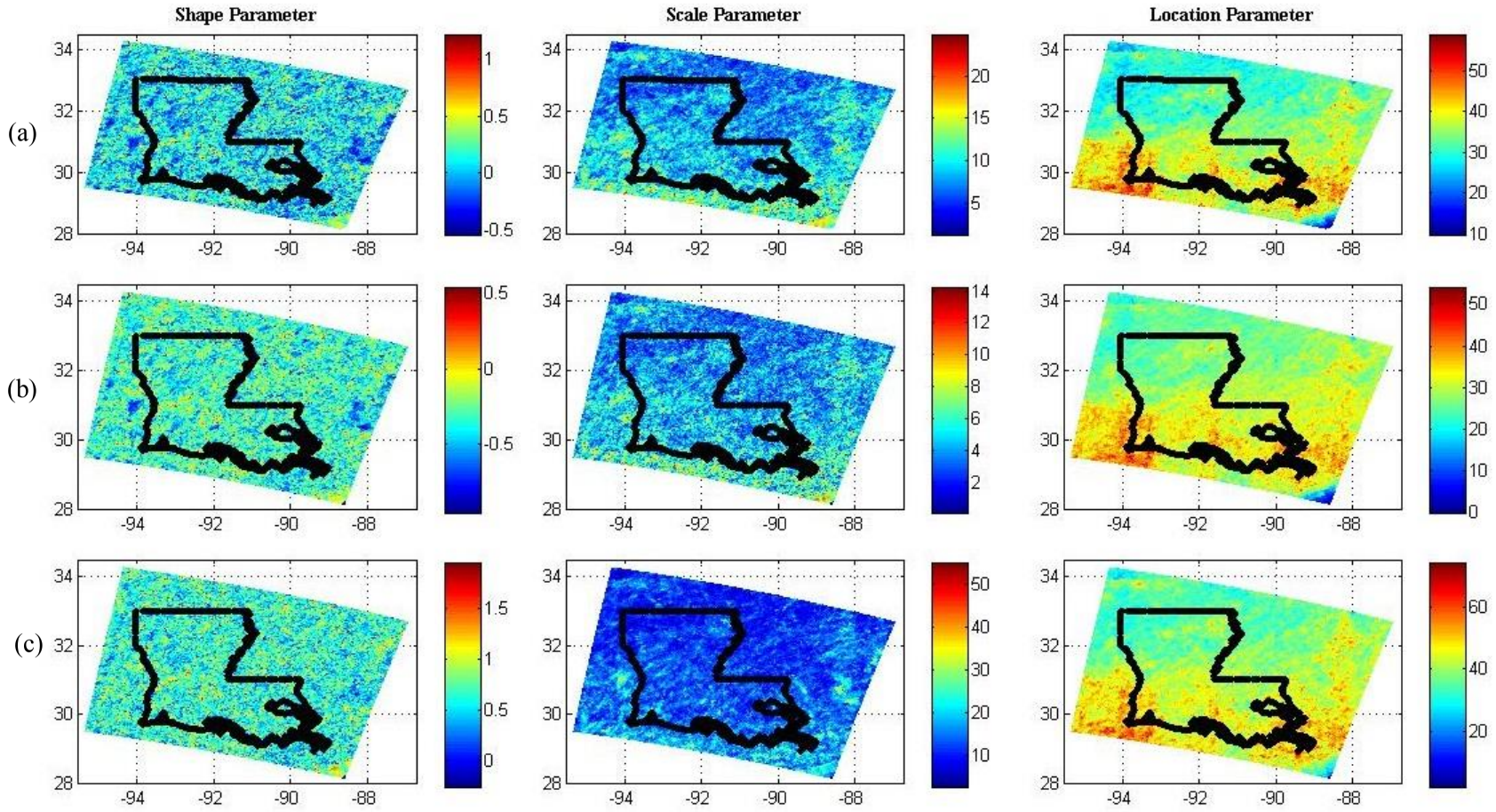

Figure 45 The GEV distribution parameters from Pixel-Based Approach; (a) Mean of 500 bootstrap runs, (b) 5% Confidence Limit, and (c) 95% Confidence Limit.

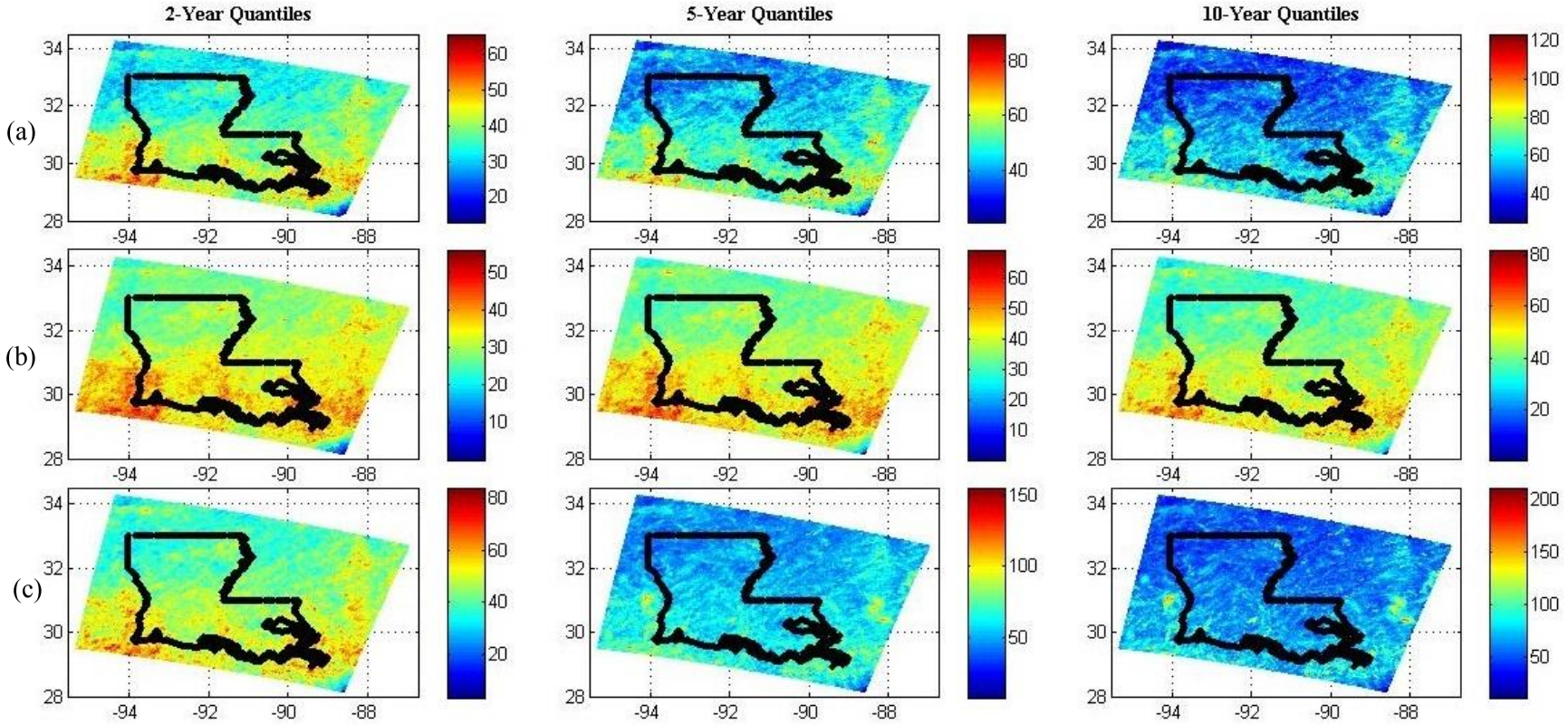

Figure 46 The rainfall depth corresponding to 2, 5, and 10 year return periods from Pixel-Based Approach; (a) Mean of 500 bootstrap runs, (b) 5% Confidence Limit, and (c) 95% Confidence Limit.

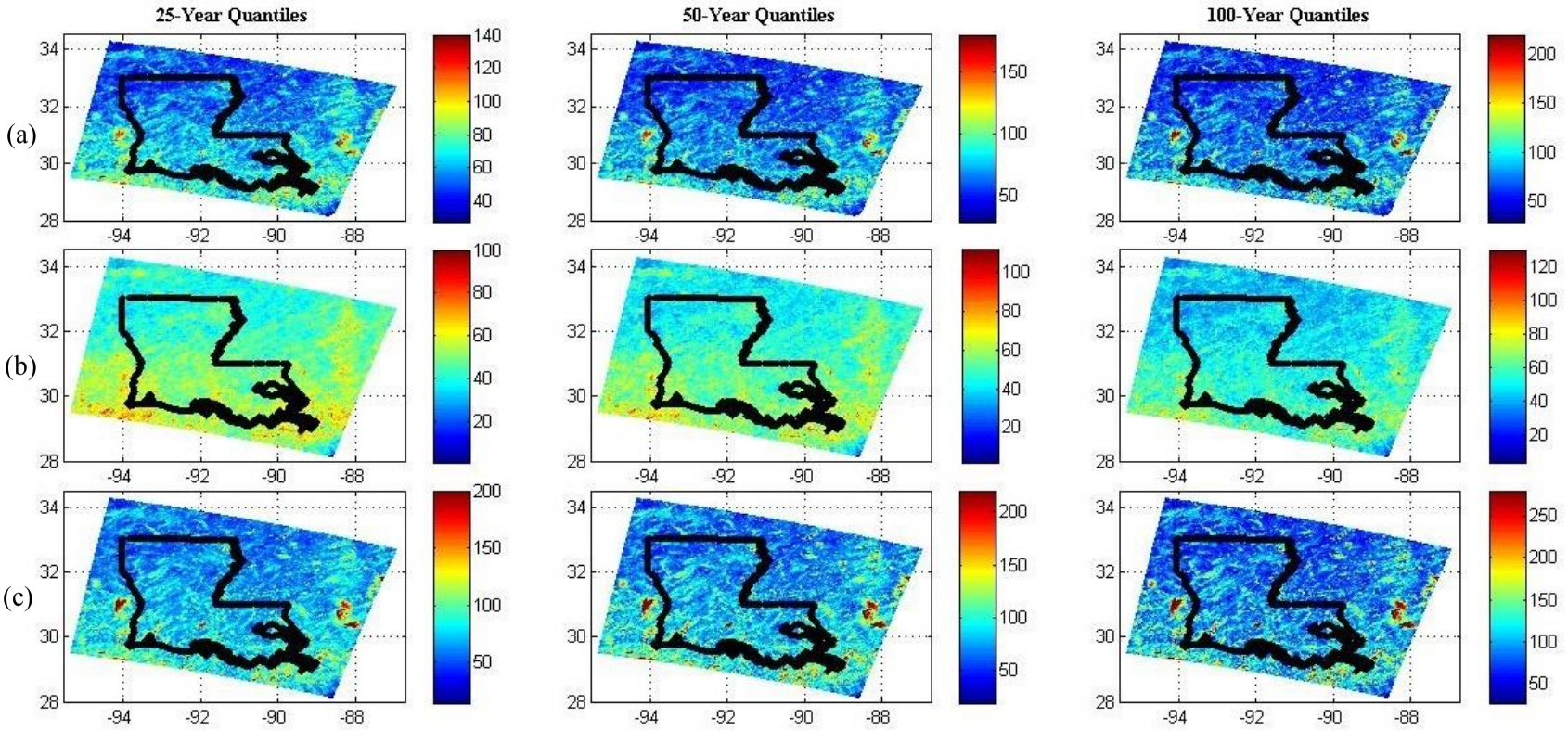

Figure 47 The rainfall depth corresponding to 25, 50, and 100 year return periods from Pixel-Based Approach; (a) Mean of 500 bootstrap runs, (b) 5% Confidence Limit, and (c) 95% Confidence Limit.

6.3 Region-Based Precipitation Frequency Estimates (PFEs)

This section presents that PFE results obtained using the region-based spatial bootstrap method that was described in Section 5.5.2. The mean estimated GEV distribution parameters and their upper and lower confidence bounds are shown in Figure 48 and Figure 49 for the region-based approach with two different moving windows; 11x11 pixels and 21x21 pixels. The confidence limits are estimated using the spatial bootstrap technique for 500 runs. Compared to the pixel-based approach, the results suggest that the region-based approach results in a reduction of the estimated parameters and in lower confidence limits. For instance, the mean shape parameters, in most of the pixels, went down to the range [-0.2, 0.2] with narrower uncertainty bounds.

The reduction in the dispersion of the estimated parameters is attributed to the gain from the repeated sampling from the surrounding pixels, which is the advantage of the regional approach as opposed to using only information available in each pixel. Sampling from a homogenous region resulted in smoother fields of the GEV parameters with less sampling variability. Because of the short record available in each pixel, only 11 years, the pixel-based estimation varies considerably from one pixel to another, which was circumvented when using the region-based estimation with the moving window at each pixel. Increasing the size of the moving window to (21x21) pixels results in lower variability and more smoothness for the estimates transition between the pixels (Figure 49).

Figure 50,Figure 51,Figure 52, and Figure 53 display the precipitation frequencies estimated using the GEV distribution parameters. Improvements in the uncertainty of the different quantiles can obviously be seen when using the regional approach over the pixel-based

approach where each pixel is treated in isolation from its surrounding region. The use of a region of influence approach with a moving widow allows for the smoother spatial transition as opposed to the pixel-based approach. Since the pixel size is only (4x4 km) and no significant climatic changes are expected to occur over the pre-set region of influence, it is more realistic to expect such smoother spatial fields for the rainfall frequency estimates. Further increases in the size of the moving window would result in more spatial smoothing and slight reduction in the uncertainty bounds obtained, nevertheless, increasing the window size is restricted by the formation of homogenous region. The smoothness in the rainfall estimates patterns by the spatial bootstrap resembles to great extent the smoothing algorithm performed by *Durrans, et al.,* (2002). They use simple distance-weighted averaging procedures to spatially smooth the estimates of sample L-moments. This smoothing algorithm reduced the effects of sampling variations caused by the short time series used, only 8 years in their study.

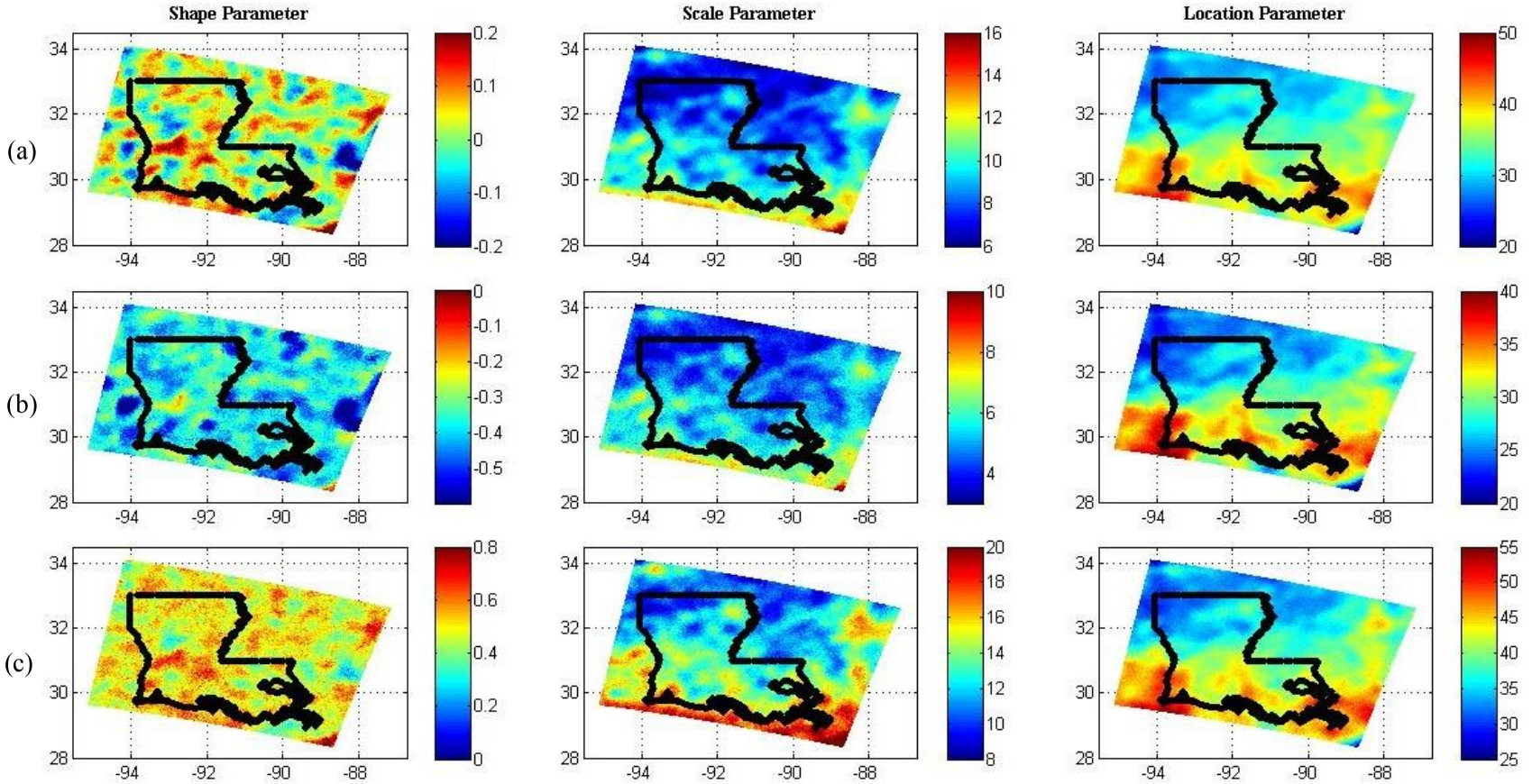

Figure 48 The GEV distribution parameters from Spatial Bootstrap Technique using moving widow (11x11 Pixels); (a) Mean of 500 bootstrap runs, (b) 5% Confidence Limit, and (c) 95% Confidence Limit.

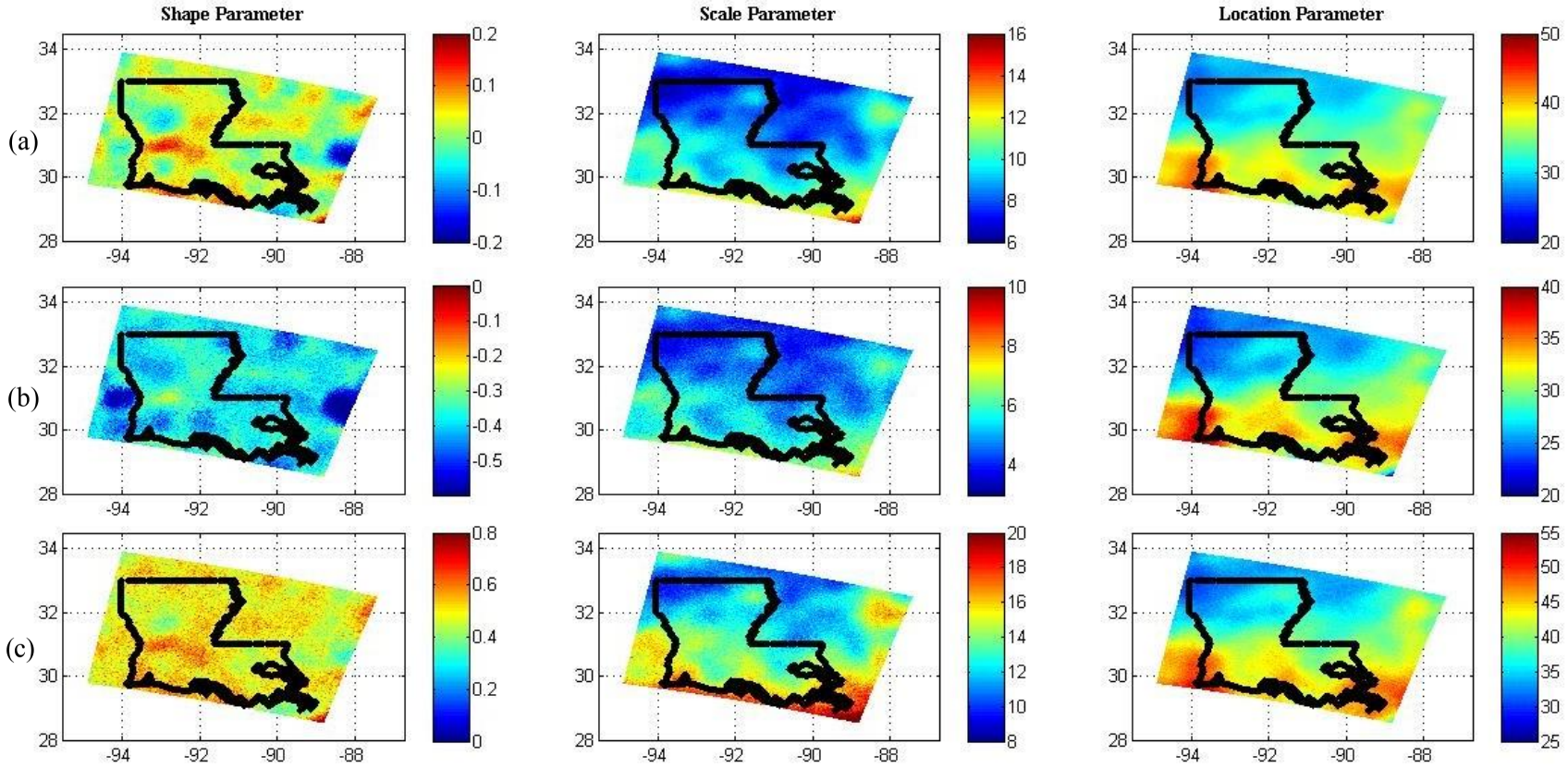

Figure 49 The GEV distribution parameters from Spatial Bootstrap Technique using moving widow (21x21 Pixels); (a) Mean of 500 bootstrap runs, (b) 5% Confidence Limit, and (c) 95% Confidence Limit.

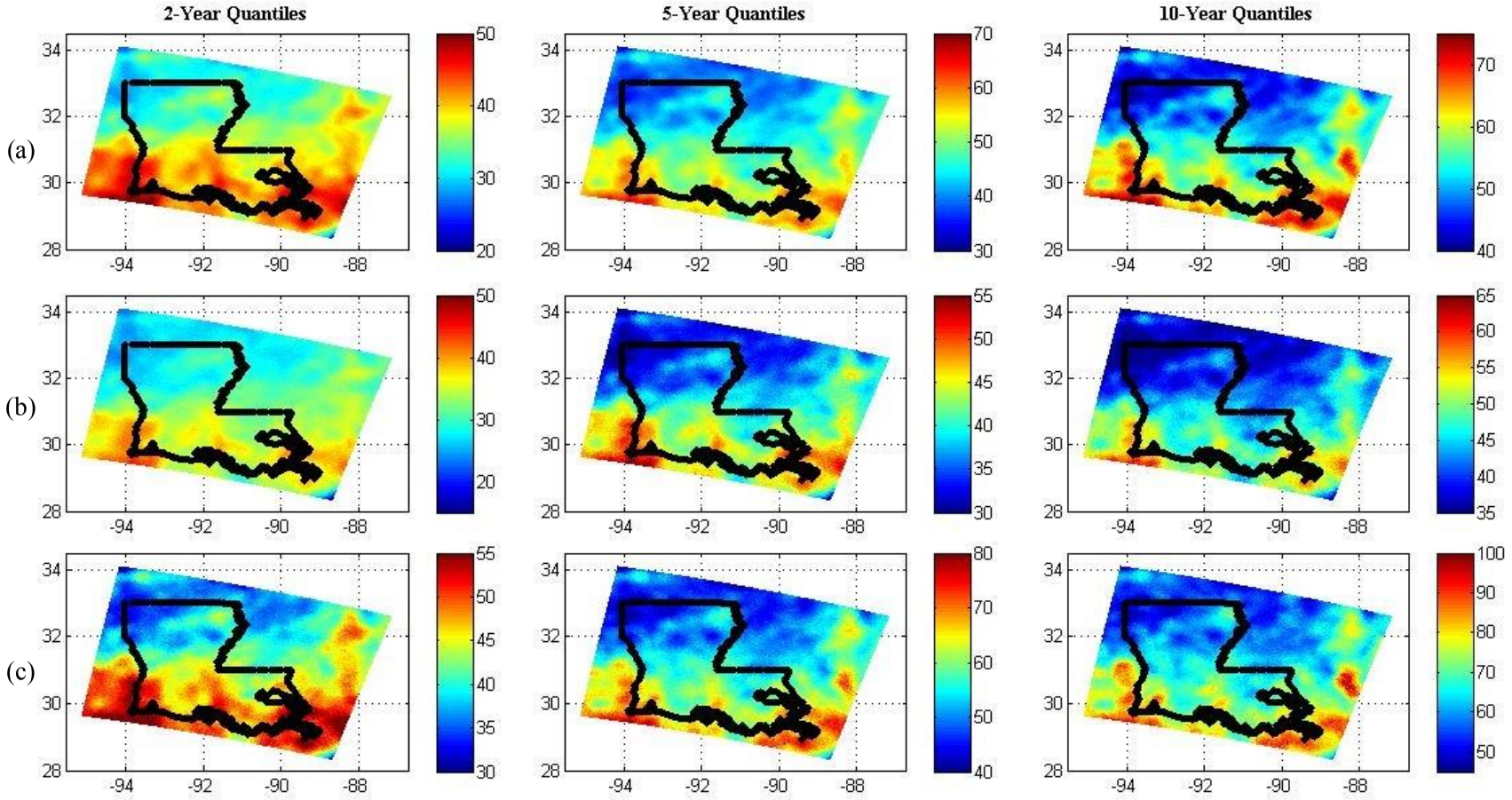

Figure 50 The rainfall depth corresponding to 2, 5, and 10 year return periods from Spatial Bootstrap Technique using moving widow (11x11 Pixels); (a) Mean of 500 bootstrap runs, (b) 5% Confidence Limit, and (c) 95% Confidence Limit

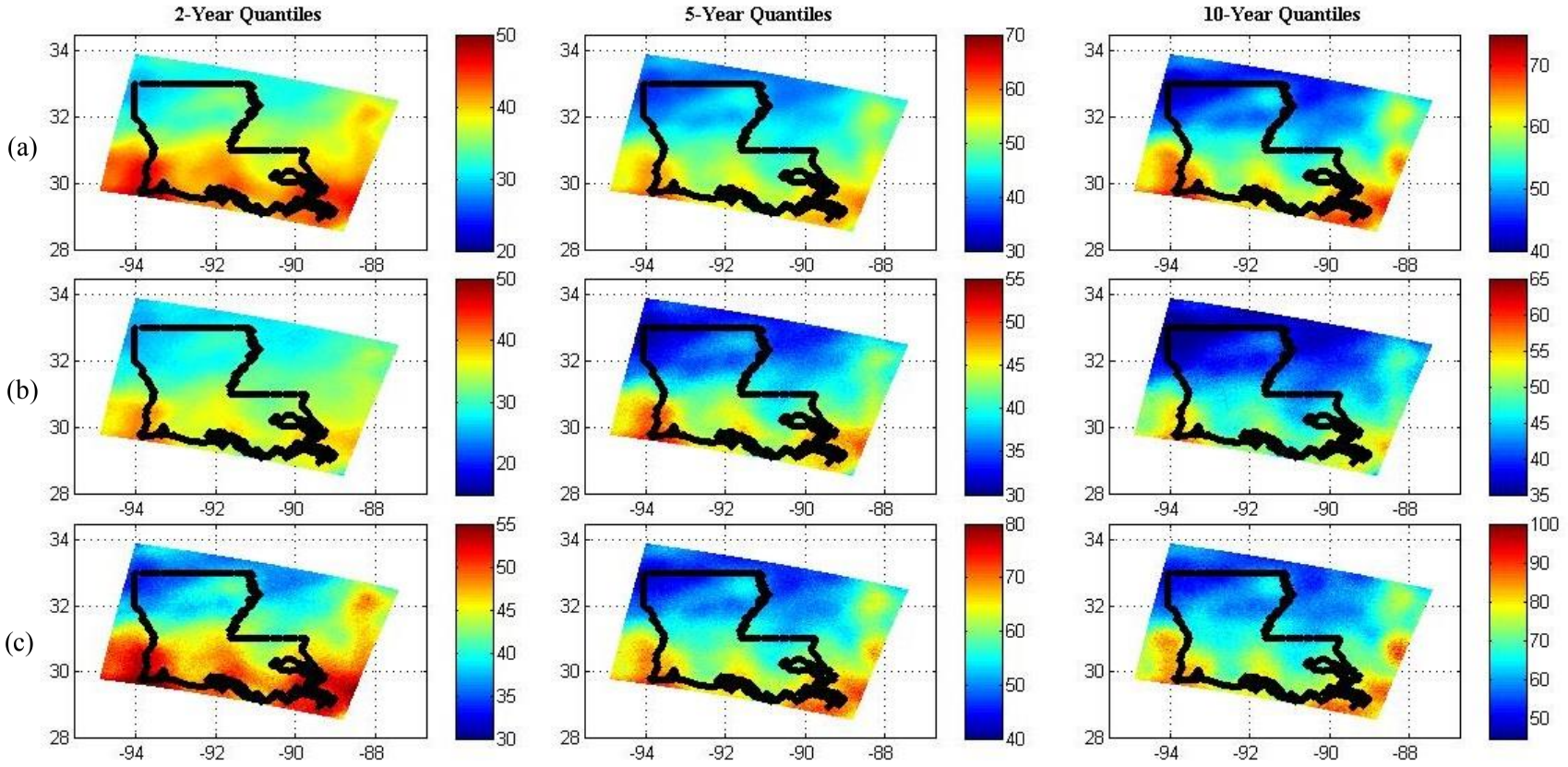

Figure 51 The rainfall depth corresponding to 2, 5, and 10 year return periods from Spatial Bootstrap Technique using moving widow (21x21 Pixels); (a) Mean of 500 bootstrap runs, (b) 5% Confidence Limit, and (c) 95% Confidence Limit.

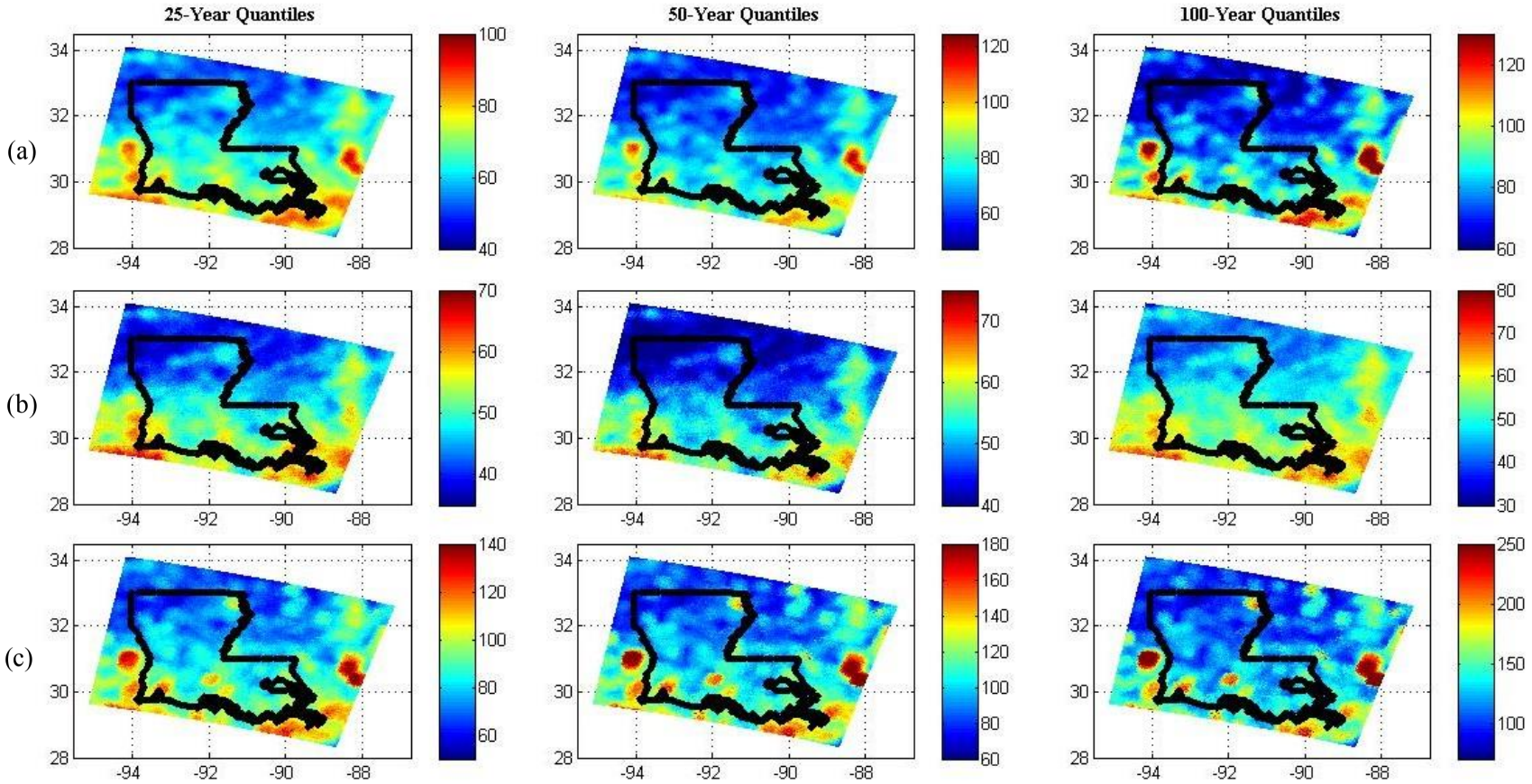

Figure 52 The rainfall depth corresponding to 25, 50, and 100 year return periods from Spatial Bootstrap Technique using moving widow (11x11 Pixels); (a) Mean of 500 bootstrap runs, (b) 5% Confidence Limit, and (c) 95% Confidence Limit.

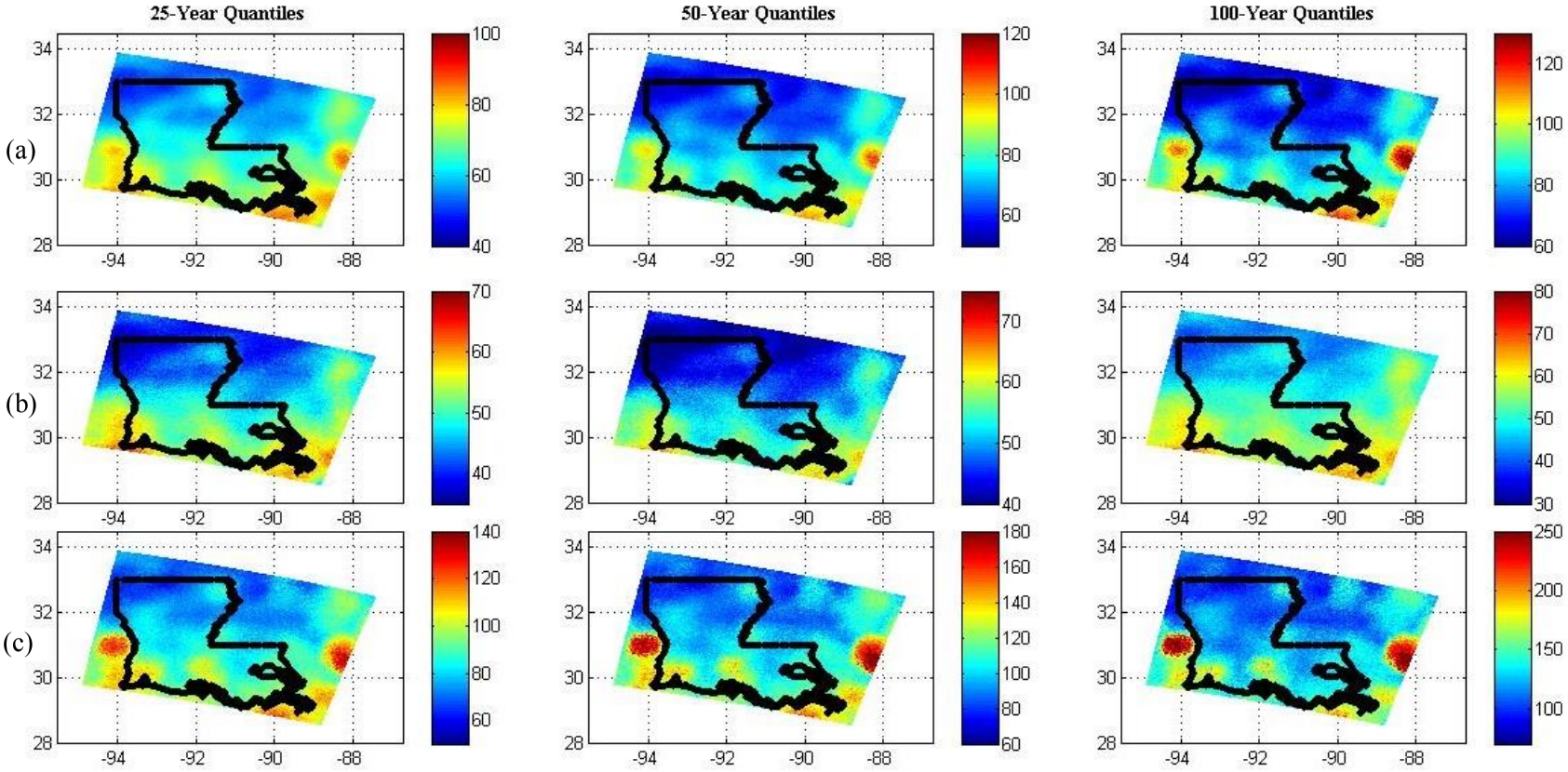

Figure 53 The rainfall depth corresponding to 25, 50, and 100 year return periods from Spatial Bootstrap Technique using moving widow (21x21 Pixels); (a) Mean of 500 bootstrap runs, (b) 5% Confidence Limit, and (c) 95% Confidence Limit.

6.4 Comparison of Radar versus Gauge PFE's

The Hydrometeorological Design Studies Center (HDSC) provides the annual maximum series used in the NOAA Atlas 14 and the corresponding PFEs with 90% confidence intervals. A network of 33 hourly gauges in Louisiana, operated by the National Climatic Data Center (NCDC), is used in the current study (Figure 54) to identify differences in the AMS extracted from the radar QPE versus those from the gauges. Moreover, the NOAA Atlas 14 gauge-based PFEs and their 90% confidence intervals are contrasted against the corresponding frequencies estimated in the current study using the two approaches described earlier, pixel-based and regional.

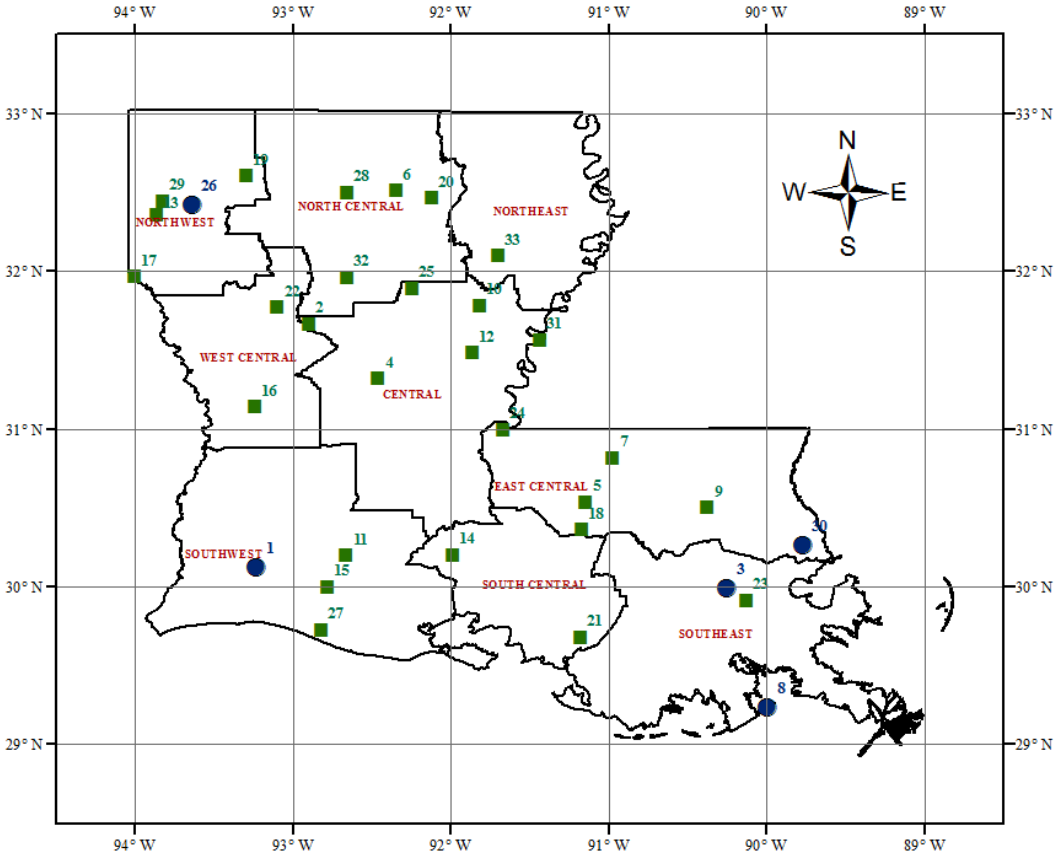

Figure 54 A network of 33 hourly gauges in Lousiana (The cicled symbols indicate gauges used in the current study for comparison with radar-based PFE estimates).

The NOAA Atlas 14 applied a regional frequency analysis approach that is different from the region-based technique used in the current study. The main difference is in how the homogenous region is formed initially for each station. In the Atlas 14 method, a homogeneous region is defined for each gauge for by grouping the closest 10 stations and then stations are added to or removed from regions based on examination of their distance from a target station, elevation difference, difference in MAMs at various durations, and inspection of their locations with respect to mountain ridges, etc. (*Perica, et al.,* 2013). The PFEs from the NOAA Atlas 14 are used as a reference for examining the radar-based PFEs. However, it is important to note that this comparison doesn't imply that gauges are the true estimates, simply because they also have some uncertainties caused by sampling variability and the estimation process itself. Nevertheless, the comparison will provide some insight into the performance of the radar-based estimates and their uncertainties.

Table 6 Location of gauges and pixels used for comparing PFEs.

Gauge Number	Latitude	Longitude	HRAP X*	HRAP Y*
1	30.1247	-93.2283	51	30
3	29.9933	-90.2511	124	44
8	29.2339	-89.9961	136	24
26	32.4219	-93.6381	28	93
30	30.265	-89.7697	134	54

* HRAP X and HRAP Y are the transformed Grids, i.e., Local HRAP.

Five representative gauges are selected for the comparison analysis. The location of these gauges and the corresponding radar pixels are listed in Table 6. Figure 55(a) shows plots of the annual maximum series available for gauge (1) and for the coincident HRAP pixel (51, 30). The gauge AMS is available for 49 years from 1962 to 2010 which is a long record

compared with the 11-year radar QPE data available from 2002 to 2012. It is noted that the 2003 annual maximum from the radar QPE is very high compared to that of the corresponding gauge, and suggests that this particular value might be an outlier. The mean and standard deviation of annual maximum series for this pixel are 58 mm and 37 mm respectively, while the standard deviation for the sample excluding this observation is only 14 mm, which indicates the high variability that might results from this individual value. Moreover, the Grubbs-Beck (GB) outlier detection test, explained in section (4.3), removes this observation and considers it as an outlier at a 5% level of significance. This high radar estimate in 2003 affects the PFE in the pixel-based approach as shown in (Figure 57), while the spatial bootstrap is less influenced by this estimate. The reduced effect of possible outliers is one of the benefits of the spatial bootstrap technique since the combined use of multiple pixels enables reducing the impact of such very rare events (*Uboldi, et al.,* 2014).

The annual maximum series for the other three gauges, i.e., gauge (8), (26), and (30), and the corresponding pixels are shown in Figure 55 (b) and Figure 56(a) and Figure 56(b). The three gauges show different patterns for the available maximum series; however, unlike gauge (1), the precipitation frequencies estimated by the NOAA Atlas 14 approach for the three gauges are quite larger than those estimated by the radar QPE dataset when using the pixel-based estimation. For instance, Figure 58 shows lower mean estimates for the quantiles and very narrow confidence intervals in the pixel-based estimation compared with Atlas 14 regional estimation and the spatial bootstrap technique used in this study. The lower quantiles estimates can be inferred from the annual maximum series shown in Figure 55 (b) in which most of the radar-based annual maximum estimates are lower than those estimated by gauge, while the less variability is due to the small standard deviation, about 11.7 mm, of the AMS.

This narrow confidence bounds discloses one of the limitations of using the conventional bootstrap resampling with small sample size. Since the conventional bootstrap will never generate an observation either larger or smaller than the maximum or minimum historical observation, this bootstrap needs sample size n greater than the planning horizon N for an effective examination of the probability distribution of the largest or smallest observation (*Vogel & Shallcross,* 1996).

Although the spatial bootstrap technique results in lower estimates compared to the NOAA Atlas 14 estimates, it again outperforms the pixel-based approach by introducing observations from surrounding pixels. The addition of observations other than those included in the pixel sample introduced more variability to the quantile estimates in a way that makes them much closer to those derived by the gauge-based regional frequency analysis approach used in NOAA Atlas 14. Unlike the expected reduced variability in most of the pixels, variability increases with opening the moving window to larger size to take advantage from more observations for pixels with AMS having similar statistical characteristics to pixel (99, 53).

The rest of gauges share the same low mean and confidence estimates as the three gauges (8), (26) and (30). Trying to quantify this estimation problem, we used gauge (3), which has the largest annual maximum series (63 observations) and it extends from 1948 to 2011, and use a sample of 10 annual maxima from 2002 to 2011 to estimate the quantiles using the at-site estimation procedures. The same procedures are performed for the corresponding pixel by using the annual maximum observations from 2002 to 2011. Having two samples, one from gauge and one from radar, with the same sample size and using annual maxima for same years, we concluded that radar estimates underestimates the annual maxima compared with

those extracted from the gauges observations (Figure 61). This underestimation affects significantly the estimation of the quantiles as shown in Figure 62. The confidence intervals are constructed using the conventional bootstrap resampling and as explained, the uncertainty bound obtained with the bootstrap resampling from small sample size is very sensitive to the magnitude of the observations in the sample, thereby, the high values of gauge annual maxima resulted in higher variability compared with the radar-based annual series. The fluctuations in the radar estimates, between underestimation and overestimation of the gauges annual maxima, was attributed to the fact that the algorithms, used to blend the gauge and radar estimates to produce the MPEs, account only for the overall bias, while a considerable conditional bias dependent on the radar rainfall values still remains. This conditional bias is a conditional statistics that provide detailed insight into how the product performs at different ranges of the rainfall amount (for more details on the uncertainty models for the radar estimation errors (see for example *Ciach, et al.,* (2000); *Habib, et al.,* (2004); *Ciach, et al.,* (2007); *Villarini, et al.,* (2009); *Habib, et al.,* (2013) and *Habib & Qin,* (2013)). These studies show that the conditional bias can be characterized to have a complete uncertainty model for the radar rainfall estimates.

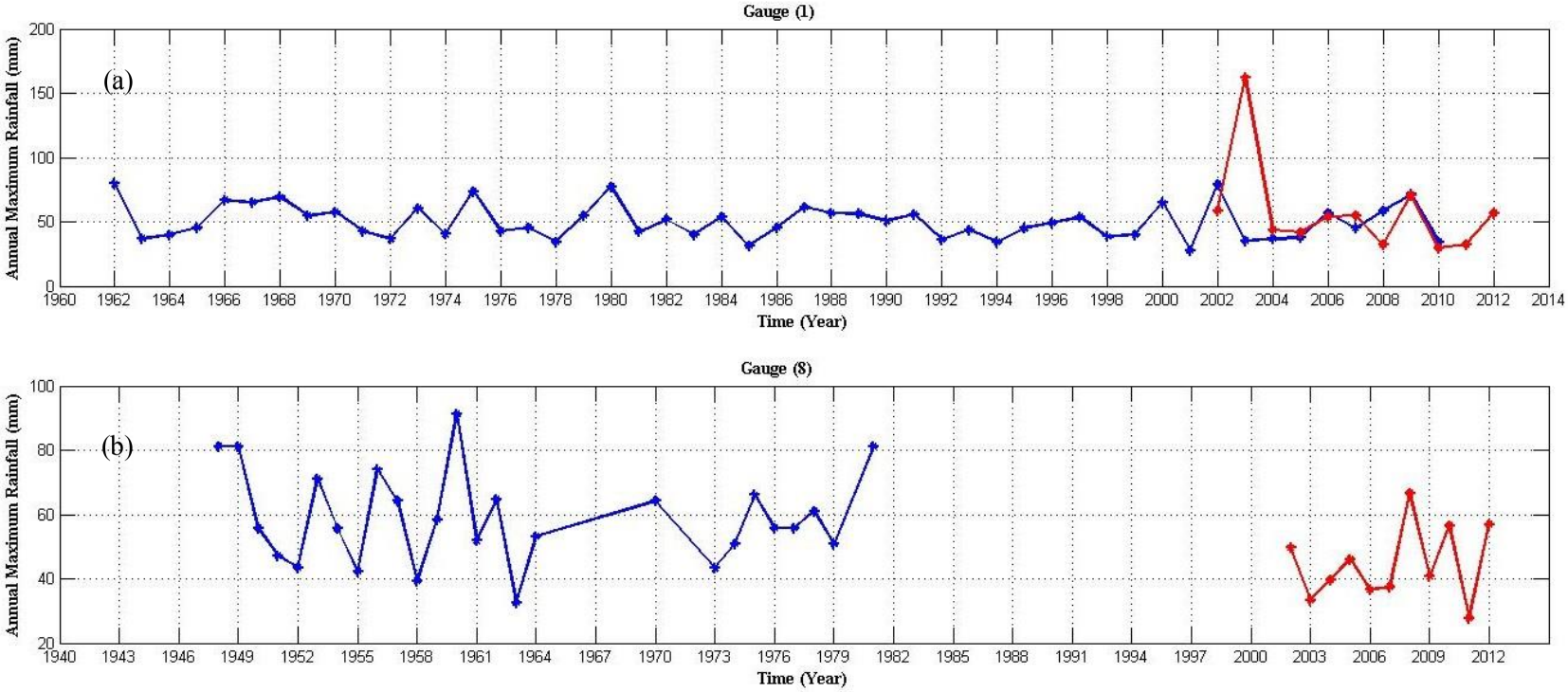

Figure 55 Annual Maximum Series (AMS) for NOAA Atlas14 gauge (1) and (8) (Blue) and the corresponding radar pixel (51,30) and (136,24) (Red) respectively.

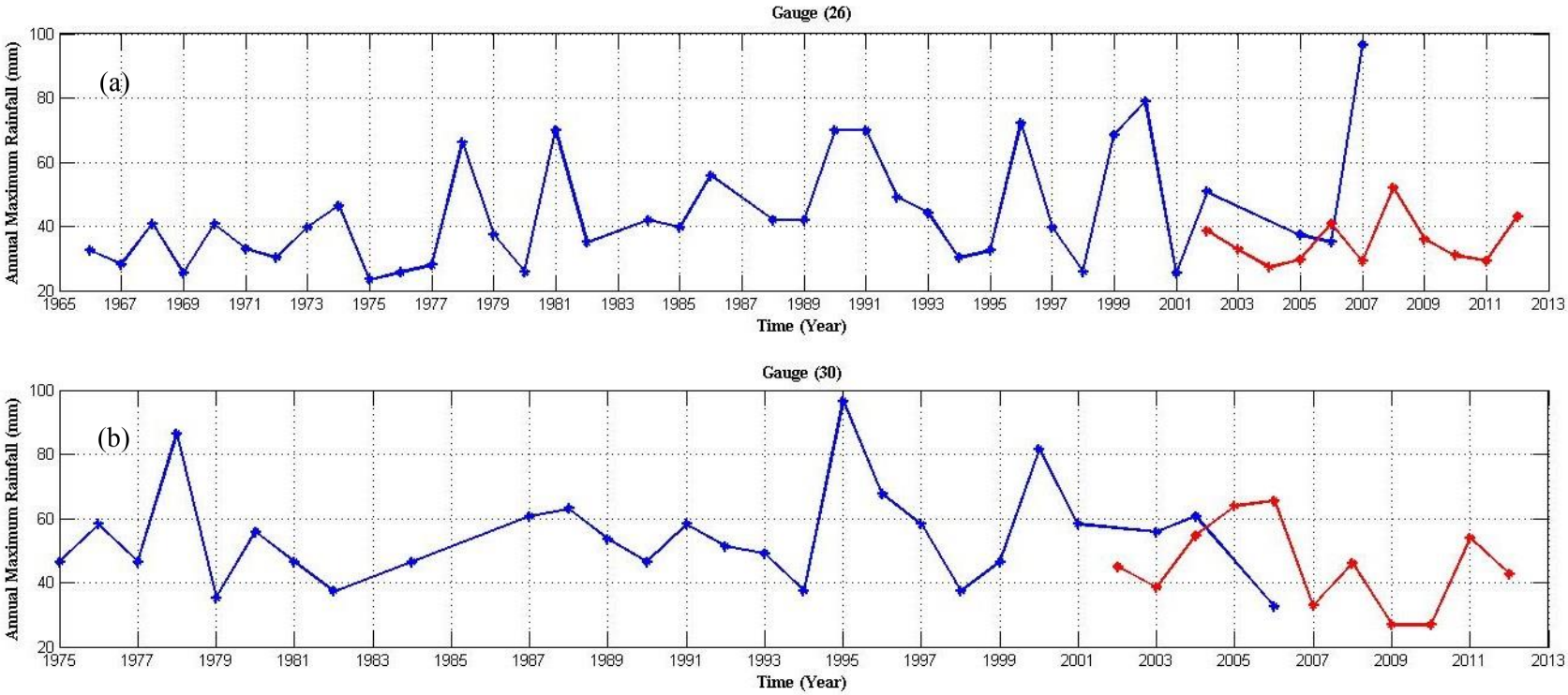

Figure 56 Annual Maximum Series (AMS) for NOAA Atlas14 gauge (26) and (30) (Blue) and the corresponding radar pixel (28,93) and (134,54) (Red) respectively.

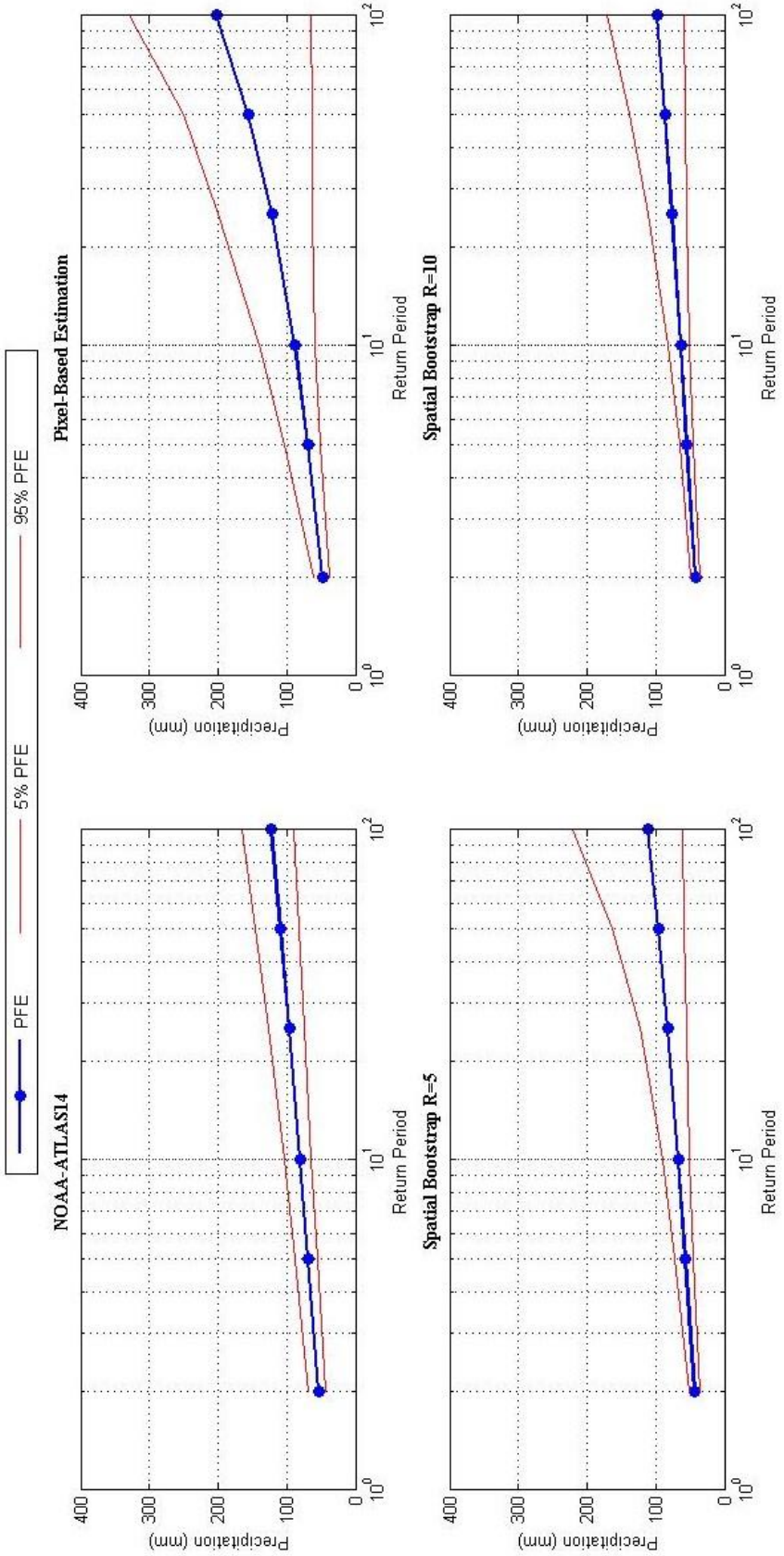

Figure 57 Precipitation Frequency Estimates (PFE) and 90% Confidence Limits at location of gauge (1).

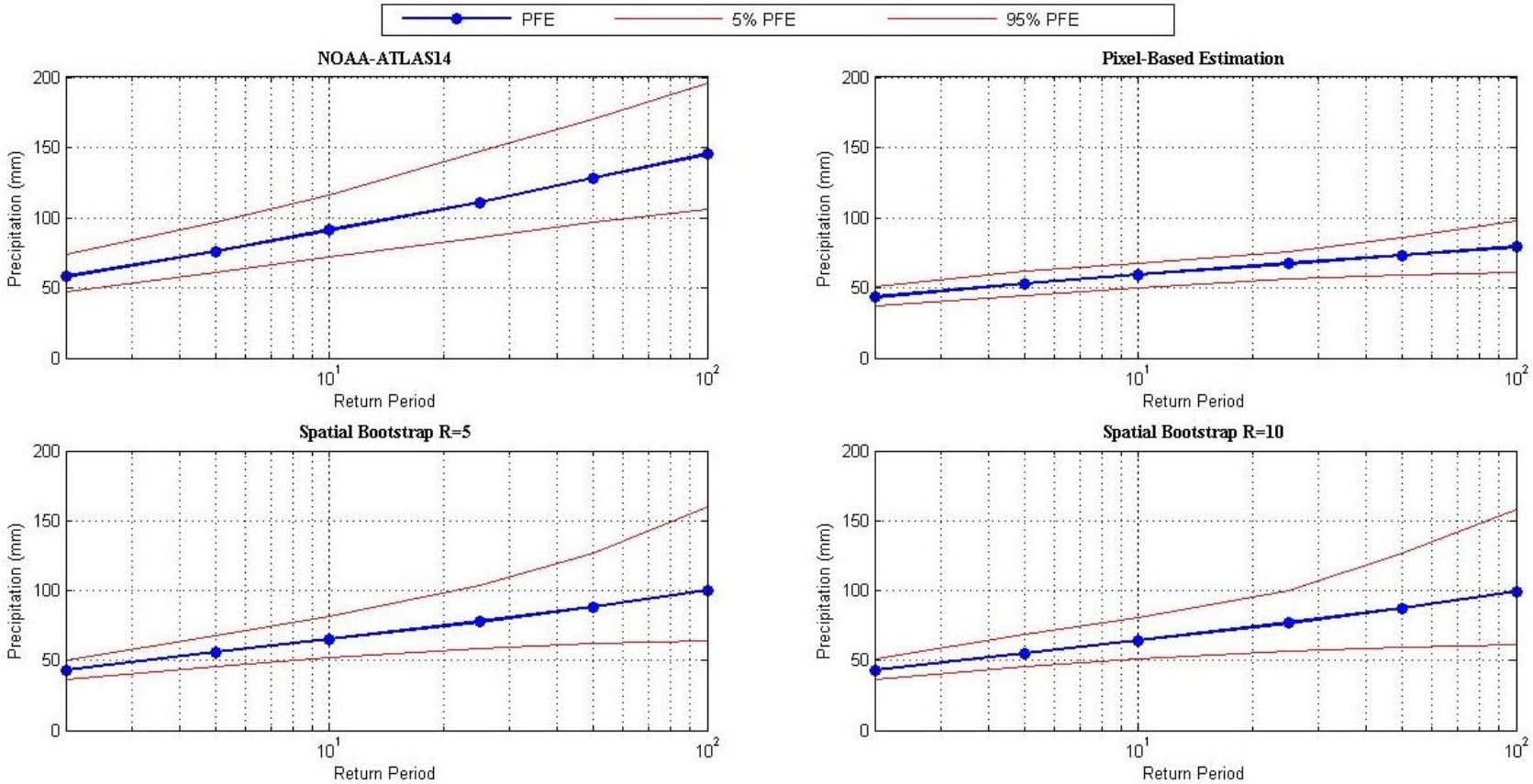

Figure 58 Precipitation Frequency Estimates (PFE) and 90% Confidence Limits at location of gauge (8).

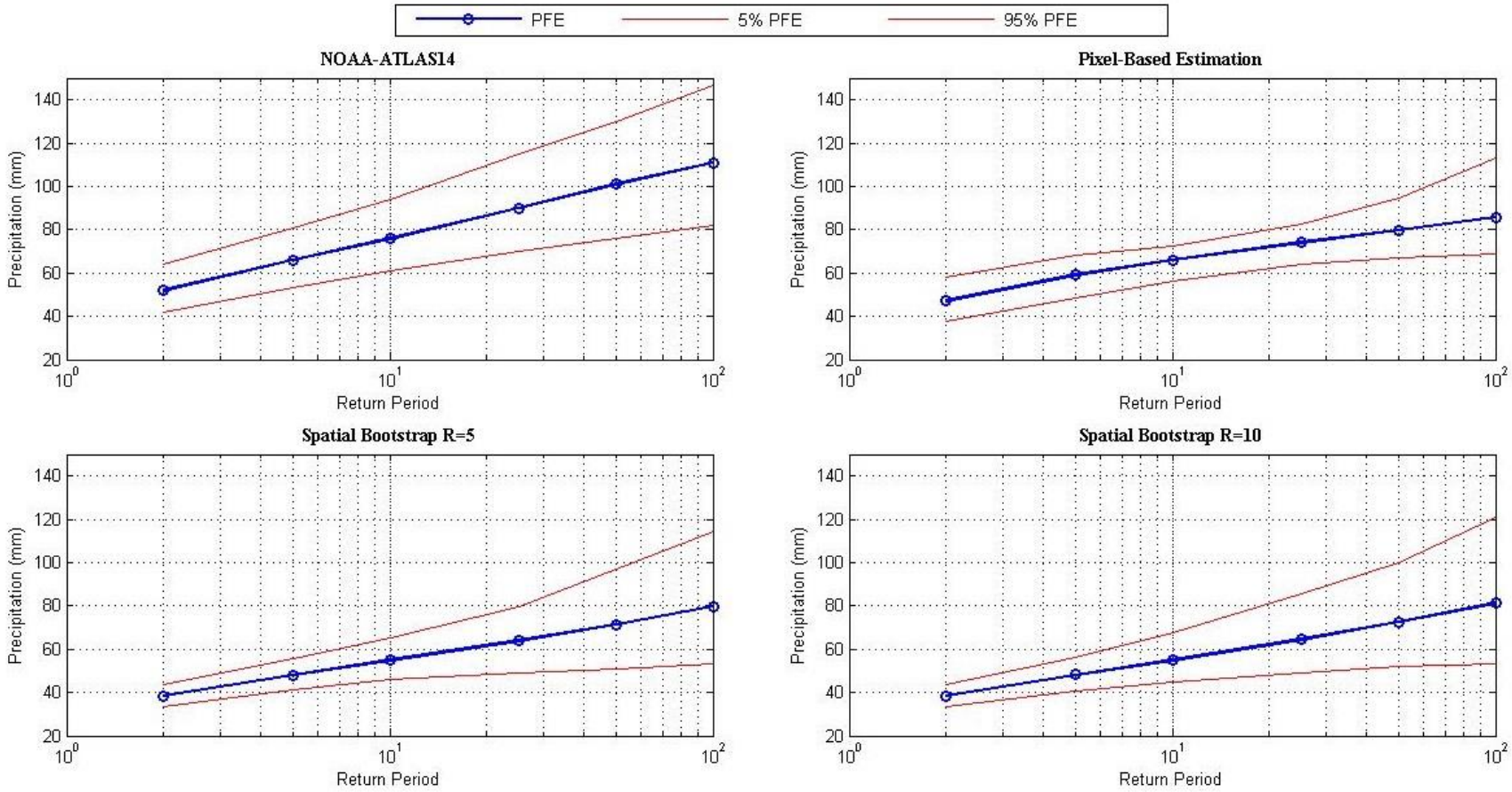

Figure 59 Precipitation Frequency Estimates (PFE) and 90% Confidence Limits at location of gauge (26).

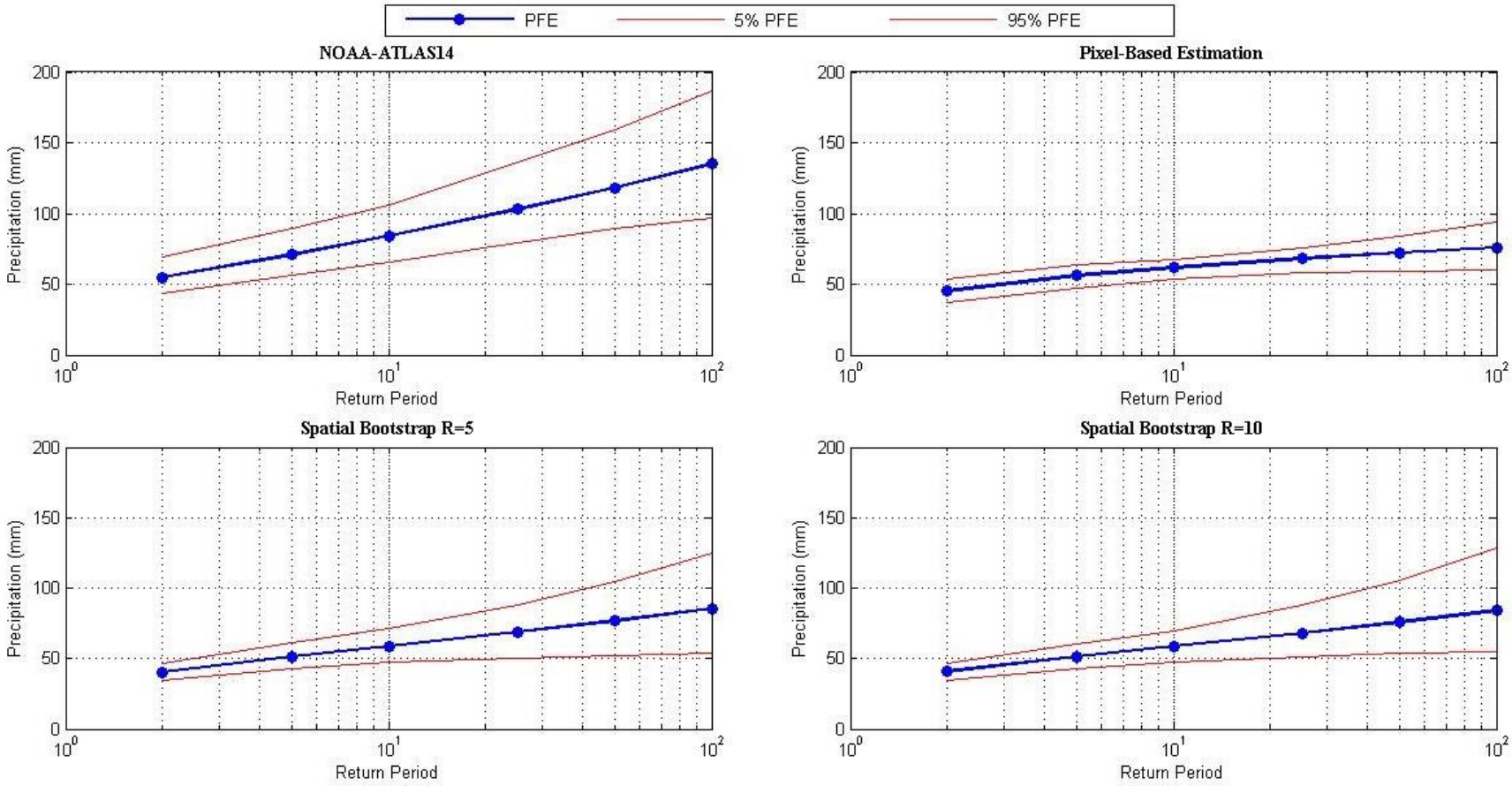

Figure 60 Precipitation Frequency Estimates (PFE) and 90% Confidence Limits at location of gauge (30).

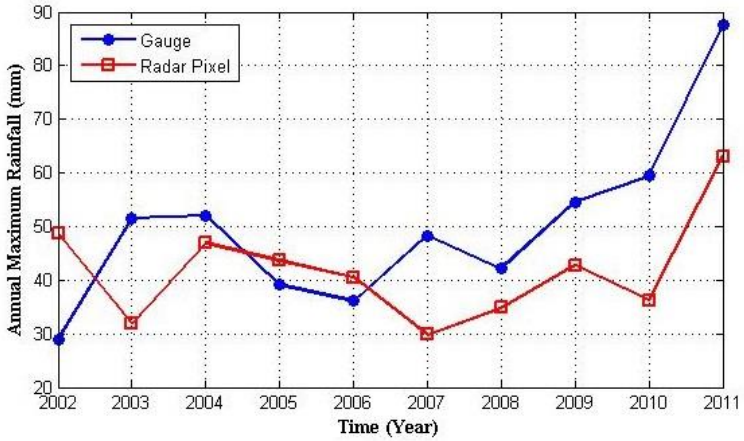

Figure 61 Annual Maximum Series (AMS) for NOAA Atlas14 gauge (3) and corresponding radar pixel (124,44).

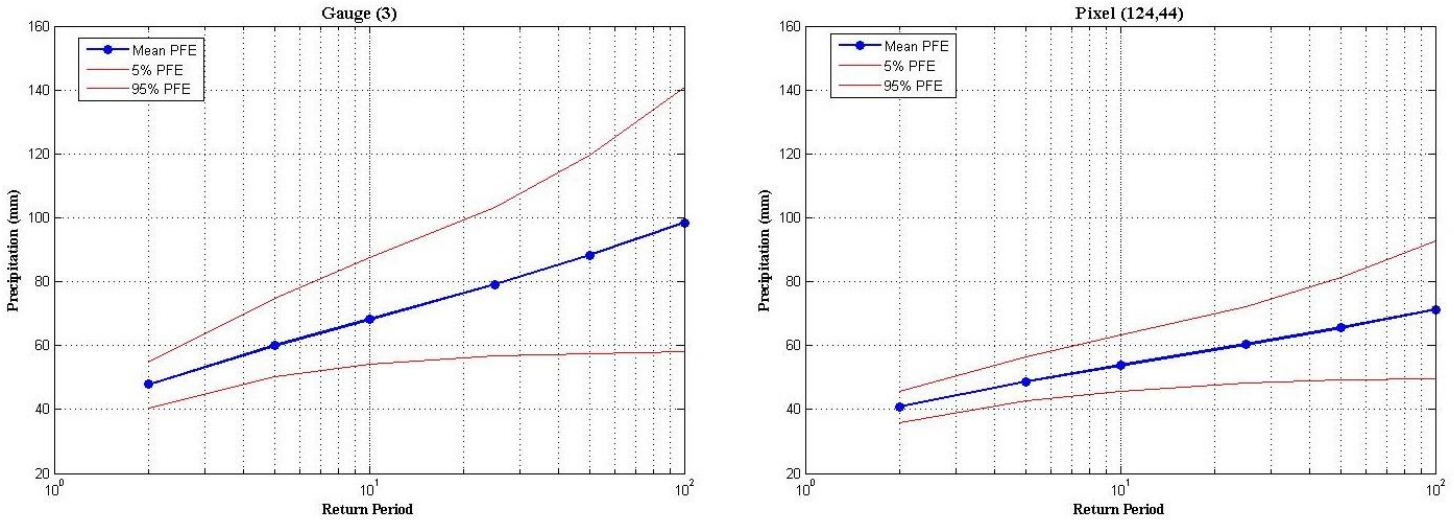

Figure 62 Precipitation Frequency Estimates (PFE) and 90% Confidence Limits at gauge (3) and corresponding radar pixel (124,44).

Chapter 7 Summary, Conclusions and Future Work

7.1 Summary

Accurate and regionally specific information on Precipitation Frequency Estimates (PFE) are critically needed for various water resources engineering planning and design purposes. Traditionally, PFE information is based on near-point observations of sparsely distributed rain gauges. The limited spatial availability of rain gauge stations and their lack of areal representation, calls for exploring the utility of weather radar techniques for PFE analysis This study examined the applicability of radar-based Quantitative Precipitation Estimates (QPE) to derive precipitation frequencies that are critically needed for engineering and environmental design purposes. Developing a quantitative assessment of radar products and their data quality is crucial for proper application of such products in design frequency analyses. The study focused first on examining the data quality of two main radar products, the near real-time Stage IV QPE product, and the post real-time RFC/MPE product. The two products are widely used in research and operational applications, with little knowledge about their quality from the perspective of heavy precipitation and frequency analysis. The procedures conducted for the assessment of the Stage IV product include constructing fields of maximum precipitation (known as Partial Duration Series) over the Contiguous U.S. domain. The Stage IV product was compared against the longer-latency MPE product. The Grubbs-Beck (GB) outlier detection test was used to identify and remove some of the artifacts detected in Stage IV product in an effort to improve the quality of this product and make it more applicable for extreme precipitation analysis.

Based on the inter-comparison analysis of the two products, Stage IV and RFC/MPE, the latter was selected for the frequency analysis carried out throughout the study. The study domain was selected to cover a region over Louisiana for the period 2002-2012 when the radar dataset was fully available. The methodology used in derivation of precipitation frequency estimates using the radar QPE dataset was composed of the following:

1. Extracting the hourly Annual Maximum Series (AMS) for each pixel for the period 2002-2012 to represent extreme precipitation.

2. The Generalized Extreme Value (GEV) distribution is selected to fit the AMS samples.

3. The method of L-moments (or probability weighted moments) is used for estimating the parameters of GEV distribution.

4. The precipitation frequencies and their 90% confidence intervals were estimated using two different approaches:

    - Pixel-based estimation, in which GEV distribution was fitted for the AMS sample at each pixel. As such, the distribution parameters and the PFE quantiles are estimated for each individual pixel. Confidence limits were established using the conventional bootstrap resampling technique.

    - Region-based estimation, in which a spatial bootstrap technique was applied at each pixel to construct AMS samples by sampling from a pre-fixed region of influence. The selected observations from the surrounding pixels were based on a

probability of extraction that depends on the horizontal and vertical distances from pixel of interest.

5. The NOAA Atlas 14 precipitation frequency estimates (PFE) are used as a reference to evaluate the capability of the radar-based QPE to estimate precipitation frequencies and to evaluate the performance of the two frequency estimation approaches.

7.2 Conclusions

Assessment of the Stage IV real-time product showed some alarming data artifacts that contaminate the identification of rainfall maxima. Such artifacts are usually undetected when dealing with average rainfall amounts as opposed to extremes. The artifacts are more dominant in the western and southeastern US, but are not uncommon in the northeastern and northern regions. The artifacts are mostly in the form of circular patterns, or rings, with very high rainfall rates surrounded by lower values. A close examination of these artifacts was performed by comparison against the corresponding precipitation estimates from the longer-latency RFC radar MPE product. Most of the very high rainfall rates were found to be due to erroneous rain gauge observations, which are used to bias-adjust the radar-only estimates within the MPE algorithm. These artifacts and erroneous data points were mostly absent in the longer latency MPE product that undergoes manual quality control by the forecasters at the NWS River Forecasting Centers. Unlike the RFC/MPE product, the real-time hourly Stage IV QPE doesn't capture any of these manual quality performed either to the MPE product or the erroneous gauges.

The Grubb's Beck outlier detection test was applied to the maximum precipitation fields to identify these artifacts statistically. Although the GB test successfully removed most of these

artifacts, it is recommended to use this test with a predetermined threshold for outlier detection to avoid removing some of actual extremes.

The presence of problematic estimates and outliers in radar-rainfall products are attributed to different factors such as delays in data transmission, insufficient time for comprehensive quality control of the ingredient data, or insufficient computational power to use better algorithms within real-time operations. Therefore it is recommended to use a Multisensor Precipitation Reanalysis (MPR) approach to produce higher quality precipitation estimates that can take full advantage of additional rain gauge data that may not have been available in real time (*Seo, et al.,* 2010). An MPR approach can introduce much-needed enhancements to the near real-time operation products such as: systematic quality control of input data, correction of systematic biases in radar precipitation data, and optimization of algorithm parameters. An MPR pilot study has been recently applied for a regional domain over the Carolinas and produced more accurate precipitation estimates compared with real-time estimates (*Nelson, et al.,* 2009). Expansion of such MPR efforts to other US domains will bring major enhancements in the quality of radar QPE's and their utility for PFE analysis.

Since the RFC/MPE product provided more reliable extreme estimates compared to the Stage IV, it was selected for frequency analysis in this study. Two different frequency analysis approaches were applied; the first is pixel-based and uses the short available record of 11 years at each pixel, while in the second approach, a region-based method, tries to overcome the short record availability by sampling from a homogenous region surrounding the pixel of interest. The latter approach has the advantage of gaining more information from a climatologically homogenous region and is expected to enhance the estimation process. The formation of homogenous regions is usually the most difficult task in regional frequency

analysis and it requires more qualitative than quantitative decisions. The region of influence (ROI) approach is used to specify a radius of influence that bounds each pixel with a homogenous region. The ROI technique provides a smooth transition between the estimates as opposed to using fixed boundary regions. The radius of influence is chosen to be lower than an upper bound defined based on the climate division classification in Louisiana. The regional PFE approach showed more smoothness in the estimation of the distribution parameters and the associated quantiles compared to the pixel-based approach. The smoothness of the estimates in this high-resolution grid, 4-km x 4-km, is more realistic, since high variations between neighboring pixels are not expected.

The radar-based PFE results were assessed versus those from the NOAA Atlas 14 that were developed using a gauge-based regional frequency analysis approach. The comparison results indicated that pixel-based approach is highly sensitive to observational and sampling variability, and can result much higher or lower PFE estimates compared to the gauge-based PFE. The region-based spatial bootstrap approach is less sensitive to sampling effects and short records of radar data due to its regional sampling mechanism. The spatial bootstrap technique applied in the region-based approach avoids misleading PFE estimates and provides more realistic representation of the PFE confidence intervals and thus can be considered more reliable when compared with the NOAA Atlas 14 frequency estimates.

The overall results of the current study indicate the potential power of radar-based QPE's for delivering frequency estimates with high spatial resolutions. However, a main limitation stems from the relatively short record radar-rainfall datasets (typically 10-20 years), as opposed to the much longer records of rain gauge datasets. A viable approach is to combine both sources of information, radar products, and rain gauge observations, and capitalize on

their respective strengths to improve the PFE estimation process and their subsequent hydrologic design applications.

7.3 Future Work

Based on the results of the current study, a number of follow-up research questions can be proposed for future investigations:

1. In this study, hourly radar-based QPEs were used in the frequency analysis, and it is of interest to perform the same analysis with different durations, e.g., 6 hours and 24 hours. The results from different durations can be used to derive Depth-Duration-Frequency (DDF) or Intensity-Duration-Frequency (IDF) curves required for design purposes.

2. In the current analysis, the annual maximum series approach was adopted; however, alternative approaches such as partial duration series or peak over threshold series modeled with Generalized Pareto (GP) distribution should be examined and evaluated against the results reported in this study.

3. Although the use of L-moment estimation is commonly applied in the precipitation frequency analysis, other estimation methods such as the maximum likelihood (ML) method and method of moments (MOM) should also be evaluated for radar-based PFE analysis.

4. The selection of homogenous regions is a critical aspect of any regional-based PFE analysis. Therefore, a procedure for identification an optimum region size, as opposed to pre-set region size, should be explored.

5. The spatial bootstrap technique is thought to be not sensitive to outliers, and as such, should be applied to test its robustness to data artifacts and possible outliers in real-time radar products such as the Stage IV product.

6. In the current study, the spatial bootstrap technique was used as regional PFE estimation approach; the use of other regional frequency analysis approaches, e.g., the index-flood method, should be explored.

7. Applying the extreme value theory implies that the maximum series are all independent and identically distributed; however, precipitation cannot be considered as independent in space. Therefore, it is of interest to study how to model the spatial dependence of extreme events and examine the consequences on frequency estimation.

8. The GEV model used in this study assumed stationary parameters; however, due to possible changes in extreme events through time, using non-stationary modeling of extreme precipitation might be more reasonable.

9. Radar-based QPE products are known to be subject to various sources of sampling and estimation uncertainties. The effect of such uncertainties on the PFE estimates should be assessed and quantified.

10. A preliminary analysis was performed to examine the sources of difference between radar and gauge-based PFE results. A comparison of gauge and radar-based AMS series was done for a common period (2002 to 2011). The comparison confirms the fact that the radar-based QPEs have conditional bias, i.e., bias relative to the

magnitude of the rainfall. The effect of such conditional biases on the estimation of PFE yet remains to be investigated.

11. The change in characteristics of extreme rainfall to known sources of climate variability such as El Niño Southern Oscillations (ENSO) is another area of research that can be pursued using procedures similar to those adopted in the current study.

References

Allen, R. J. & DeGaetano, A. T., 2005. Considerations for the use of radar-derived precipitation estimates in determining return intervals for extreme areal precipitation amounts. *Journal of Hydrology,* 315(1), pp. 203-219.

Anagnostou, E. N., Krajewski, W. F. & Smith, J., 1999. Uncertainty quantification of mean-areal radar-rainfall estimates. *Journal of Atmospheric and Oceanic Technology,* 16(2), pp. 206-215.

Athreya, K. B., Fukuchi, J.-i. & Lahiri, S. N., 1999. On the bootstrap and the moving block bootstrap for the maximum of a stationary process. *Journal of Statistical Planning and Inference,* 76(1), pp. 1-17.

Atlas, D. & Ulbrich, C. W., 1977. Path-and area-integrated rainfall measurement by microwave attenuation in the 1-3 cm band. *Journal of Applied Meteorology,* 16(12), pp. 1322-1331.

Ausherman, D. A. et al., 1984. Developments in radar imaging. *IEEE Transactions on Aerospace and Electronic Systems,* AES-20(4), pp. 363-400.

Barnett , V. & Lewis, T., 1994. *Outliers in statistical data (Volume 3).* New York: Wiley.

Barnett, V., 1978. The study of outliers: purpose and model. *Journal of the Royal Statistical Society. Series C (Applied Statistics),* 27(3), pp. 242-250.

Battan, L. J., 1973. *Radar Observation of the Atmosphere*.

Bedient, P. B., Hoblit, B. C., Gladwell, D. C. & Vieux, B. E., 2000. NEXRAD radar for flood prediction in Houston. *Journal of Hydrologic Engineering,* 5(3), pp. 269-277.

Bhunya, P. K., Singh, R. D., Berndtsson, R. & Panda, S. N., 2012. Flood analysis using generalized logistic models in partial duration series. *Journal of Hydrology,* 420, pp. 59-71.

Bodine, D. et al., 2011. Understanding radar refractivity: sources of uncertainty. *Journal of Applied Meteorology and Climatology,* 50(12), pp. 2543-2560.

Borga, M., 2002. Accuracy of radar rainfall estimates for streamflow simulation. *Journal of Hydrology,* 267, pp. 26-39.

Boyles, R. et al., 2006. Evaluation and applications of NCEP stage II and stage IV gage-corrected radar precipitation estimates over the Carolinas. Preprints, 20th Hydroogical Conference Atlanta, GA, American Meteorological Society (CD-ROM, 1.1).

Buishand, T. A., 1989. Statistics of extremes in climatology. *Statistica Neerlandica,* 43(1), pp. 1-30.

Bureau, U. S. W., 1953. Rainfall intensities for local drainage design in the United States, for durations of 5 to 240 minutes and 2, 5, and 10-year return periods, part 1: west of the 115th meridian, Washington D. C.: U. S. Department of Commerce, Weather Bureau.

Bureau, U. S. W., 1954. Rainfall intensities for local drainage design in the United States, for durations of 5 to 240 minutes and 2, 5, and 10-year return periods, part II: between 105° W and 115° W, Washington D. C.: U. S. Department of Commerce, Weather Bureau.

Bureau, U. S. W., 1955. Rainfall intensity-duration-frequency curves for selected stations in the United States, Alaska, Hawaiian Islands, and Puerto Rico. *Technical Paper 25.*

Bureau, U. S. W., 1957. Rainfall intensity-frequency regime, part 1-The Ohio valley. *Technical Paper 29.*

Bureau, U. S. W., 1958. Rainfall intensity-frequency regime, part 2-Southeastern United States. *Technical Paper 29.*

Bureau, U. S. W., 1958. Rainfall intensity-frequency regime, part 3-The Middle Atlantic region. *Technical Paper 29.*

Bureau, U. S. W., 1959. Rainfall intensity -frequency regime, Part 4-Northeastern United States. *Technical Paper 29.*

Bureau, U. S. W., 1960. Rainfall intensity-frequency regime, Part 5-Great Lakes region. *Technical Paper 29.*

Bureau, U. S. W., 1964. Two- to ten-day precipitation for return period of 2 to 100 years in the contiguous United States. *Technical Paper 49.*

Burn, D. H., 1990a. Evaluation of regional flood frequency analysis with a region of influence approach. *Water Resources Research,* 26(10), pp. 2257-2265.

Burn, D. H., 1990b. An appraisal of the "region of influence" approach to flood frequency analysis. *Hydrological Sciences Journal,* 35(2), pp. 149-165.

Chen, V. C., Li, F., Ho, S.-S. & Wechsler, H., 2006. Micro-Doppler effect in radar: phenomenon, model, and simulation study. *IEEE Transactions on Aerospace and Electronic Systems,* 42(1), pp. 2-21.

Chowdhury, J. U., Stedinger, J. R. & Lu, L.-H., 1991. Goodness-of-fit tests for regional generalized extreme value flood distributions. *Water Resources Research,* 27(7), pp. 1765-1776.

Chow, V. T., Maidment, D. R. & Mays, L. W., 1988. *Applied Hydrology*.

Chwala, C. et al., 2012. Precipitation observation using microwave backhaul links in the alpine and pre-alpine region of Southern Germany. *Hydrology and Earth System Scciences,* 16, pp. 2647-2611.

Ciach, G. J., Krajewski, W. F. & Villarini, G., 2007. Product-error-driven uncertainty model for probabilistic quantitative precipitation estimation with NEXRAD data. *Journal of Hydrometeorology,* 8(6), pp. 1325-1347.

Ciach, G. J., Morrissey, M. L. & Krajewski, W. F., 2000. Conditional bias in radar rainfall estimation. *Journal of Applied Meteorology,* 39(11), pp. 1941-1946.

Cohn, T. A. et al., 2013. A generalized Grubbs-Beck test statistic for detecting multiple potentially influential low outliers in flood series. *Water Resources Research,* 49(8), pp. 5047-5058.

Cunnane, C., 1973. A particular comparison of annual maxima and partial duration series methods of flood frequency prediction. *Journal of Hydrology,* 18(3), pp. 257-271.

Cunnane, C., 1988. Methods and merits of regional flood frequency analysis. *Journal of Hydrology,* 100(1), pp. 269-290.

Davison, A. C., Hinkley, D. V. & Schechtman, E., 1986. Efficient bootstrap simulation. *Biometrika,* 73(3), pp. 555-556.

Doviak, R. J. & Zrnić, D. S., 1993. *Doppler radar and weather observations.*

Durrans, S. R., 2010. Intensity-duration-frequency curves. In: F. Y. Testik & M. Gebremichael, eds. *Rainfall: State of the Science.* Washington, DC: American Geophysical Union, pp. 159-169.

Durrans, S. R., Julian, L. T. & Yekta, M., 2002. Estimation of depth-area relationships using radar-rainfall data. *Journal of Hydrologic Engineering,* 7(5), pp. 356-367.

Ebert, E. E., Janowiak, J. E. & Kidd, C., 2007. Comparison of near-real-time precipitation estimates from satellite observations and numerical models. *Bulletin of the American Meteorological Society,* 88(1), pp. 47-64.

Ebtehaj, M., Moradkhani, H. & Gupta, H. V., 2010. Improving robustness of hydrologic parameter estimation by the use of moving block bootstrap resampling. *Water Resources Research,* 46(7).

Efron , B. & Tibshirani, R., 1986. Bootstrap methods for standard errors, confidence intervals, and other measures of statistical accuracy. *Statistical Science,* 1(1), pp. 54-75.

Efron, B., 1979. Bootstrap methods: another look at the Jackknife. *The Annals of Statistics,* 7(1), pp. 1-26.

Efron, B. & Tibshirani, R. J., 1994. *An Introduction to the Bootstrap.*

El Adlouni, S. & Ouarda, T. B. M. J., 2010. Frequency analysis of extreme rainfall events. In: F. Y. Testik & M. Gebremichael, eds. *Rainfall: State of the Science.* Washington, DC: American Geophysical Union, pp. 171-188.

Fabry, F. & Zawadzki, I., 1995. Long-term radar observations of the melting layer of precipitation and their interpretation. *Journal of the Atmospheric Sciences,* 52(7), pp. 838-851.

Faiers, G. E., Keim, B. D. & Hirschboeck, K. K., 1994. A Synoptic evaluation of frequencies and intensities of extreme three-and 24-hour rainfall in Louisiana. *The Professional Geographer,* 46(2), pp. 156-163.

Fang, Z., Bedient, P. B., Benavides, J. & Zimmer, A. L., 2008. Enhanced radar-based flood alert system and floodplain map library. *Journal of Hydrologic Engineering,* 13(10), pp. 926-938.

Faulkner , D. S. & Jones, D. A., 1999. The FORGEX method of rainfall growth estimation III: examples and confidence intervals. *Hydrology and Earth System Sciences,* 3(2), pp. 205-212.

Fowler, H. J. & Kilsby , C. G., 2003. Regional frequency analysis of United Kingdom extreme rainfall from 1961 to 2000. *International Journal of Climatology,* 23(11), pp. 1313-1334.

Franchini, M., Galeati, G. & Lolli, M., 2005. Analytical derivation of the flood frequency curve through partial duration series analysis and a probabilistic representation of the runoff coefficient. *Journal of Hydrology,* 303(1), pp. 1-15.

Frederick, R. H., Myers, V. A. & Auciello, E. P., 1977(a). Five to 60 minute precipitation frequency for the eastern and central United States. *NOAA Technical Memorandum NWS HYDR0-35.*

Frederick, . R. H., Myers, V. A. & Auciello, E. P., 1977(b). Storm depth-area relations from digitized radar returns. *Water Resources Research,* 13(3), pp. 675-679.

Fulton, R. A., 1998. WSR-88D polar-to-HRAP mapping, Silver Spring, Maryland: Hydrologic Research Laboratory, Office of Hydrology, National Weather Service Technical Memorandum.

Fulton, R. A., Breidenbach, J. P., Seo, D.-J. & Miller, D. A., 1998. The WSR-88D rainfall algorithm. *Weather and Forecasting,* 13(2), pp. 377-395.

Garcia, F. A. A., 2012. Tests to identify outliers in data series, Rio de Janeiro, Brazil: Pontifical Catholic University of Rio de Janeiro, Industrial Engineering Department.

Greene , D. R. & Hudlow, M. D., 1982. Hydrometeorologic grid mapping procedures. Denver, Colorado, AWRA International Symposium on Hydrometeorology.

Greenwood, A. J., Matalas, N. C., Landwehr, M. J. & Wallis, J. R., 1979. Probability weighted moments: definition and relation to parameters of several distributions expressable in inverse form. *Water Resources Research,* 15(5), pp. 1049-1054.

Gregersen, I. B., Madsen, H., Rosbjerg, D. & Arnbjerg-Nielsen, K., 2013. A spatial and nonstationary model for the frequency of extreme rainfall events. *Water Resources Research,* 49(1), pp. 127-136.

Grubbs , F. E. & Beck, G., 1972. Extension of sample sizes and percentage points for significance tests of outlying observations. *Technometrics,* 14(4), pp. 847-854.

Grubbs, F. E., 1950. Sample criteria for testing outlying observations. *The Annals of Mathematical Statistics,* 21(1), pp. 27-58.

Grubbs, F. E., 1969. Procedures for detecting outlying observations in samples. *Technometrics,* 11(1), pp. 1-21.

Guttman, N. B. & Quayle, R. G., 1996. A historical perspective of US climate divisions. *Bulletin of the American Meteorological Society,* 77(2), pp. 293-303.

Habib, E., Ciach, G. J. & Krajewski, W. F., 2004. A method for filtering out raingauge representativeness errors from the verification distributions of radar and raingauge rainfall. *Advances in Water Resources,* 27(10), pp. 967-980.

Habib, E., Henschke, A. & Adler, R. F., 2009. Evaluation of TMPA satellite-based research and real-time rainfall estimates during six tropical-related heavy rainfall events over Louisiana, USA. *Atmospheric Research,* 94, pp. 373-388.

Habib, E., Lee, G., Kim, D. & Ciach, G. J., 2010. Ground-based direct measurement. In: F. Y. Testik & M. Gebremichael, eds. *Rainfall: State of the Science.* Washington, DC: American Geophysical Union, pp. 61-77.

Habib, E. & Qin, L., 2013. Application of a radar-rainfall uncertainty model to the NWS multi-sensor precipitation estimator products. *Meteorological Applications,* 20(3), pp. 276-286.

Habib, E. et al., 2013. Independent assessment of incremental complexity in NWS multisensor precipitation estimator algorithms. *Journal of Hydrologic Engineering,* pp. 143-155.

Hailegeorgis, T. T., Thorolfsson, S. T. & Alfredsen, K., 2013. Regional frequency analysis of extreme precipitation with consideration of uncertainties to update IDF curves for the city of Trondheim. *Journal of Hydrology,* 498(19), pp. 305-318.

Hanel, M., Buishand, T. A. & Ferro, C. A. T., 2009. A nonstationary index flood model for precipitation extremes in transient regional climate model simulations. *Journal of Geophysical Research: Atmospheres,* 114(D15), pp. 1984-2012.

Heiser, W. J. & Meulman, J. J., 1992. Homogeneity analysis: Exploring the distribution of variables and their nonlinear relationships, University of Leiden.

Hershfield, D. M., 1961. Rainfall frequency atlas of the United States for durations from 30 minutes to 24 hours and return periods from 1 to 100 years. *Technical Paper 40, U.S. Weather Bureau, Washington, D. C.*.

Hosking, J., 1990. L-moments: Analysis and estimation of distributions using linear combinations of order statistics. *Journal of the Royal Statistical Society,* 52(1), pp. 105-124.

Hosking, J. R. M. & Wallis, J. R., 1997. *Regional Frequency Analysis.* Cambridge University Press.

Hou, D. et al., 2012. Climatology-calibrated precipitation analysis at fine scales: statistical adjustment of stage IV towards CPC gauge based analysis. *Journal of Hydrometeorology*.

Hubbert, J. C., Dixon, M., Ellis, S. M. & Meymaris, G., 2009. Weather radar ground clutter. Part I: identification, modeling, and simulation. *Journal of Atmospheric and Oceanic Technology,* 29(7), pp. 1165-1180.

Iglewicz , B. & Hoaglin, D., 1993. *How to Detect and Handle Outliers (Volume 16).* Milwaukee, Wisconsin: ASQC Quality Press.

Jayakrishnan, R., Srinivasan, R. & Arnold, J. G., 2004. Comparison of raingage and WSR-88D Stage III precipitation data over the Texas-Gulf basin. *Journal of Hydrology,* 292(1), pp. 135-152.

Johnson, D., Smith, M., Koren, V. & Finnerty, B., 1999. Comparing mean areal precipitation estimates from NEXRAD and rain gauge networks. *Journal of Hydrologic Engineering,* 4(2), pp. 117-124.

Kachroo , R. K., Mkhandi , S. H. & Parida , B. P., 2000. Flood frequency analysis of southern Africa: I. Delineation of homogeneous regions. *Hydrological Sciences Journal,* 45(3), pp. 437-447.

Katz, R. W., Brush, G. S. & Parlan, M. B., 2005. Statistics of extremes: modeling ecological disturbances. *Ecology,* 86(5), pp. 1124-1134.

Katz, R. W., Parlange, M. B. & Naveau, P., 2002. Statistics of extremes in hydrology. *Advances in Water Resources,* 25, pp. 1287-1304.

Klazura, G. E. & Imy, D. A., 1993. A description of the initial set of analysis products available from the NEXRAD WSR-88D system. *Bulletin of the American Meteorological Society,* 74, pp. 1293-1311.

Kotz, S. & Nadarajah, S., 2000. *Extreme Value Distribuutions, Theory and Applications.* London: Imperial College Press.

Krajewski, W. F. & Smith, J. A., 2002. Radar hydrology: rainfall estimation. *Advances in Water Resources,* p. 1387–1394.

Krajewsk, W. F. et al., 2007. Towards better utilization of NEXRAD data in hydrology: an overview of Hydro-NEXRAD. *World Environmental and Water Resources Congress 2007,* pp. 1-8.

Kuligowski, R. J., 1997. An overview of National Weather Service quantitative precipitation estimates. *TDL Office Note 97-4.*

Kursinski , A. L. & Mullen, S. L., 2008. Spatiotemporal variability of hourly precipitation over the eastern contiguous United States from stage IV multisensor analyses. *Journal of Hydrometeorology,* 9, pp. 3-21.

Lall, U. & Sharma, A., 1996. A nearest neighbor bootstrap for resampling hydrologic time series. *Water Resources Research,* 32(3), pp. 679-693.

Landwehr, J. M., Matalas, N. C. & Wallis, J. R., 1979. Probability weighted moments compared with Some traditional techniques in estimating Gumbel parameters and quantiles. *Water Resources Research,* 15(5), pp. 1055-1064.

Langford , E., 2006. Quartiles in elementary statistics. *Journal of Statistics Education,* 14(3).

Lee, S. H. & Maeng, S. J., 2003. Frequency analysis of extreme rainfall using L-moment. *Irrigation and Drainage,* 52(3), pp. 219-230.

Leijnse, H., Uijlenhoet, R. & Stricker, J. N. M., 2007. Rainfall measurement using radio links from cellular communication networks. *Water Resources Research,* 43(3).

Lin, B. et al., 2006. Regional frequency studies of annual extreme precipitation in the United States based on regional L-moments analysis. *World Environmental and Water Resource Congress 2006,* pp. 1-11.

Lin, Y. & Mitchell , K. E., 2005. The NCEP stage II/IV hourly precipitation analyses: development and applications. 19th Conf. on HydrologySan Diego, CA,American Meteorological Society,1.2.

Liu, Z., 2015. Comparison of precipitation estimates between version 7 3-hourly TRMM multi-satellite precipitation analysis (TMPA) near-real-time and research products. *Atmospheric Research,* 153, pp. 119-133.

Lombardo, F., Napolitano, F. & Russo, F., 2006. On the use of radar reflectivity for estimation of the areal reduction factor. *Natural Hazards and Earth System Science,* 6(3), pp. 377-386.

Lopez, P., 2011. Direct 4D-Var assimilation of NCEP stage IV radar and gauge precipitation data at ECMWF. *Monthly Weather Review,* 139(7), p. 2098–2116.

Lopez, P. & Bauer, P., 2007. 1D+4D-VAR assimilation of NCEP stage-IV radar and gauge hourly precipitation data at ECMWF. *Monthly Weather Review,* 135, pp. 2506-2524.

Maddox, R. A., Chappell, C. F. & Hoxit, L. R., 1979. Synoptic and meso-α scale aspects of flash flood events 1. *Bulletin of the American Meteorological Society,* 60(2), pp. 115-123.

Madsen, H., Rasmussen, P. F. & Dan Rosbjerg, 1997. Comparison of annual maximum series and partial duration series methods for modeling extreme hydrologic events: 1. At-site modeling. *Water Resources Research,* 33(4), pp. 747-757.

Marshall, J. S. & Palmer, W. M. K., 1948. The distribution of raindrops with size. *Journal of Meteorology,* 5(4), pp. 165-166.

Martins , E. S. & Stedinger, J. R., 2000. Generalized maximum-likelihood generalized extreme-value quantile estimators for hydrologic data. *Water Resources Research,* 36(3), pp. 737-744.

Martins, E. S. & Stedinger, J. R., 2001. Historical information in a generalized maximum likelihood framework with partial duration and annual maximum series. *Water Resources Research,* 37(10), pp. 2559-2567.

Meischner, P., 2004. *Weather Radar: Principles and Adavnaced Applications.*Springer.

Messer, H., Zinevich, A. & Alpert, P., 2006. Environmental monitoring by wireless communication networks. *Science,* 312(5774).

Miller, J. F., Frederick, R. H. & Tracey, R. J., 1973. Precipitation-frequency atlas of the western United States. *NOAA Atlas 2.*

Naghavi, B. & Yu, F. X., 1995. Regional frequency analysis of extreme precipitation in Louisiana. *Journal of Hydraulic Engineering,* 121(11), p. 819–827.

NCEP/EMC/NOAA, 2013. *Questions & Answers about NCEP Stage II/Stage IV.* [Online] Available at: http://www.emc.ncep.noaa.gov/mmb/ylin/pcpanl/QandA/#1HVS6H

Neary, V. S., Habib, E. & Fleming, M., 2004. Hydrologic modeling with NEXRAD precipitation in middle Tennessee. *Journal of Hydrologic Engineering,* 9(5), pp. 339-349.

Nelson, B. R., Seo, D.-J. & Kim, D., 2009. Multisensor precipitation reanalysis. *Journal of Hydrometeorology,* 11, pp. 666-682.

Olivera, F., Choi, J., Kim, D. & Li, M.-H., 2008. Estimation of average rainfall areal reduction factors in Texas using NEXRAD data. *Journal of Hydrologic Engineering,* 13(6), pp. 438-448.

Overeem, A., Buishand, A. & Holleman, I., 2008. Rainfall depth-duration-frequency curves and their uncertainties. *Journal of Hydrology,* 348, pp. 124-134.

Overeem, A., Buishand, T. A. & Holleman, I., 2009. Extreme rainfall analysis and estimation of depth-duration-frequency curves using weather radar. *Water Resources Research ,* 45(10).

Overeem, A., Buishand, T. A., Holleman, I. & Uijlenhoet, R., 2010. Extreme value modeling of areal rainfall from weather radar. *Water Resources Research,* 46(9).

Overeem, A., Leijnse, H., Gaona, M. F. R. & Uijlenhoet, R., 2014. Calling for rain: Rainfall maps from cellular communication networks.

Pal, N., Jin, C. & Lim, W. K., 2006. *Handbook of Exponential and Related Distribuations for Engineers and Scientists.* Boca Raton, FL, USA: Chapman & Hall/CRC, Taylor & Francis Group.

Pearson , E. S. & Sekar, C. C., 1936. The efficiency of statistical tools and a criterion for the rejection of outlying observations. *Biometrika,* 28(3-4), pp. 308-320.

Pecho, J., Fasko, P., Lapin, M. & Gaál, L., 2009. Analysis of rainfall intensity-duration-frequency relationships in Slovakia (estimation of extreme rainfall return periods). Vienna, Austria, EGU General Assembly.

Perica, S. et al., 2013. Precipitation-frequency atlas of the United States, NOAA Atlas 14, Volume 9, Version 2: Southeastern States, Silver Spring, Maryland, 2013: U.S. Department of Commerce, National Oceanic and Atmospheric Adminstration, National Weather Service.

Pilona, P. J., Adamowskib, K. & Alilab, Y., 1991. Regional analysis of annual maxima precipitation using L-moments. *Atmospheric Research,* 27(1), pp. 81-92.

Ryzhkov, A., Diederich, M., Zhang, P. & Simmer, C., 2014. Potential utilization of specific attenuation for rainfall estimation, mitigation of partial beam blockage, and radar networking. *Journal of Atmospheric and Oceanic Technology,* 31, pp. 599-619.

Schumacher, R. S. & Johnson, R. H., 2006. characteristics of U.S. extreme rain events during 1999–2003. *Weather and Forecasting,* 21(1), pp. 69-85.

Scofield, R. A. & Kuligowski, R. J., 2003. Status and outlook of operational satellite precipitation algorithms for extreme-precipitation events. *Weather and Forecasting,* 18(6), pp. 1037-1051.

Seo, B.-C.et al., 2011. Radar-rainfall estimation algorithms of Hydro-NEXRAD. *Journal of Hydroinformatics,* 13(2).

Seo, D. J., 1998. Real-time estimation of rainfall fields using radar rainfall and rain gauge data. *Journal of Hydrology,* 208, pp. 37-52.

Seo, D.-J., Seed, A. & Delrieu, G., 2010. Radar and multisensor rainfall estimation for hydrologic applications. In: F. Y. T. a. M. Gebremichael, ed. *Rainfall:State of Science.* Washington, D. C.: American Geophysical Union.

Sharma, S. & Tiwari , K., 2009. Bootstrap based artificial neural network (BANN) analysis for hierarchical prediction of monthly runoff in Upper Damodar Valley Catchment. *Journal of Hydrology,* 374, pp. 209-222.

Skolnik, M. I., 1970. *Radar Handbook.*

Smalley, M., L'Ecuyer, T., Lebsock, M. & Haynes, J., 2014. A comparison of precipitation occurrence from the NCEP stage IV QPE product and the CloudSat cloud profiling radar. *Journal of Hydrometeorology,* 15, pp. 444-458.

Smith, J. A., Seo, D. J. & Baeck, M. L., 1996. An intercomparison study of NEXRAD precipitation estimates. *Water Resources Research,* 32(7), pp. 2035-2045.

Srikanthan, R., 1995. A review of the methods for estimating areal reduction factors for design rainfalls. *CRC for Catchment Hydrology, Department of Civil Engineering, Monash University.*

Stedinger, J. R., Vogel, R. M. & Foufoula-Georgio, E., 1993. Frequency analysis of extreme events. In: D. R. Maidment, ed. *Handbook of Hydrology.* New York: McGraw-Hill, p. 18.1 – 18.66.

Sugahara, S., Da Rocha, R. P. & Silveira, R., 2009. Non-stationary frequency analysis of extreme daily rainfall in Sao Paulo, Brazil. *International Journal of Climatology,* 29(9), pp. 1339-1349.

Sveinsson , O. G. B., Boes , D. C. & Salas, J. D., 2001. Population index flood method for regional frequency analysis. *Water Resources Research,* 37(11), pp. 2733-2748.

Sveinsson, O. G. B., Boes, D. C. & Salas , J. D., 2001. Population index flood method for regional frequency analysis. *Water Resources Research,* 37(11), pp. 2733-2748.

Svensson, C. & Jones, D. A., 2010. Review of rainfall frequency estimation methods. *Journal of Flood Risk Management ,* 3(4), pp. 296-313.

Tallaksen, L. M. & van Lanen, H. A. J., 2004. *Hydrological Drought: Processes and Estimation Methods for Streamflow and Groundwater.* 1st ed. Amsterdam, The Netherlands: Elsevier.

Thompson, W. R., 1935. On a criterion for the rejection of observations and the distribution of the ratio of deviation to sample standard deviation. *The Annals of Mathematical Statistics,* 6(4), pp. 214-219.

Trefry, C. M., Watkins, D. W. & Johnson, D., 2005. Regional rainfall frequency analysis for the state of Michigan. *Journal of Hydrologic Engineering,* 10(6), pp. 437-449.

Uboldi, F. et al., 2014. A spatial bootstrap technique for parameter estimation of rainfall annual maxima distribution. *Hydrology and Earth System Sciences,* 18, pp. 981-995.

USGS, I. A. C. o. W. D., 1982. Guidlines for determining flood flow frequency, Bulletin#17B of the hydrology subcommittee, Reston, Virginia.

Villarini, G. & Krajewski, W. F., 2010a. Review of the different sources of uncertainty in single polarization radar-based estimates of rainfall. *Surveys in geophysics,* pp. 107-129.

Villarini, G., Krajewski, W. F., Ciach, G. J. & Zimmerman, D. L., 2009. Product-error-driven generator of probable rainfall conditioned on WSR-88D precipitation estimates. *Water Resources Research,* 45(1).

Villarini, G. et al., 2010b. Radar analyses of extreme rainfall and flooding in urban drainage basins. *Journal of Hydrology,* 381, pp. 266-286.

Vogel, R. M. & Shallcross, A. L., 1996. The moving blocks bootstrap versus parametric time series models. *Water Resources Research,* 32(6), pp. 1875-1882.

Watson, R. J., Holt, A. R., Marecal, V. & Testud, J., 1999. A rainrate-attenuation-reflectivity relation for use in the spaceborne and airborne sensing of rain. *IEEE Transactions on Geosecience and Remote Sensing ,* 37(3), pp. 1447-1450.

Westrick, K. J., Mass, C. F. & Colle, B. A., 1999. The limitations of the WSR-88D radar network for quantitative precipitation measurement over the coastal Western United States. *Bulletin of the American Meteorological Society,* 80(11), pp. 2289-2298.

Wilks, D. S., 1993. Comparison of three-parameter probability distributions for representing annual extreme and partial duration precipitation series. *Water Resources Research,* 29(10), pp. 3543-3549.

Wright, D. B., Smith, J. A., Villarini, G. & Baeck, M. L., 2013. Estimating the frequency of extreme rainfall using weather radar and stochastic storm transposition. *Journal of Hydrology,* 488, pp. 150-165.

Xie, P. & Arkin, P. A., 1996. Analyses of global monthly precipitation using gauge observations, satellite estimates, and numerical model predictions. *Journal of Climate,* 9(4), pp. 840-858.

Yarnell, D. L., 1935. Rainfall intensity-frequency data. No. 204. *US Government Printing Office.*

Young, B. C. et al., 2000. Evaluating NEXRAD multisensor precipitation estimates for operational hydrologic forecasting. *Journal of Hydrometeorology,* 1, pp. 241-254.

Young, C. B. & Brunsell, N. A., 2008. Evaluating NEXRAD estimates for the Missouri river basin: analysis using daily raingauge data. *Journal of Hydrologic Engineering,* 13(7), pp. 549-553.

Zagrodnik , J. P. & Jiang, H., 2013. Investigation of PR and TMI version 6 and version 7 rainfall algorithms in landfalling tropical cyclones relative to the NEXRAD stage-IV multisensor precipitation estimate dataset. *Journal of Applied Meteorology and Climatology,* 52, pp. 2809-2827.

Zhang, J., Langston, C. & Howard, K., 2008. Brightband identification based on vertical profiles of reflectivity from the WSR-88D. *Journal of Atmospheric and Oceanic Technology,* 25(10), pp. 1859-1872.

Zhang, Y., Reed, S. & Kitzmiller, D., 2011. Effects of retrospective gauge-based readjustment of multisensor precipitation estimates on hydrologic simulations. *Journal of Hydrometeorology,* 12, pp. 429-443.

Zhang, Z. et al., 2004. Use of next generation weather radar data and basin disaggregation to improve continuous hydrograph simulations. *Journal of Hydrologic Engineering,* 9(2), pp. 103-115.

El-Dardiry, Hisham A. Bachelor of Science, Faculty of Engineering, Alexandria University, Egypt, 2010; Master of Science, University of Louisiana at Lafayette, Fall 2014
Major: Engineering, Civil Engineering option
Title of Thesis: The Use of Multi-Sensor Quantitative Precipitation Estimates for Deriving Extreme Precipitation Frequencies with Application in Louisiana
Thesis Director: Dr. Emad Habib
Pages in Thesis: 180; Words in Abstract: 290

ABSTRACT

The Radar-based Quantitative Precipitation Estimates (QPE) is one of the NEXRAD products that are available in a high temporal and spatial resolution compared with gauges. Radar-based QPEs have been widely used in many hydrological and meteorological applications; however, a few studies have focused on using radar QPE products in deriving of Precipitation Frequency Estimates (PFE). Accurate and regionally specific information on PFE is critically needed for various water resources engineering planning and design purposes. This study focused first on examining the data quality of two main radar products, the near real-time Stage IV QPE product, and the post real-time RFC/MPE product. Assessment of the Stage IV product showed some alarming data artifacts that contaminate the identification of rainfall maxima. Based on the inter-comparison analysis of the two products, Stage IV and RFC/MPE, the latter was selected for the frequency analysis carried out throughout the study. The precipitation frequency analysis approach used in this study is based on fitting Generalized Extreme Value (GEV) distribution as a statistical model for the hydrologic extreme rainfall data that based on Annual Maximum Series (AMS) extracted from 11 years (2002-2012) over a domain covering Louisiana. The parameters of the GEV model are estimated using method of linear moments (L-moments). Two different approaches are suggested for estimating the precipitation frequencies; Pixel-Based approach, in which PFEs are estimated at each individual pixel and Region-Based approach in which a

synthetic sample is generated at each pixel by using observations from surrounding pixels. The region-based technique outperforms the pixel based estimation when compared with results obtained by NOAA Atlas 14; however, the availability of only short record of observations and the underestimation of radar QPE for some extremes causes considerable reduction in precipitation frequencies in pixel-based and region-based approaches.

BIOGRAPHICAL SKETCH

Hisham Abd El-Kareem El-Dardiry was born on October 23, 1987 in Egypt. He received a Bachelor of Science with degree of honor in Civil Engineering from Alexandria University in 2010. He joined Alexandria University as a teaching assistant in 2011 and worked there for almost two years. Hisham has studied in the master's program in Engineering with concentration in Civil Engineering at the University of Louisiana at Lafayette since August 2013 and is expected to graduate in fall 2014.